

Aus dem Zentrum für Medizinische Forschung
der Medizinischen Fakultät Mannheim
Direktor: Prof. Dr. med. Norbert Gretz
(Aufgelöst zum 16.04.2020)

Impact of photobiomodulation on human skin melanocytes

Inauguraldissertation
zur Erlangung des akademischen Grades
Doctor scientiarum humanarum (Dr. sc. hum.) der
Medizinischen Fakultät Mannheim
der Ruprecht-Karls-Universität
zu
Heidelberg

vorgelegt von
Aparna Chauhan

aus
Ghaziabad, India
2020

Dekan: Prof. Dr. med. Sergij Goerd
Referent: Prof. Dr. med. Norbert Gretz

Table of Contents

1. Introduction	1
1.1 Photobiomodulation	1
1.2 Human skin	7
1.3 Human skin melanocytes	8
1.4 Blue light and optical properties of skin	9
2. Aims of the study.....	12
3. Material and methods.....	13
3.1 Material	13
3.2 Methods	17
4. Results.....	27
4.1 Assessment of effects of different blue light irradiation time points with corresponding doses.....	27
4.2 Influence of blue light on melanin content	30
4.3 Effect of blue light treatment on cell apoptosis	32
4.4 Blue light irradiation influences the energy metabolism level in NHEM	34
4.5 Intracellular redox level changes inflicted by blue light	35
4.6 Gene expression analysis	36
5. Discussion.....	65
5.1 Blue light doses resulted in a biphasic dose response	65
5.2 Blue light induces hyperpigmentation	66
5.3 No induction of cell death via apoptosis by blue light.....	67
5.4 Blue lights increases ATP amount.....	69
5.5 Blue light increases ROS level	69
5.6 AHR as a possible target for oxidative stress management from blue light.....	71
5.7 Conclusion and outlook	73
6. Summary.....	75

7. References.....	77
8. Appendix.....	88
9. Curriculum vitae and Publications	90
Abbreviations	92
Acknowledgements	97

1. Introduction

1.1 Photobiomodulation

The term photobiomodulation (PBM) is referred to as the use of visible (VIS) and infrared (IR) spectrum of light that leads to modulation in the biological functions. It was previously known as low-level laser (or light) therapy (LLLT) that was a well-established and searchable MeSH term ¹. In September 2014, a joint conference of the North American Association for Light Therapy (NAALT) and the World Association for Laser Therapy (WALT) held a nomenclature consensus meeting. In this meeting, after the discussion about the pros and cons of several terms used for this therapy, the term 'Photobiomodulation Therapy' was accepted as the new MeSH term and added to the MeSH vocabulary for its 2016 version of the vocabulary thesaurus. As the term, LLLT is vague because the words 'low' and 'level' are not well defined and the word 'laser' also is not correct anymore because of the use of other types of light sources like light-emitting diodes (LEDs) in this field ². The new suggested definition of PBM therapy is as follows:

“A light therapy that utilizes non-ionizing light sources, including lasers, LEDs and broadband light, in the visible and infrared spectrum. It is a non-thermal process involving endogenous chromophores eliciting photophysical (i.e. linear and non-linear) and photochemical events at various biological scales. This process results in beneficial therapeutic outcomes including but not limited to the alleviation of pain or inflammation, immunomodulation, and promotion of wound healing and tissue regeneration” ³.

1.1.1 History

Sunlight is the natural source of light on the planet earth, and it has been known to have both beneficial and detrimental effects on living beings. Hence, the use of light therapy dates back to ancient times. However, Niels Ryberg Finsen carried out the first pioneered work in the medical phototherapy field in the late eighteenth century ⁴.

He used ultraviolet (UV) radiation to treat various human ailments, especially *Lupus vulgaris*. In 1895, he demonstrated the concentrated beams of UV radiation could have bactericidal as well as stimulating the surrounding tissue and won Nobel Prize in 1903 for the same work ⁴. After the invention of ruby laser in 1960 and the helium-neon (HeNe) laser in 1961 led to another milestone work by Endre Mester in 1967, at the Semmelweis Medical University, Hungary ⁵. He provided the first evidence and described the potential effect of the low-level laser therapy by applying the ruby laser on the back of shaved mice implanted with tumour via an incision in the skin. Although he could not cure the tumour, as an outcome of this treatment he observed a faster rate of hair growth in the laser-treated mice as compared to non-treated controls ⁶. The 'Laser Biostimulation' term was coined due to beneficial effects of the laser treatment⁷. In modern medicine, the use of this therapy gained momentum from this point onwards and since then, several studies have been carried out to assess the effects of light. Also progress in this field led to the development of many other light devices, for example, non-coherent LEDs. As a result, different terms came into existence like low-level laser (or light) therapy, low-intensity laser therapy, low-power laser therapy, cold laser, soft laser, photobiostimulation and photobiomodulation ³. The most commonly used was LLLT and due to this having an ambiguous definition, the term 'Photobiomodulation' or 'Photobiomodulation Therapy' was accepted.

1.1.2 Irradiation parameters

The irradiation parameters and the doses applied are very basic and critical specifications in the light therapy field. The biggest concern in this field is improper reporting of the irradiation parameters, which affects the reproducibility and reliability of the experimental outcome obtained from one group to validate the results by another⁸. The most important parameters are listed in Table 1.

Table 1. List of the irradiation parameters

Irradiation parameter	Measurement unit
Wavelength	nm
Irradiance	W/cm ² (or mW/cm ²)
Energy density	J/cm ²
Irradiation time	s
Operating mode	Continuous or pulsed

Among the important parameters, wavelength (λ) of the light is defined as the length of a full oscillation of the wave. It is the most fundamental parameter for studying the effects of different colours of visible light on the living organisms. Light is part of the electromagnetic spectrum, which constitutes the range from gamma rays to radiowaves ⁹, as shown in Figure 1.

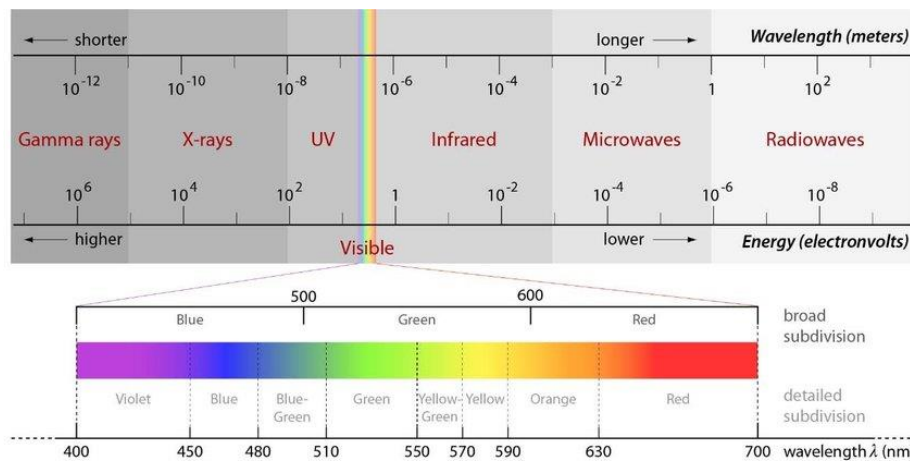


Figure 1. The electromagnetic spectrum. Complete electromagnetic spectrum with spectral subdivision including the visible light spectrum ¹⁰.

Next, irradiance is the intensity of the radiation incident on a patient (or an object). It is also known as power density, where it corresponds to power (W) divided by the area (in per cm²).

Another very essential specification include energy density, which is an important descriptor of the dose and defined as the time integral of the irradiance (unit: J/cm²) ¹¹.

1.1.3 Mechanism of action

The effectiveness of any kind of applied therapy or medicine holds the key to its mechanism of action. The use of PBM still as an alternative treatment is in fact due to lack of understanding of complete biochemical mechanisms. According to the first law of photobiology, also called Grotthus-Draper law, light must be absorbed by the system for a biologic effect to take place. Moreover, this could include some molecular photoacceptors or chromophores ¹². Numerous chromophores and photoacceptors can be found in the living system, for example, chlorophyll, haemoglobin, cytochrome C oxidase (Cox), myoglobin, flavins, flavoproteins, porphyrins ¹³. Also endogenous nucleic acids, aromatic amino acids, tryptophan, tyrosine, melanin and melanin precursors, bilirubin, β -carotene or water molecules are photoacceptors ^{14, 15}. The primary and secondary mechanisms of action of visible and near-infrared (NIR) have been summarized by Karu, T. et al., 1999 ^{13, 16}. They are as follow: First, photoexcitation of the electronic states of the components of the respiratory chain can alter their redox properties via an acceleration of electron transfer. Second, during the process of photoexcitation, a certain amount of excitation energy is converted to heat and this enhances the local temperature of the absorbing chromophore. As a result, a conformational change occurs, and this possibly triggers the biochemical reactions like activation or inhibition of enzymes. Third, secondary messenger like H_2O_2 or reactive oxygen species (ROS) like $O_2^{\cdot-}$ change the redox potential of mitochondria and/or the redox status of the cell. Fourth, some photoabsorbing molecules, for example, porphyrin and flavoproteins can be reversibly converted to photosensitizers, which transfer the energy to adjacent molecules. These changes activate molecules responsible for cellular homeostasis and initiate a series of biochemical reactions, which might be involved in further promoting the secondary responses. Furthermore, the effects of light on respiration are oxygen-dependent.

The photodynamic reactions are stimulated by certain respiratory chain components that include flavins, hemes and Fe-S centres ^{17, 18} and a classic example that has been extensively studied and reported include cytochrome C oxidase ^{19, 20}.

1.1.4 Clinical applications

PBM is known to have a wide range of clinical applications, which are mainly involved in stimulating, healing and restoration. These applications have emerged in diverse medical fields, ranging from dermatology, to dentistry, to rheumatology and physiotherapy, as summarized in Figure 2.

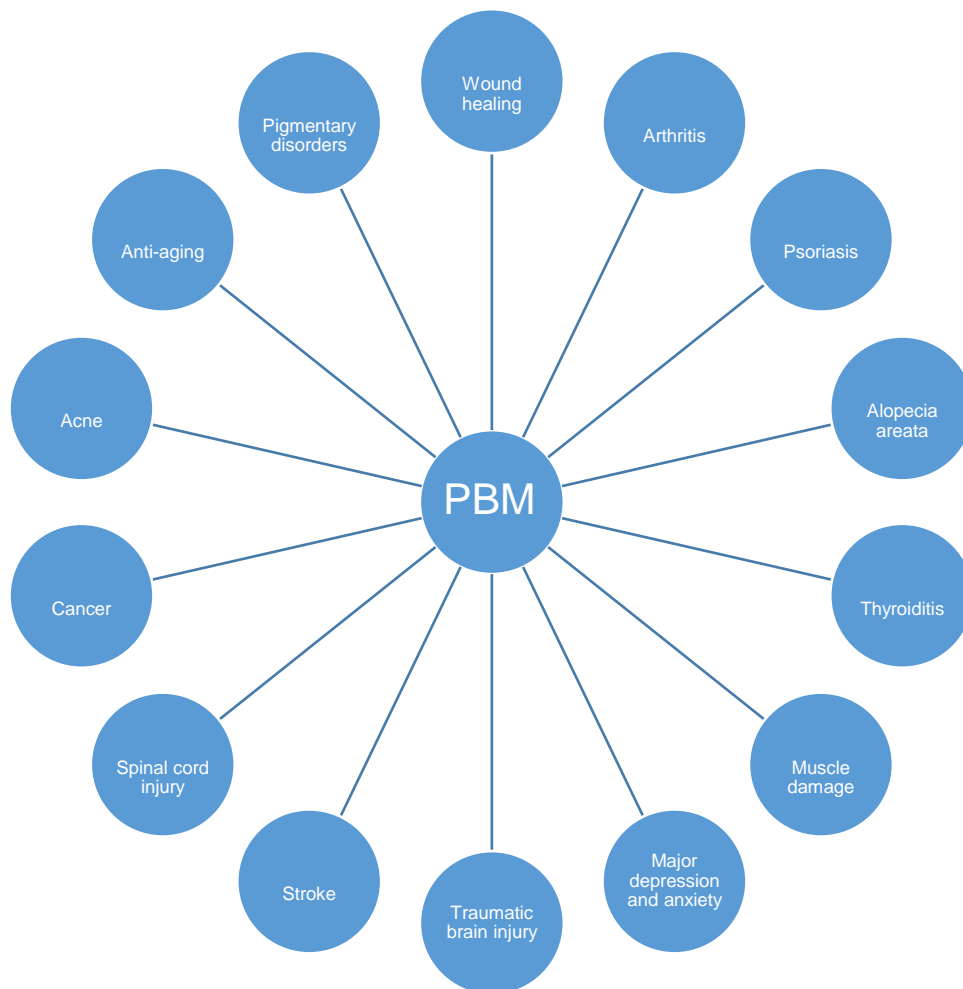


Figure 2. Summarized clinical applications of PBM ^{21, 22, 9}.

Besides, there are several devices based on these clinical applications. Table 2 lists some devices used in dermatology which are manufactured by different companies.

Table 2. Examples of PBMT devices used for dermatological applications ²²

Supplier	Product Name	Wavelength (nm)	Power Density (mW/cm ²)	Standard Dose (J/cm ²)	Application
PhotoMedex (Manchester, UK)	Omnilux	415 (±5) 633 (±6) 830 (±5)	40 105 55	48 126 66	Acne, photodamage, nonmelanoma skin cancers, skin rejuvenation, vitiligo, and wound healing after elective surgery
Edge Systems (Signal Hill, CA)	Delphia del Sol	420 600-700 700-1000		7.4 J per treatment area	Acne, improving skin texture, firmness and resilience, increasing lymphatic system activity, fine lines, wrinkles, and superficial hyperpigmentation
Flip 4 (Sainte-Julie, Quebec, Canada)	Max7	420-700	≤4		Acne, rejuvenation and injured skin healing, including the shortening of the post-skin resurfacing erythema duration
Light BioSciences (Virginia Beach, VA)	Gentlewaves	588 (10)	Variable		Antiaging
OPUSMED (Montreal, Canada)	LumiPhase-R	660	150		Skin firmness, rhytid depth, and wrinkles
Revitalight (Chicago, IL)	Revitalight 747 Hand Spa Food Spa Evolution	420 590 625 940	80 80 80 80	7.2 J per 90 s per treatment area	Fine lines, wrinkles, and age spots on the face, neck, and hands
Soli-Tone (Woburn, MA)	LumiFacial Lumilift	470 525 590 640	84 27 10 89		Acne, antiaging, hyperpigmentation, and rosacea
DUSA (Wilmington, MA)	BLU-U	417	10		Acne
Curelight (Rehovot, Israel)	iClearXL Clear100XL	405-420 890-900		60	Acne, antiaging, skin rejuvenation, acceleration of healing of post peel, and postsurgical suture sites
Lumenis (Santa Clara, CA)	ClearLight Clear100	405-420	200	60	Acne
Lightwave Technologies (Phoneix, AZ)	Lightwave Professional Deluxe LED System	417 630 880			Antiaging and skin rejuvenation
Dynatronics (Salt Lake City, UT)	Synergie LT2	660 880	500 mW (total power)	6 J per treatment area	Antiaging, skin firmness, wrinkles, skin tone, and texture for face and neck

1.2 Human skin

The skin is referred as the largest organ in the human body and consists for a surface area of 1.5-1.8 m². It is 1.5-4mm thick and accounts for approximately 15% of the total adult body weight^{23, 24}. It serves as the physical barrier for the host body by protecting against chemical, mechanical and microbial factors²³. Likewise, other key functions include sensation, prevention of water loss from the body as well as thermoregulation^{25, 26}. The skin is divided into three layers (from top to bottom), the epidermis, the dermis and the hypodermis (or the subcutaneous layer)²⁶ (Figure 3).

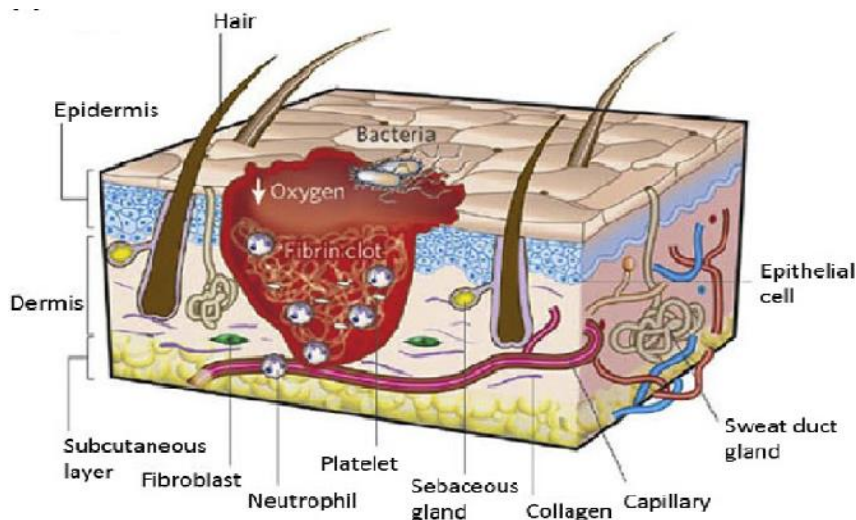


Figure 3. The human skin. Schematic diagram showing the different layers of human skin²⁷.

The epidermis is the superficial and stratified layer, where the epithelium is being continuously renewed. It is composed of different cell types, namely keratinocytes, melanocytes, Langerhans cells and Merkel cells. All these cells densely pack the epidermis to a depth of 75-150 μm (up to 600 μm thick on the soles and palms). The keratinocytes (constitute 90-95%) are either self-replicating in the basal layer or differentiating towards the upper layer, also known as cornification and via this sequential process the epidermis is divided into four distinct layers²⁸. Whereas the rest of the epidermis is made up of melanocytes, Langerhans cells and Merkel cells. On the other hand, dermis has a thickness of <2mm and gives mechanical strength to the skin. It is further divided into superficial papillary dermis and deeper reticular dermis²⁹. It mainly comprises of collagen, elastin, glycosaminoglycans, which collectively form the extracellular-matrix (ECM) as well as fibroblasts. Also, the hypodermis consists of

loose connective tissue, rich in adipose tissue that insulates and protects the skin ^{28, 30}.

1.3 Human skin melanocytes

In the human skin, the melanocytes are dendritic cells located in the lower most layer of the skin epidermis as illustrated in Figure 4, as well as hair follicles ³¹. Their origin is from the embryonic cells called neural crest cells ³². The principle function of these cells are their ability to produce the pigment termed melanin, hence responsible for the pigmentation of skin ³³. The pigment melanin is formed in specialised membrane-bound organelles named melanosomes and these are transferred via their dendrites to the neighbouring keratinocytes ³⁴, known to protect against UV ^{35, 36}. The ratio of melanocyte to keratinocytes is 1:10 in the basal layer of the epidermis and this balance is maintained through the human live but the exact mechanism is unknown ³⁷. Approximately 1200 melanocytes exist per mm² of the skin irrespective of the human race ³⁸. Melanocyte biology is influenced by paracrine factors from both keratinocytes as well as fibroblasts.

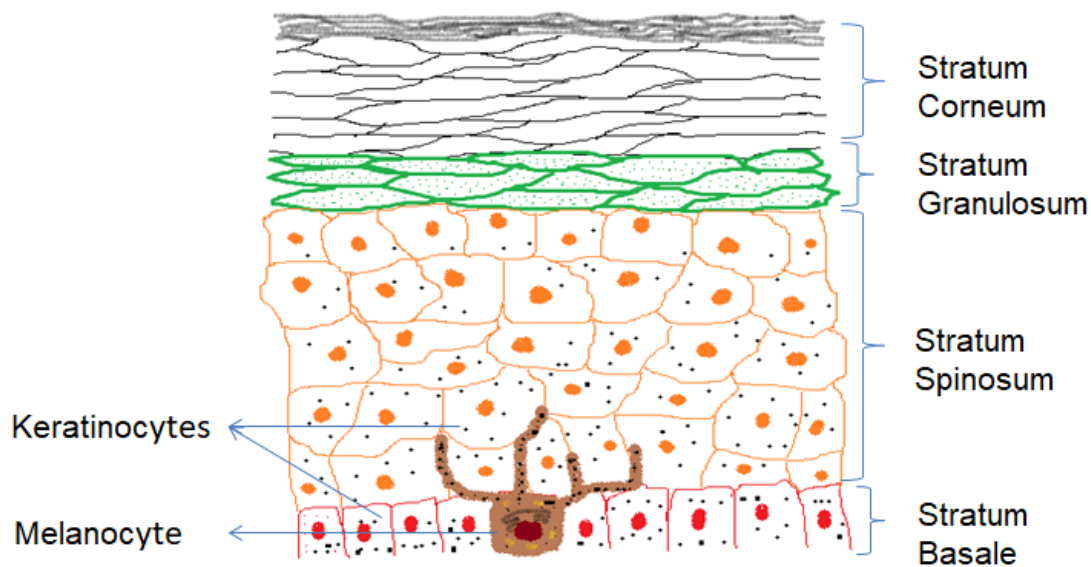


Figure 4. Skin epidermis. Schematic showing different layers of the epidermis of skin with keratinocytes and melanocyte.

Briefly, the synthesis of melanin is a complex biochemical process known as melanogenesis ³⁹. Two different types of melanin are produced by melanocytes: pheomelanin and eumelanin, which differ in their colour and the mode of synthesis.

Melanin production is known to be regulated by various factors, foremost by UV as well as many hormones and other extrinsic factors ⁴⁰.

1.4 Blue light and optical properties of skin

Blue light (400-500 nm) is a major portion of the visible light spectrum (Figure 1). It has relatively high energy due to its shorter wavelength range. The use of blue light has been a bit debatable, firstly, due to its proximity with UV radiation (UV-C: ~100-280 nm, UV-B: ~280-315 nm and UV-A: ~315-400 nm), which is known for its cytotoxic effects like DNA damage and mutagenesis ^{41, 42}. Secondly, due to low penetration depth through the tissue in comparison to red or NIR light. It has a penetration depth of ~1 mm into the skin ⁴³ (Figure 5).

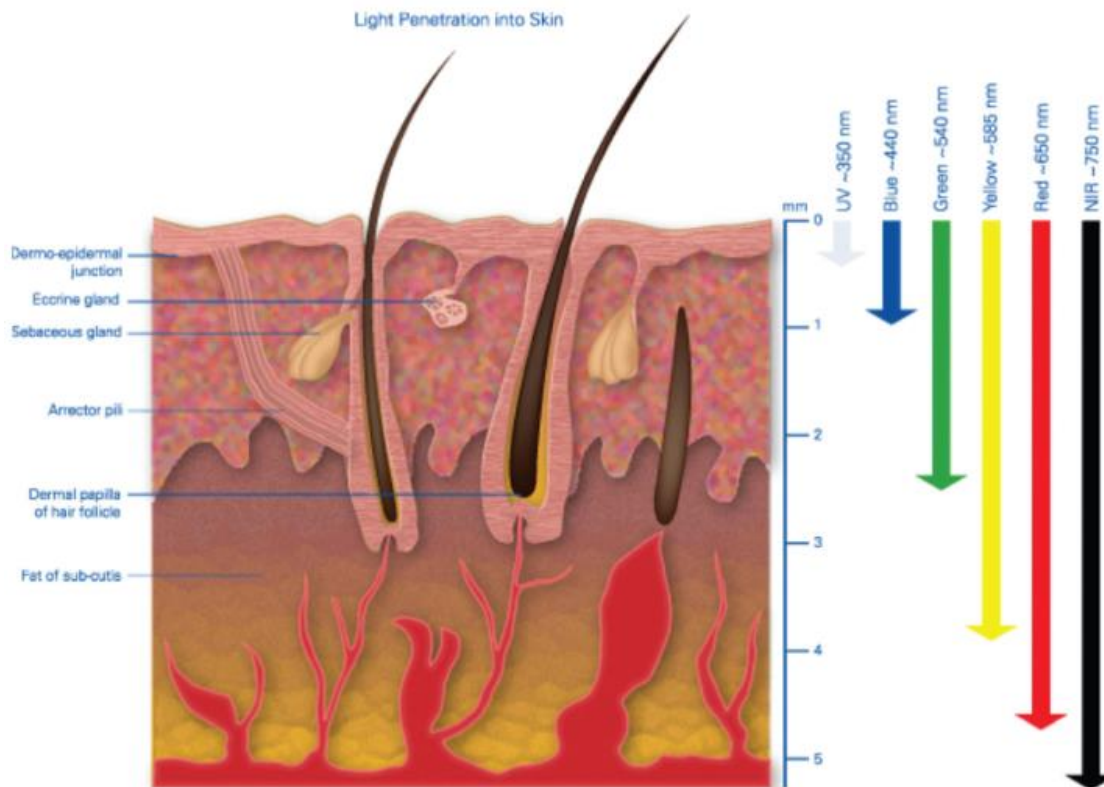


Figure 5. Light penetration depth into the skin. Penetration depth of different wavelengths of light into human skin ⁴³.

Skin is the primary target organ for exposure to natural or artificial light in comparison to the other organs of the human body. As the photons of light strike the skin surface, they are either reflected, scattered or absorbed. Molecules known as chromophores absorb these radiations, which results in a photochemical reactions and hence

activating the downstream processes⁴⁴. The identified photoreceptors (chromophores) include flavins, porphyrins, opsins and nitrosated proteins⁴⁵.

Blue light has been shown to have harmful effects like age-related macular degeneration or induction of cataract formation in the eye lens⁴⁶. Despite this, there is a major chunk of literature, which have reported beneficial effects of this wavelength of light. Some effects of blue light reported recently in literature have been summarized in Table 3.

Table 3. Summary of the literature with blue light effects.

Year	Author	Model system (cell/tissue/organ)	Parameters	Conclusion
2009	Kleinpenning, M. M. et al. ⁴⁷	Human skin	$\lambda=420$ nm Dose: 20 J/cm ² per day	Transient melanogenesis
2010	Kushibiki, T. et al. ⁴⁸	Prechondrogenic cells	$\lambda=405$ nm Irradiance: 100 mW/cm ² Time: 180 s	Increase in intracellular ROS
2012	Lavi, R. et al. ⁴⁹	Sperm membrane	$\lambda=400-505$ nm Dose: 20 J/cm ²	Increase in ROS production
2013	Kushibiki, T. et al. ⁵⁰	3T3-L1, ATDC5, C2C12, KUSA-A1, LLC, MIN6, NIH-3T3, HeLa, THP-1 & RBL-2H3	$\lambda=405$ nm Irradiance: 100 mW/cm ² Time: 60-120 s	Increase in intracellular ROS in all cell types
2013	Buravlev, E.A., et al. ⁵¹	Rat liver mitochondria	$\lambda=442$ nm Dose: 6 J/cm ²	Increase in mitochondrial respiration by 40%
2014	Duteil, L. et al. ⁵²	Human skin	$\lambda=415$ nm Dose: 87.5 J/cm ²	Hyperpigmentation

2015	AlGhamdi, K. M. et al. ⁵³	Human epidermal melanocytes	$\lambda=457$ nm Dose: 0.5-5.0 J/cm ²	Increase in cell viability at 0.5-2.0 J/cm ²)
2016	AlGhamdi, K. M. et al. ⁵⁴	Human epidermal melanocytes	$\lambda=457$ nm Dose: 2.0 J/cm ²	Increase in stage 1 melanosome
2017	D. Bennet, et al. ⁵⁵	Human epidermal keratinocytes, melanocytes, fibroblasts	$\lambda=460$ nm Dose: 0.2-300 mJ/cm ²	Effect of different color light on cellular functions. May contribute to premature aging.
2017	Yuan, Y., et al. ⁵⁶	Bone marrow-derived mesenchymal stem cells (BMSCs)	$\lambda=470$ nm Irradiance: 20 mW/cm ² Time: 60-3600 s	Inhibition of osteogenic differentiation, induction of apoptosis due to increase in ROS and DNA damage
2017	Nakashima, Y., et al. ⁵⁷	Mouse skin	$\lambda=460$ nm Irradiance: 133mW/cm ² Time: 5s Duty cycle: 50%	Induction of oxidative stress
2018	C. Regazzetti, et al. ⁵⁸	Human melanocytes	$\lambda=415$ nm and $\lambda=465$ nm Dose: 50-62.5 J/cm ²	Hyperpigmentation
2018	Mignon et al. ⁵⁹	Human reticular and dermal fibroblasts	$\lambda=450$ nm Dose: 30 J/cm ²	Reduction in cell metabolic activity by 50%

2. Aims of the study

The main objective of this dissertation was to investigate the impact of PBM using blue light on human skin melanocytes. The intensity and different doses were studied to optimize and create an effective irradiation cycle. Also, the induced biological effects were analyzed on the metabolic and gene expression level in detail, thereby determining possible side effects to keep them to a minimum.

The key cellular processes were studied to understand the impact of PBM using blue light on melanocytes: The following factors were analysed:

1. Assessing different irradiation time points and corresponding doses on melanocytes.
2. Changes in the pigmentation level induced by blue light dose.
3. Effects on the cellular apoptosis as a marker of cytotoxicity.
4. Evaluation of ATP level as a status of cellular metabolism.
5. Status of reactive oxygen species inside the cellular environment to bring further changes in the downstream signalling processes.
6. Lastly, with the help of gene expression profiling revealing the gene and pathway networks induced by the respective dose and wavelength used in this project to shed light on the possible application(s).

3. Material and methods

3.1 Material

3.1.1 Cell Line

The primary cells named Normal Human Epidermal Melanocyte (NHEM) were obtained cryopreserved at passage 2 from PromoCell GmbH, Heidelberg, Germany. NHEM were obtained from donors with lightly, moderately and darkly pigmented skin. These cells were isolated from juvenile foreskin and from different body parts, for example face, breast, abdomen and thighs, culturing the cells in serum-free and PMA-free Melanocyte Growth Medium M2.

NHEM have a star-like morphology with long elongated dendrites, more than one per cell (Figure 6).

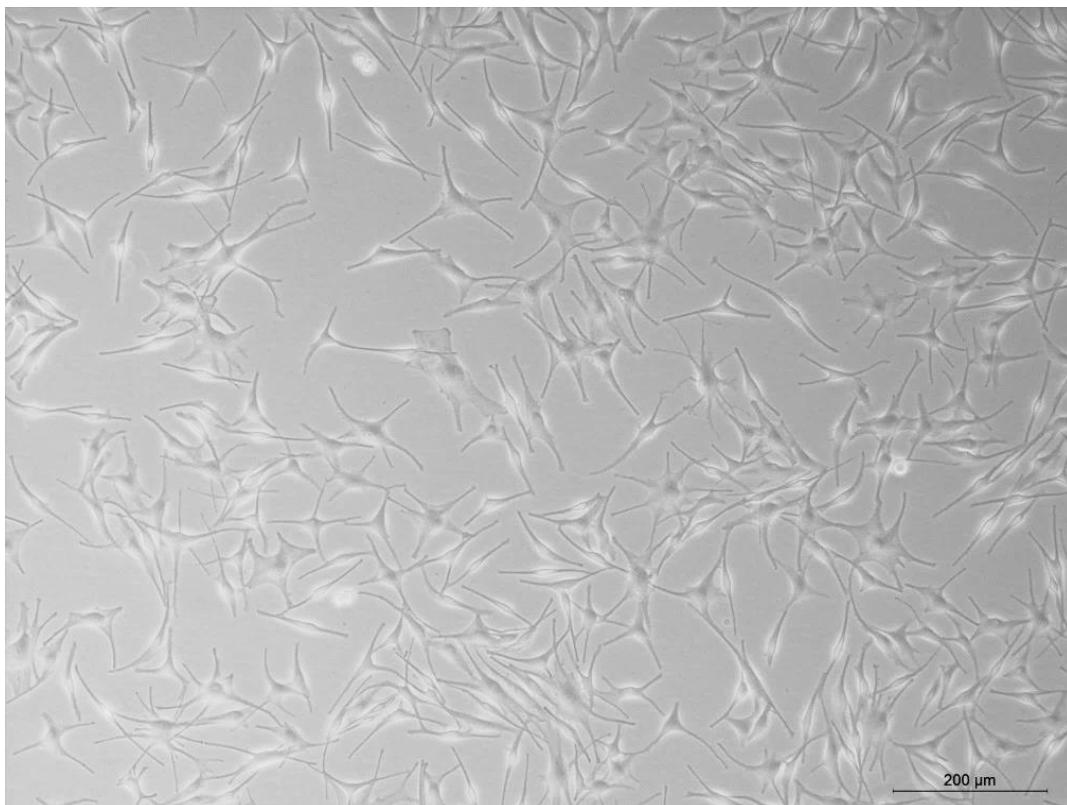


Figure 6. Normal human epidermal melanocytes (NHEM) morphology in passage 4. Image captured using a brightfield microscope with 10x magnification in phase contrast.

3.1.2 Light source

A BioLight LED lamp provided by Philips Research, Eindhoven, Netherlands was used to irradiate NHEM. The setup consisted of the lamp unit, current modulator, main power supplies and fan (Figure 7).



Figure 7. Bio-Light LED blue lamp set-up. (A) The experimental setup used for the blue light irradiation of NHEM *in vitro*. (B) LED apertures covered with lenses.

The light source comprised of two main power supplies, one delivered a direct current of 1A at 300V and another one powered the fan with a direct current of 0.1A and a fixed voltage of 24V in order to provide protection against overheating. The illumination field composed of LEDs (LUXEON Rebel LXML-PR01-0275 (blue) from Lumileds (Amsterdam, Netherlands) was covered by a set of lenses. The current modulator enabled pulsed driving of the LEDs. The radiation source provided a homogeneous blue light with a peak wavelength at 453 nm at a central irradiance of 12 mW/cm² at a distance of 50 mm. The maximum time-averaged emittance was 100 mW/cm² that corresponded to 15 W for the 10 cm X 15 cm emission aperture and the maximum peak emittance was equivalent to 350 mW/cm². According to the company's specification, the LED device delivered a fixed irradiance of 23 mW/cm² at the surface of the cell culture plates kept at a distance of 5 cm. The irradiation field was 150 cm² (Figure 8).

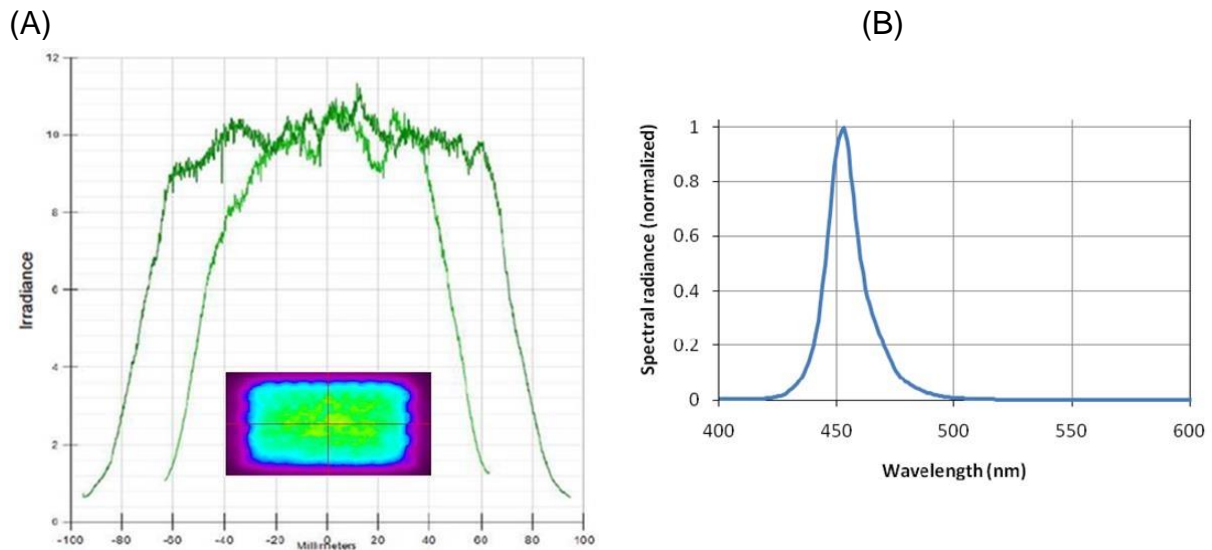


Figure 8. Bio-Light LED blue lamp specification. (A) homogeneous distribution of the light from casing at a distance of 50mm (B) emission spectrum at 12 mW/cm² irradiance with peak wavelength at 453 nm.

All the experiments were performed with continuous irradiation with a duty cycle of 100%. 96-well and 6-well plates were irradiated using this set-up.

Also, before each irradiation cycle for an experiment, the LEDs were pre-run to stabilize the output.

3.1.3 Redox sensor

For reactive oxygen species measurement, lentivirus particles with a redox sensor (Grx1-roGFP3) were utilized from our collaborator, Dr Prama Pallavi, Department of Vascular Surgery, Medical Faculty of Mannheim, Mannheim, Germany.

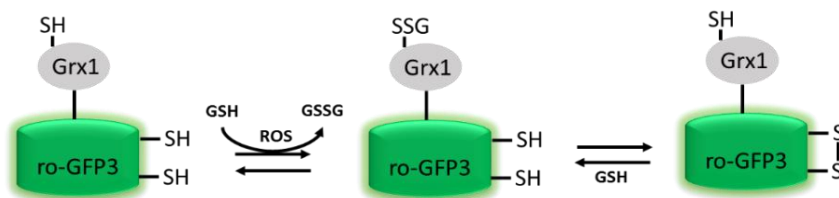


Figure 9. Redox sensor. Schematic illustration explaining the principle of the functioning of redox sensor (unpublished data, Courtesy: Dr. Prama Pallavi).

3.1.4 Reagents and kits

Product	Company
Colorimetric Cell Viability Kit III (XTT)	Promokine™ by PromoCell GmbH, Heidelberg, Germany
CellTiter-Glo® Luminescent Cell Viability Assay	Promega Corporation, Madison, WI, USA
FITC Annexin V Apoptosis Detection Kit with PI	BioLegend, San Diego, CA
Cell Staining Buffer	BioLegend, San Diego, CA
Purified Annexin V	BioLegend, San Diego, CA
Staurosporine (<i>Streptomyces staurosporeus</i>)	Sigma Aldrich, St. Louis, MO, USA
RNeasy mini kit	Qiagen, Hilden, Germany
RNase-Free DNase set	Qiagen, Hilden, Germany
Sodium hydroxide	Sigma Aldrich, St. Louis, MO, USA
Ethanol, ROTIPURAN®, > 99.8%, p.a.	Carl Roth GmbH & Co. KG, Karlsruhe, Germany
2-Mercaptoethanol	Sigma Aldrich, St. Louis, MO, USA
2-Propanol, ROTIPURAN®, > 99.8%, p.a.	Carl Roth GmbH & Co. KG, Karlsruhe, Germany

3.1.5 Cell culture reagents

Product	Company
Melanocyte Growth Medium M2	PromoCell GmbH, Heidelberg, Germany
SupplementMix, Melanocyte Growth Medium M2	PromoCell GmbH, Heidelberg, Germany
Phosphate buffer saline	Gibco™ by Thermo Fisher Scientific, Waltham, MA, USA
Cryo-SFM	PromoCell GmbH, Heidelberg, Germany
Trypan Blue stain (0.4%)	Gibco™ by Thermo Fisher Scientific, Waltham, MA, USA
0.25% Trypsin-EDTA (1x)	Gibco™ by Thermo Fisher Scientific, Waltham, MA, USA
Phosphate Buffer Saline	Sigma Aldrich, St. Louis, MO, USA
Melanin Synthetic	Sigma Aldrich, St. Louis, MO, USA

3.1.6 Devices

Product Description	Company
BioLight LED Lamp with Lumileds LUXEON Rebel LXML-PR01-0275	Philips Electronics Nederland B.V. Philips Research, Eindhoven, Netherlands Koninklijke Philips N.V., Eindhoven, Netherlands
Microplate reader, Spark® 10M	Tecan Austria GmbH, Grödig, Austria
Leica DM IRB, IRBE	Leica Mikroskopie & Systeme GmbH, Wetzlar, Germany
Flow cytometer, BD FACSCanto™ II	BD Biosciences, San Jose, CA, USA
NanoQuant plate™	Tecan Austria GmbH, Grödig, Austria
Agilent 2100 Bioanalyzer	Agilent Technologies, Santa Clara, CA, USA

3.1.7 Softwares

Analysis Software	Source
SparkControl, version 1.2	Tecan Austria GmbH, Grödig, Austria
JMP® Genomics, version 7.1	SAS Institute Inc., Cary, NC, USA
BD FACSDiva, version V8.0.1	BD Biosciences, San Jose, CA, USA
Fiji, Image processing package of ImageJ	Free software for image analysis
ZEN 2 pro	Carl Zeiss AG, Oberkochen, Germany

3.2 Methods

3.2.1 Cell culture

The human primary melanocytes, NHEM-lightly, moderately and darkly pigmented (Promocell GmbH) were cultured in Melanocyte growth medium M2 with an addition of Melanocytes supplement mix M2.

All the cells were maintained under the standard condition in a humidified incubator at 37°C in 5% CO₂. Cells were thawed rapidly in a 37°C water bath, then suspended in pre-warmed medium and seeded in a T-75 flask. At a confluence of 70%-90% the cells were sub-cultured after washing twice with PBS and 0.05% trypsin EDTA (in PBS) was used to detach the cells and neutralized using 10% FBS in Melanocyte growth medium M2. The cell suspension was centrifuged at 220Xg for 3 minutes. The supernatant was removed and cells were suspended in fresh medium and after counting the cells, they were seeded in the respective flask.

For the preparation of freeze-downs, the cells were detached in the same way as explained above and cell number- 1×10^6 cells per cryovial were used. Cell suspension in the fresh medium was centrifuged and the cell pellet was suspended in freezing medium known as Cryo-SFM. Aliquots of this cell suspension were prepared in cryovials, placed in isopropanol chamber and stored at -80°C overnight. The frozen cells were transferred the next day to liquid nitrogen.

For the study, cells from three skin phototypes were seeded in 96-well black plate with a clear bottom in triplicates. Black well plates were incorporated into the study to avoid the cross-link of light between the wells.

The cells were seeded in a concentration of 6000/well and 5500/well for 24 hours and 48 hours of harvesting time post-irradiation, respectively and in triplicates with three repetitions performed in all the experiments.

3.2.2 Light treatment

24 hours after seeding, the medium was renewed and plates were incubated for 30 minutes before irradiation for the cells to be stabilized to the new supply of nutrients in fresh medium. A special plate lid (Figure 10) was used during the light treatment which was divided into two halves using an aluminium sheet to cover one half to have the untreated control and treated part in the same plate to avoid a plate effect.

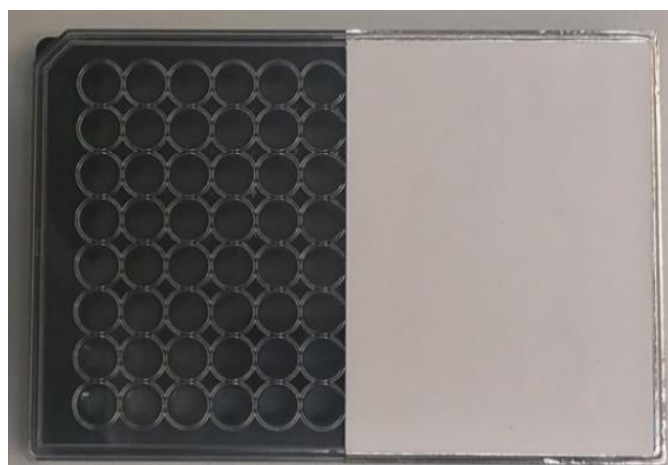


Figure 10. Special lid for irradiation. Plate lid used for 96-Well plate while irradiation.

Different irradiation doses of blue light were studied on melanocytes outside the incubator and at room temperature. The plates were maintained at a distance of 5cm under the LED casing. The lamp operated at a steady level of 23 mW/cm² of irradiance at the surface of plates used. Taking into consideration the power loss due to light absorption by the black well plate, the lid and medium correspond to approximately 50%, this reduced the irradiance level to 12 mW/cm² ⁶⁰.

Accordingly, the respective doses of blue light for the irradiation time have been listed in Table 4. As the irradiance of the lamp was fixed, the dose amount was modulated with the change in the time duration of irradiation.

Table 4: Different irradiation times (min) with respective doses (J/cm²). The list of irradiation time-points and corresponding doses used for the initial testing on NHEM.

Time (min)	Dose (J/cm ²)
0	0
2.5	1.8
5	3.6
7.5	5.4
10	7.2
15	10.8
20	14.4
30	21.6
60	43.2
90	64.8

3.2.3 Cell metabolism assay

The metabolic activity of the cells post-irradiation was measured using the colorimetric Cell Viability Kit III (XTT) from PromoKine (PromoCell GmbH). The kit consists of the XTT reagent and activation reagent-PMS (N-methyl dibenzopyrazine methyl sulfate). This assay measures an integrated set of enzyme activities that are related in various ways to cell metabolism. NADH is utilized as a cofactor by metabolically active cells

and contributes to the reduction of the tetrazolium salt XTT in the presence of PMS to the orange colored formazan compound.

This dye is water-soluble and the intensity of this dye is proportional to the amount of metabolically active or viable cells. After the respective treatment and depending on the harvesting time point, a reaction solution of XTT and the activation reagent (1:200) was added to the medium in cell culture plates and incubated for 1 hour at 37°C at 5% CO₂.

The same reaction mixture was also added to the row with the only medium which serves as chemical blank in the same plate. The absorbance intensities were measured using Spark[®] 10M microplate reader (Tecan Austria GmbH) at 450nm with a reference wavelength of 690nm.

3.2.4 Melanin content quantification assay

To quantify the melanin content after blue light treatment, 6-well plates were used as a higher number of cells is required for this assay. Melanin assay was performed using the standard protocol (Gruber and Holtz, 2013) with minor modifications. First, cells were trypsinized and counted. Then, cells (500,000) were collected in fresh tubes and centrifuged at 1000 rcf for 5 min. Next, media was removed from the tubes and cells were lysed with 1N NaOH at 80°C for 2 hours. After the incubation period, the lysate was centrifuged at 12,000 rcf for 10 min. The supernatant was collected and transferred to fresh 96-well transparent, clear bottom plates in duplicates. Absorbance values were measured at 405nm. Melanin content was determined using the standard curve obtained from synthetic melanin (Figure 11).

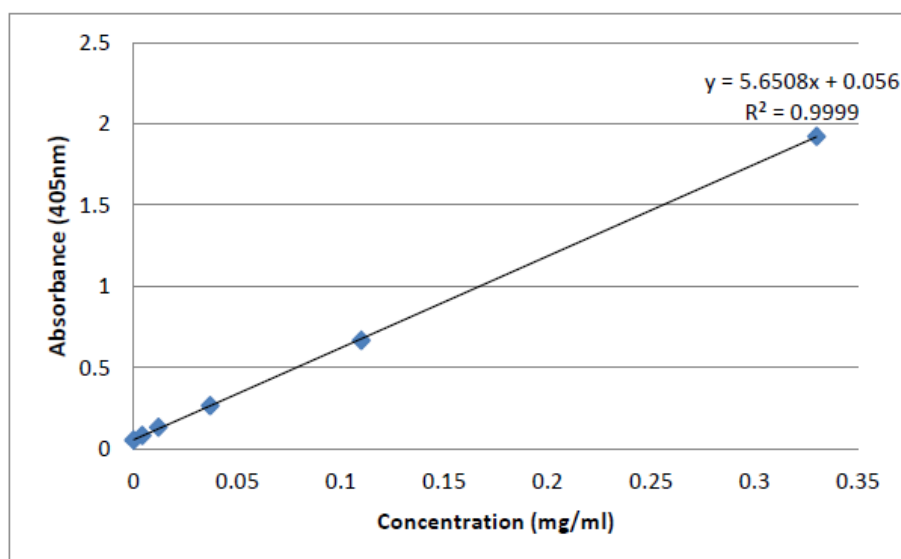


Figure 11. Standard curve obtained from synthetic melanin. Standard curve was obtained with a standard series of 0.0041 mg/ml-0.33 mg/ml.

A standard stock solution (1 mg/ml) was prepared by dissolving synthetic melanin with 1N NaOH. A melanin standard curve was developed from the standard stock solution of 1 mg/ml ranging from 0.0041 mg/ml-0.33 mg/ml.

3.2.5 Cell apoptosis-FACS analysis

To assess whether blue light induces cell apoptosis, Fluorescence-activated cell sorting (FACS) technique was incorporated for the study. Wherein cells post-irradiation were detached using trypsin and stained using the FITC Annexin V Apoptosis Detection Kit with PI. Staurosporine (1 μ m) was used to induce apoptosis in the cells. This approach was used for a positive control. Cells were incubated in Staurosporine for 4 hours at 37°C at 5% CO₂. Blocking control was prepared by staining with Annexin V pure (5 μ l) and further stained as described below.

To evaluate the level of apoptosis after blue light, the treated and untreated cells were firstly trypsinized and washed twice with cell staining buffer. After washing, the cells were resuspended in Annexin V binding buffer (1ml). Then, they were stained with 1 μ l of FITC (1:10) and followed by 2.5 μ l of PI (staining details in Table 5). The cells were vortexed and incubated for 15 minutes in dark at room temperature. After incubation, 100 μ l of stained cell suspension was added to 5 ml FACS tubes and 400 μ l of Annexin V binding buffer was added. The analysis was done using pre-adjusted BD

FACSCanto™ II, where 10,000 events were recorded per sample and data analysis was performed using BD FACS Diva software.

Table 5: FACS staining details for different controls and samples. Summary of tubes stained with necessary controls and treated and non-treated samples.

Tube type	Cell type	Annexin V pure	FITC Annexin V	PI
Unstained	NHEM	-	-	-
Blocking control	NHEM	+	+	+
Stained treated	NHEM+light treatment	-	+	+
Stained untreated	NHEM+no light treatment	-	+	+
Positive control-apoptosis	NHEM+staurosporine	-	+	-
Positive control-necrosis	NHEM (After staining incubated in sonicator for 1-2 min.)	-	-	+

3.2.6 ATP measurement assay

ATP quantitation, an indicator of metabolically active cells was performed using the CellTiter-Glo® Luminescent Cell Viability Kit (Promega Corporation).

CellTiter-Glo® substrate and CellTiter-Glo® buffer are mixed to form the CellTiter-Glo® reagent, this reagent is added to cell culture plates after irradiation. Afterwards, the shaking was performed for 2 minutes followed by incubation at RT for 10 minutes. Then, the contents of each well was mixed by pipetting up and down and transferred to the 96-well white, opaque-walled, clear bottom plate. Luminescence was recorded using the Spark® 10M microplate reader with an integration time of 500 ms. The luminescent signal is supposed to be directly proportional to the ATP amount present in cells, representing the count of viable and thus metabolically active cells. Upon mono-oxygenation of luciferin, light and oxyluciferin are formed, which is catalyzed by Ultra-Glo™ Recombinant Luciferase in the presence of ATP, Mg²⁺ and molecular oxygen.

3.2.7 Reactive Oxygen Species measurement

The generation of ROS was measured by incorporating a redox sensor. The redox sensor is a fusion of GRX1-roGFP3 tag.

The lentivirus particles with the sensor were transduced into the cells on day 1 in T-25 flask (approximately 60% confluency). Next day the medium was changed and once the confluence of 80-90%, was achieved the cells were trypsinized and seeded in a bigger flask for obtaining cells in a larger amount for the experiment. At a confluence of 80%-90% the cells were seeded in 96-black well plates and after 24 hours of seeding the cells were irradiated after a medium change.

The fluorescence signal was measured at different harvesting time points: 0, 0.5, 1, 2, 3, 4, 5, 6, 24, 48 hours. Two excitation wavelengths were 395 nm and 485 nm and the emission wavelength was 510 nm.

3.2.8 Gene expression analysis

3.2.8.1 RNA Isolation

48 hours after irradiation cells were harvested and RNA was isolated from melanocytes using RNeasy mini kit (Qiagen).

The protocol from the manufacturer was followed. The medium was removed from the cell culture plates and washed twice with PBS. Then, a working solution of Buffer RLT with β -ME (10 μ l β -ME per 1 ml Buffer RLT) was added to the wells to lyse the cells. The lysate was disrupted and homogenized using a tip. The content was transferred to 2 ml tubes and 1 volume of 70% ethanol was added to the lysate. Then it was mixed by pipetting and 700 μ l of the sample was transferred to an RNeasy spin column placed in a 2 ml collection tube. The tubes were centrifuged for 15 s at $\geq 8000 \times g$ ($\geq 10,000$ rpm) and the flow-through was discarded. Now, 350 μ l of Buffer RW1 was added to the RNeasy spin column and tubes were centrifuged for 15 s at $\geq 8000 \times g$ ($\geq 10,000$ rpm) to wash the spin column membrane. The flow-through was discarded. On-column DNase digestion was performed to eliminate the genomic DNA contamination by adding a mix of 10 μ l of DNase I stock solution (10 μ l of aliquots prepared by dissolving the lyophilized DNase I in 550 μ l of the RNase-free water) with 70 μ l Buffer RDD onto the RNeasy spin column and incubated for 15 minutes at room temperature. Afterwards, again 350 μ l of Buffer RW1 was added to the RNeasy spin column and tubes were centrifuged for 15 s at $\geq 8000 \times g$ ($\geq 10,000$ rpm) to wash the spin column membrane. The flow-through was discarded. Further washing of the membrane was

done using 500 µl Buffer RPE and again the tubes were centrifuged for 15 s at $\geq 8000 \times g$ ($\geq 10,000$ rpm). A second washing step included the addition of 500 µl Buffer RPE and the tubes were centrifuged for 2 minutes at $\geq 8000 \times g$ ($\geq 10,000$ rpm) to ensure the spin column membrane dries well and that no ethanol is carried over during RNA elution. As residual ethanol may interfere with downstream reactions. To eliminate any possible carryover of Buffer RPE, or if residual flow-through remains on the outside of the RNeasy spin column after the last step, the RNeasy spin column was placed in a new 2 ml collection tube and centrifuged at full speed for 1 min. Now, the RNeasy spin column was placed in a new 1.5 ml collection tube. 30 µl of RNase-free water was added directly to the spin column membrane and centrifuged for 1 min at $\geq 8000 \times g$ ($\geq 10,000$ rpm) to elute the RNA. The RNA samples were transferred on ice (4°C) and took for nanodrop quantification.

3.2.8.2 RNA quantification and quality control

The extracted RNA samples were quantified by nucleic acid quantification analysis using the Spark® 10M microplate reader. In addition to the concentration, RNA purity was determined by measuring the absorbance ratio at A260/280 with acceptable values of 1.7 – 2.1.

Furthermore, the RNA integrity was assessed by capillary electrophoresis on an Agilent 2100 Bioanalyzer (Agilent Technologies) providing the read-outs as the RNA Integrity Number (RIN), with $RIN \geq 7.0$ indicating sufficient RNA quality.

3.2.8.3 RNA sequencing

RNA samples were sent for RNA sequencing to BGI, Tech Solution, Co. Limited, Hongkong with sample requirements including the concentration of 10-1000 ng/µl, $RIN \geq 7.0$, $28s/18s \geq 1.0$, also baseline is smooth; 5s is normal and there is no DNA or protein contamination in the sample. As a first step, the samples went through the company's quality control check wherein all the samples were qualified and following this procedure, the RNA samples proceeded for RNA sequencing.

3.2.8.4 RNA sequence analysis

RNA sequencing data was analyzed using R and Bioconductor using NGS analysis package systempipeR⁶¹. Quality control of raw sequencing was done using FastQC (Babraham Bioinformatics). Low-quality reads were removed using trim-galore, version 0.6.4. The resulting reads were aligned to human genome version GRCh38.p13 from Genecode and counted using Kallisto version 0.46.1⁶². The counted data were transformed to log₂-counts per million (log CPM) using the voom-function from the limma package in R. A false positive rate of $\alpha = 0.05$ with FDR (adjusted p-value) correction was considered as the level of significance.

Volcano plots and heatmaps were created using ggplot2 package, version 2.2.1 and the complex Heatmap, version 2.0.0⁶³. The pathway analysis was made with fgsea package⁶⁴ and the enrichment browser package⁶⁵ in R using the pathway information from the public database KEGG (<https://www.genome.jp/kegg/pathway.html>).

For Gene expression analysis, Fisher's exact test was also applied.

miRWalk (<http://mirwalk.umm.uni-heidelberg.de/>) database was used for searching the possible target genes for the significant miRNAs in RNA sequence data. The search strategy is outlined in the Fig 12 and followed from Dweep, H. et al.⁶⁶ with minor changes.

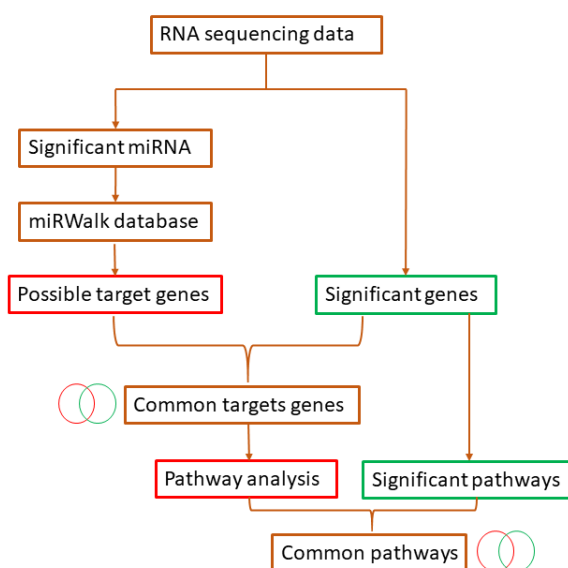


Figure 12. Outline of the search strategy. Search strategy applied for predicting the possible target genes and the respective pathways of the significant miRNA and parallel analysis with the RNA seq. data set.

STRING (<https://string-db.org/>), a biological database was used for understanding protein-protein interaction. This database provided information about the known and predicted protein-protein interactions from the published data on the web. The information is obtained from the experimental data, computational prediction methods and public text collections.

3.2.9 Statistical analysis

All the numerical data were represented as means \pm standard deviation (SD).

The fold changes were obtained by normalizing the data to time-matched, non-irradiated controls. Complete statistical analyses were performed using JMP® Genomics, version 7.1. One-way ANOVA and a Student's t-test for each pairwise comparisons were performed. For all statistical tests, differences were considered statistically significant at a false positive rate of $\alpha = 0.05$. The number of repetitions and replicates performed for each test method is indicated as N (repetitions, replicates).

4. Results

4.1 Assessment of effects of different blue light irradiation time points with corresponding doses

NHEM cells were treated for different irradiation times with corresponding doses of blue light and the effect of blue light treatment was assessed using Colorimetric Cell Viability Kit III (XTT) from PromoKine (PromoCell GmbH) as a preliminary test.

Initially, the dose-effect was studied at the harvesting time 24 hours post-irradiation. Short-term irradiation time points of 2.5 min (1.8 J/cm^2), 5 min (3.6 J/cm^2), 7.5 (5.4 J/cm^2), 10 min (7.2 J/cm^2) led to an increase in in the absorbance values with a significant difference ($p < 0.0001$) between the treated and non-irradiated control (Figure 13).

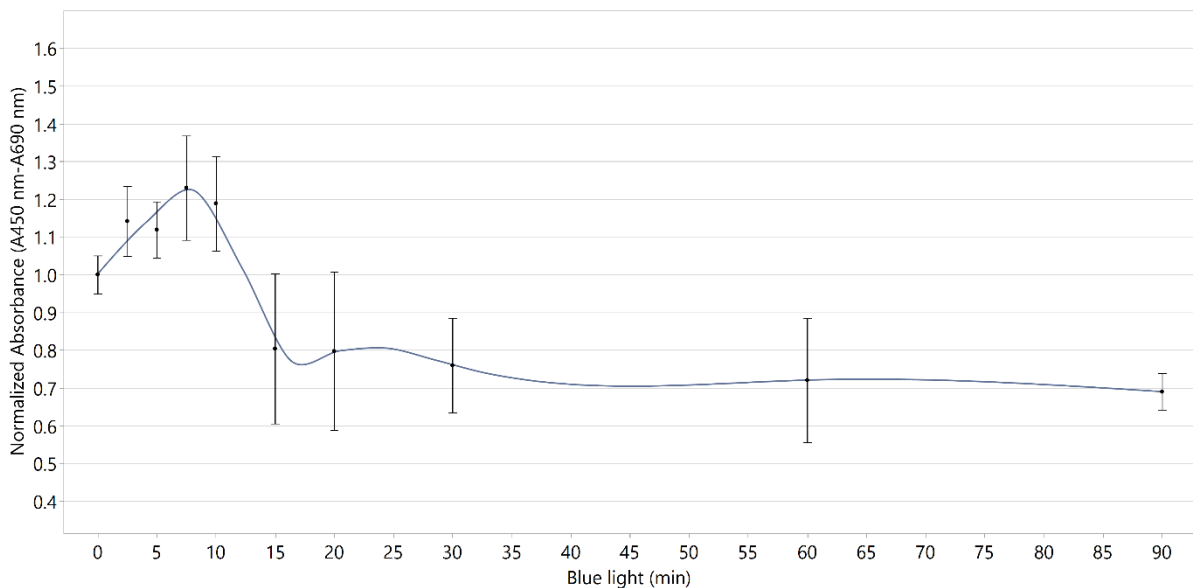


Figure 13. Colorimetric cell viability (XTT) assay. NHEM treated with blue light at different irradiation time points (2.5, 5, 7.5, 10, 15, 20, 30, 60, and 90 min) with respective doses after 24 hours of harvesting after irradiation. Data are presented as mean \pm standard deviation. (N=3 repetitions, 3 replicates). Corresponding statistics summarized in Appendix 1.

On the other hand, an exposure of 15 min (10.8 J/cm^2) resulted in a sharp decrease in the signal ($p < 0.0001$) as compared to the non-treated control. Additionally, treatment with long-term irradiation of 30 min (21.6 J/cm^2) led to further inhibition in the signal and the effect remained almost constant after 60 min (43.2 J/cm^2), and 90 min (64.8 J/cm^2) of blue light irradiation.

As a result, a biphasic dose-response curve was obtained (represented by the smooth curve) after application of different blue light doses after 24 hours of harvesting time (Figure 13).

Furthermore, irradiation times 7.5, 30 and 90 min were chosen and tested for 48 hours of harvesting time after irradiation. As these time-points represented the stimulatory (7.5 min) and inhibitory (30 min, 90 min) effects (Figure 14).

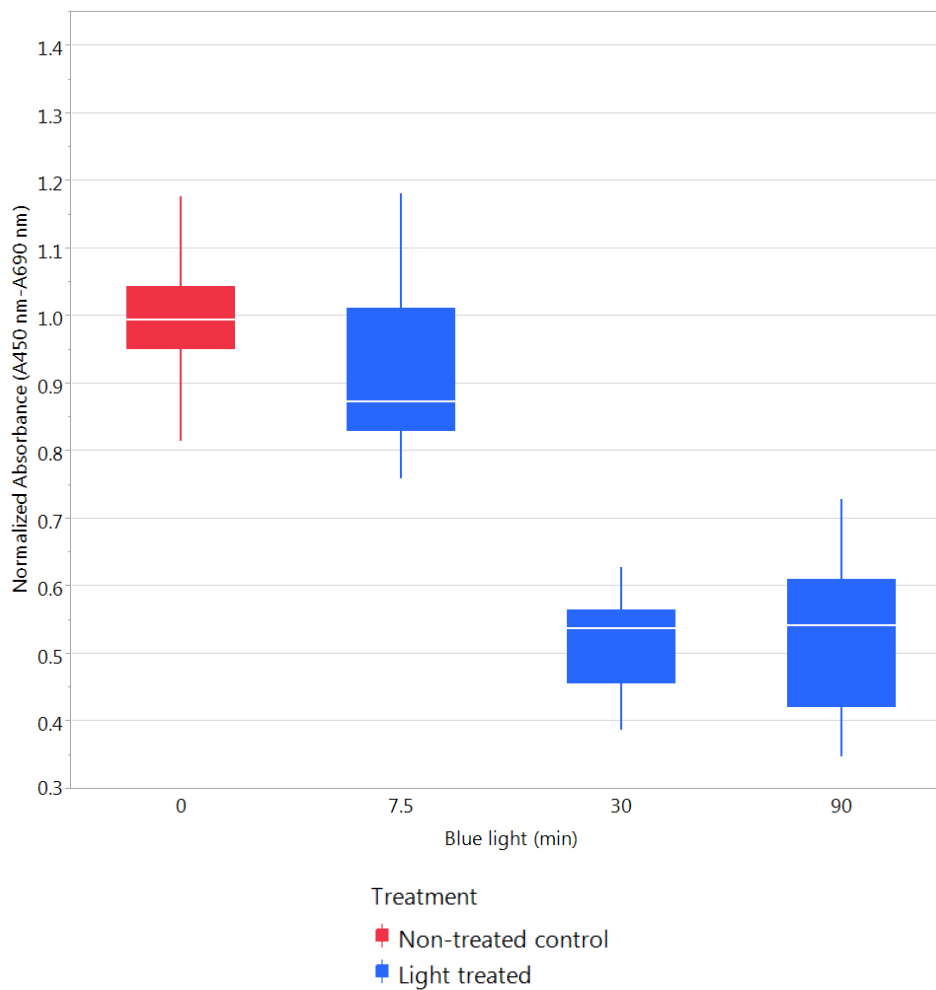


Figure 14. Colorimetric cell viability (XTT) assay. NHEM treated with blue light at different irradiation time points (7.5, 30 and 90 min) with respective doses after 48 hours of harvesting after irradiation. Data are presented as box plots (non-treated control: red, treated: blue) with median, upper and lower quartile (interquartile range (IQR) and whiskers (1.5x IQR) (N=3 repetitions, 3 replicates).

It was observed that after 48 hours after blue light treatment, the signal was suppressed ($p < 0.0001$) for all the doses as compared to the non-irradiated control (Figure 14).

Moreover, 90 min (64.8 J/cm^2) was examined 48 hours of harvesting time for the three-skin phototypes (lightly pigmented, moderately pigmented and darkly pigmented) as simultaneous experiments for melanin assay showed an increase in melanin content using this dose (Figure 5). XTT assay showed a significant ($p < 0.0001$) decrease in absorbance values between treated and respective non-treated control for all the three different pigmented NHEM (Figure 15).

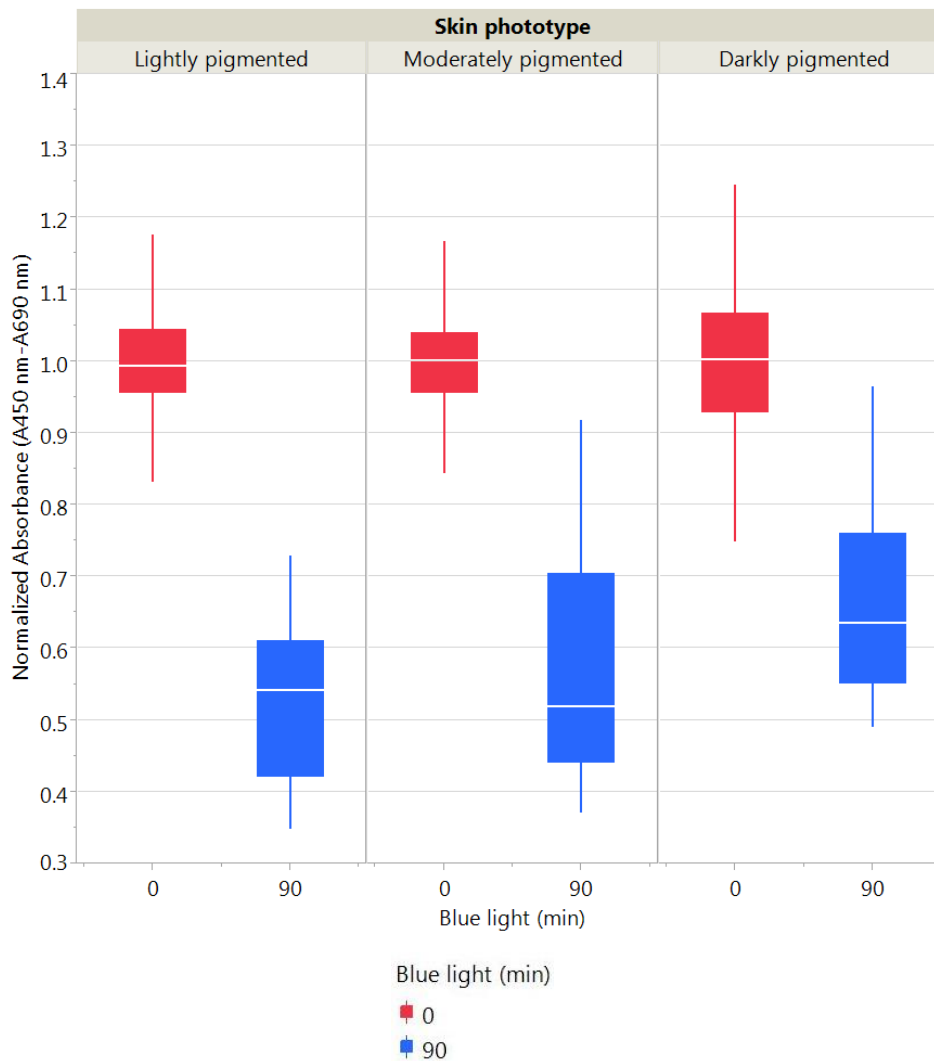


Figure 15. Colorimetric cell viability (XTT) assay. NHEM from three skin phototypes (lightly pigmented, moderately pigmented and darkly pigmented) exposed to 90 min blue light with 48 hours of harvesting time. Data are presented as box plots (non-treated control: red, treated: blue) with median, upper and lower quartile (interquartile range (IQR) and whiskers (1.5x IQR). (N=3 repetitions, 3 replicates).

4.2 Influence of blue light on melanin content

Melanin production is considered as the main function of melanocytes. Hence, to study the effect of blue light on the amount of melanin in NHEM, irradiation time point 7.5 min, 30 min and 90 min were used to assess the change in melanin content from all three different skin phototypes NHEM.

Amongst the different doses evaluated for melanin estimation, there was no significant change observed in the melanin amount for 7.5 min, 30 min and 90 min for the harvesting time of 24 hours, although there was a slight increase in the signal (Figure 16).

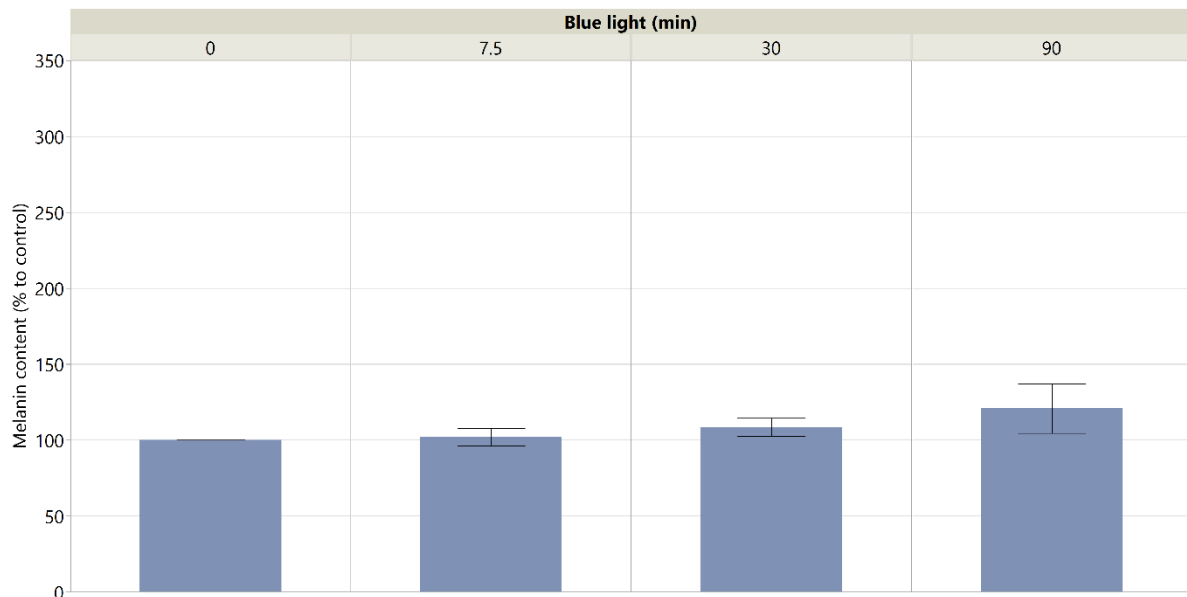


Figure 16. Melanin content estimation assay. Melanin content quantified from NHEM after an irradiation with 7.5 min, 30 min and 90 min of blue light with 24 hours of harvesting time. Bars represent mean \pm standard deviation. (N=3 repetitions, 3 replicates).

90 min (64.8 J/cm²) of irradiation led to an increase in melanin content after 48 hours (Figure 17). Although no significant change in the melanin amount was observed for 7.5 min and 30 min post 48 hours of harvesting time post-irradiation (Figure 17).

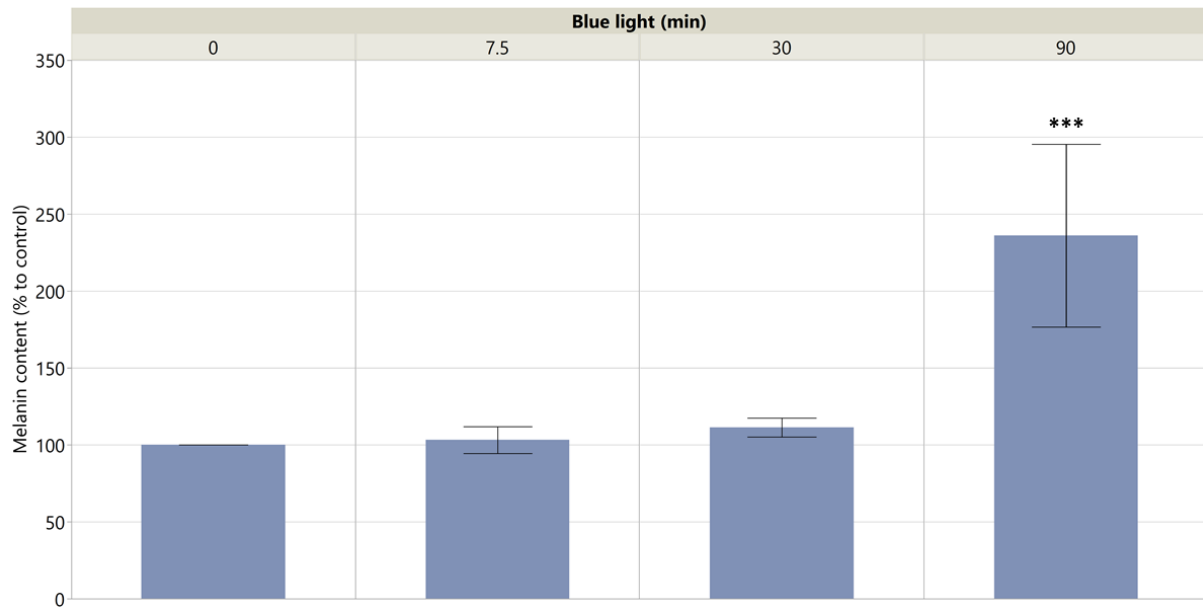


Figure 17. Melanin content estimation assay. Melanin content quantified from NHEM after an irradiation with 7.5 min, 30 min and 90 min of blue light with 48 hours of harvesting time. Bars represent mean \pm standard deviation. (N=3 repetitions, 3 replicates). Values significantly different (non treated control vs light treated (90 min)) are indicated as *** $p < 0.0001$.

Hence, this dose (90 min, 64.8 J/cm²) was used to estimate the change in melanin for all the three skin phototype NHEM. Melanin content was quantified using a standard curve obtained from synthetic melanin. Lightly pigmented ($p < 0.0001$), moderately pigmented ($p < 0.0001$) and darkly pigmented ($p < 0.0001$) showed a significant increase in melanin amount as compared to non-treated control 48 hours after blue light irradiation (Figure 18).

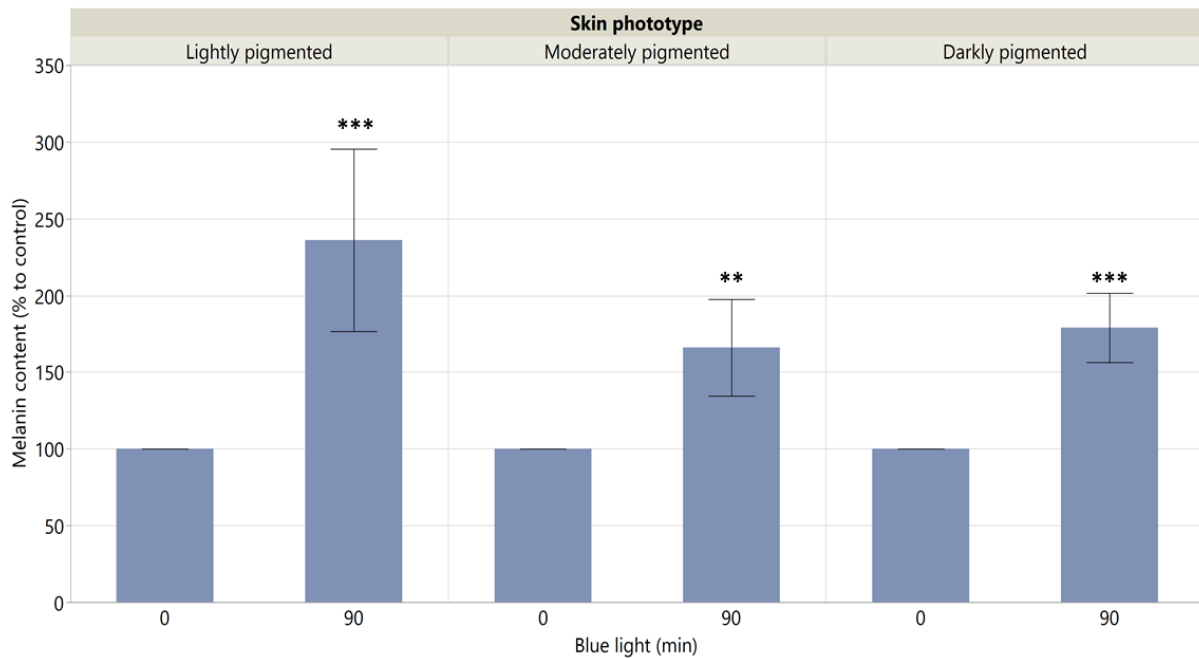


Figure 18. Melanin content estimation assay. Melanin content quantified from the three skin phototypes NHEM after an irradiation with 90 min of blue light with 48 hours of harvesting time. Bars represent mean \pm standard deviation. (N=3 repetitions, 3 replicates). Values significantly different (non treated control vs light treated (90 min)) are indicated as ** $p < 0.001$ and *** $p < 0.0001$.

As well as the similar dose (90 min, 64.8 J/cm²) was chosen to study various other cellular functions known to be affected by light, on these three skin phototype melanocytes.

4.3 Effect of blue light treatment on cell apoptosis

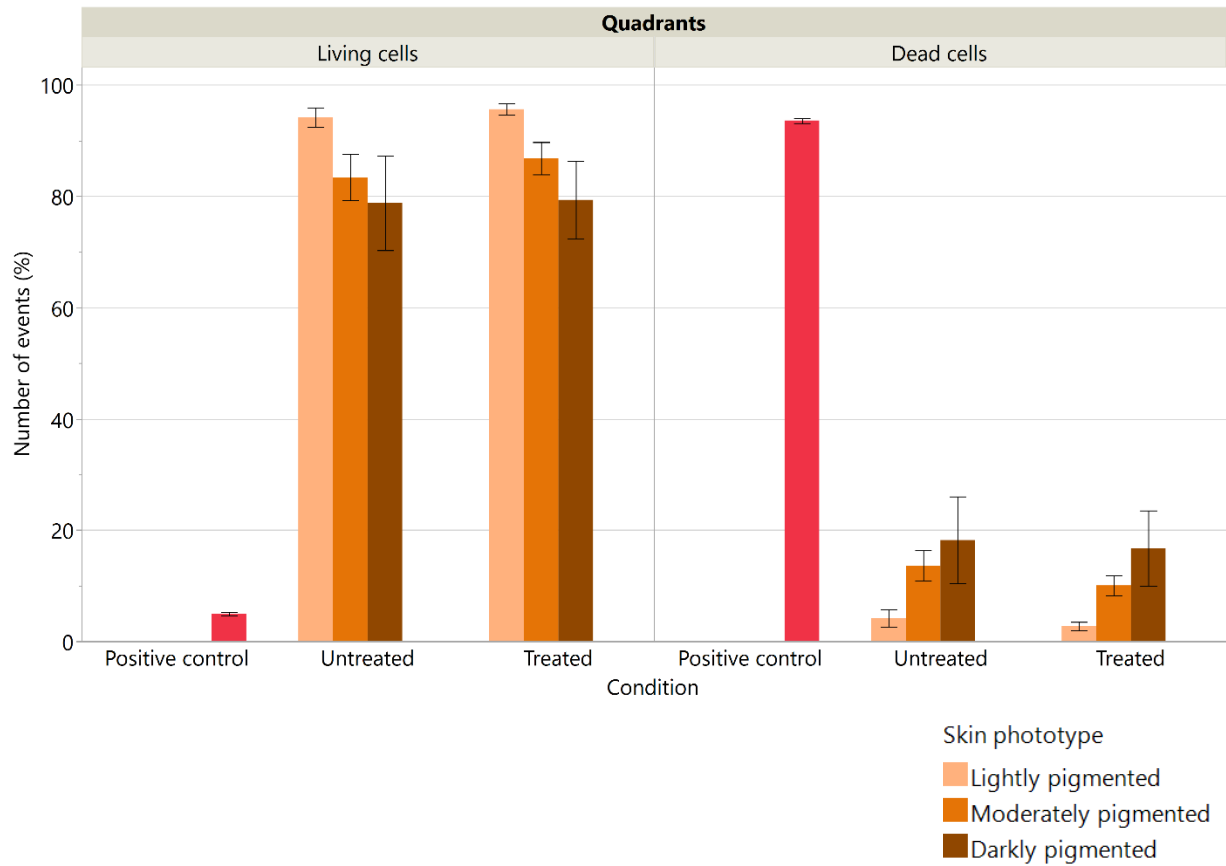
To evaluate the effect of blue light on cell apoptosis after irradiation with 90 min both at 24h and at 48h of harvesting time after-irradiation, fluorescent activated cell sorting (FACS) was performed using FITC-Annexin V and PI staining.

For positive control, 1 μ M of staurosporine (*Streptomyces staurospores*) was utilized to induce cytotoxic effects in the NHEM cell. The cells were treated with staurosporine, a non-selective protein kinase inhibitor, at 37°C and 5% CO₂.

After 4h the cells had circularized, a mark of cell detachment from the surface, cell morphology was documented by acquiring phase-contrast images using a light microscope (Data shown in Appendix 2). Cell treated with 1 μ M of staurosporine had approximately 95% dead cells and less than 5% living cells.

No significant impact on the cell apoptosis was observed between the untreated control and treated samples after 24 hours and 48 hours of harvesting time (Figure 19). All the three skin phototype NHEM had approximately 85%-95% living cells and the percentage of dead cells was around 5%-15%.

(A)



(B)

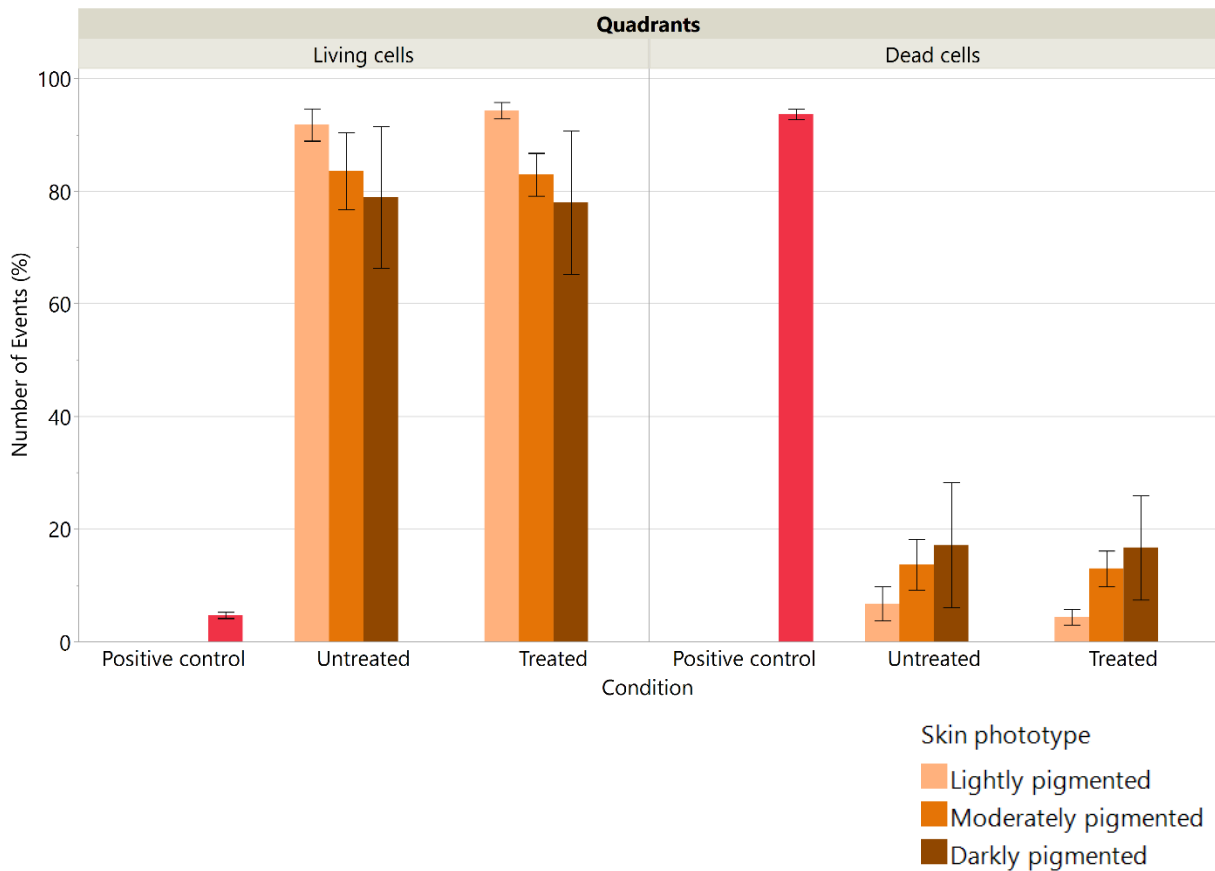


Figure 19. Cell apoptosis using FACS. Number of events for living and dead NHEM cells from the three skin phototypes was detected after an irradiation with 90 min of blue light with (A) 24 hours and (B) 48 hours of harvesting time. Bars represent mean \pm standard deviation. (N=3 repetitions, 3 replicates).

4.4 Blue light irradiation influences the energy metabolism level in NHEM

The ATP level inside the cell is the indicator of energy metabolism, which represents viable and metabolically active cells. Hence, a luminescence-based assay (CellTiter-GLO®) was applied to understand the cellular metabolic status.

The concentrations of ATP following the treatment with a dose of 90 min of blue light resulted in an increase (** $p < 0.001$, *** $p < 0.0001$) after both 24h and 48h of harvesting time points for all the three skin phototypes (Figure 20).

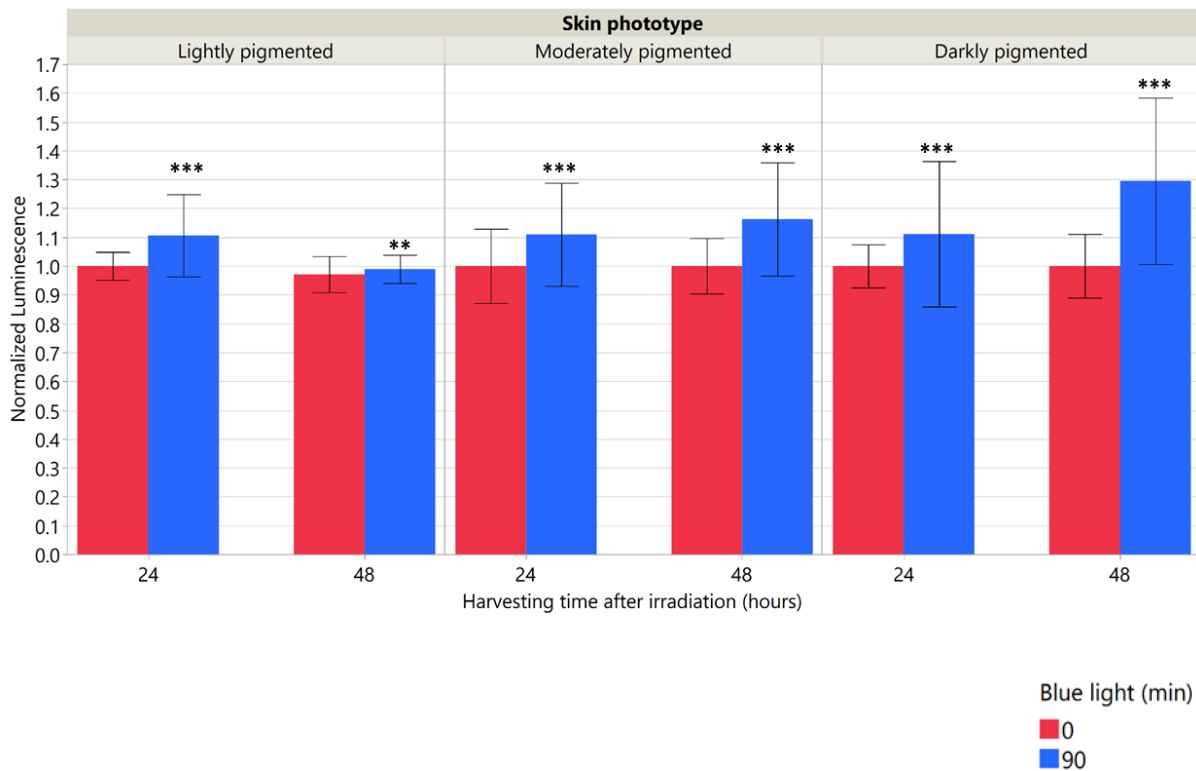


Figure 20. Cell ATP assay. Changes in ATP level of NHEM cells from the three skin phototypes was detected after an irradiation with 90 min of blue light with 24 hours (left-hand side) and 48 hours (right-hand side) of harvesting time. Bars represent mean \pm standard deviation. (N = 3 repetitions, 3 replicates). Values significantly different (non treated control vs light treated (90 min)) are indicated as ** $p < 0.001$ and *** $p < 0.0001$.

4.5 Intracellular redox level changes inflicted by blue light

Blue light is known to alter the level of oxidative stress inside the cell by producing reactive oxygen species (ROS). Hence, a redox sensor (Grx1-roGFP3) was used to determine intracellular redox changes after treatment with 90 min of blue light for different harvesting time points (0h, 0.5h, 1h, 2h, 3h, 4h, 5h, 6h, 24h and 48h) post-irradiation (Figure 21)

The blue light exposure resulted in a sharp increase in signal following irradiation as compared to non-irradiated control. Immediately after the light treatment, for lightly and moderately pigmented NHEM the oxidative stress elevated approximately 100% ($p < 0.0001$) whereas for the darkly pigmented it increased by approximately 300% ($p < 0.0001$) (Figure 21).

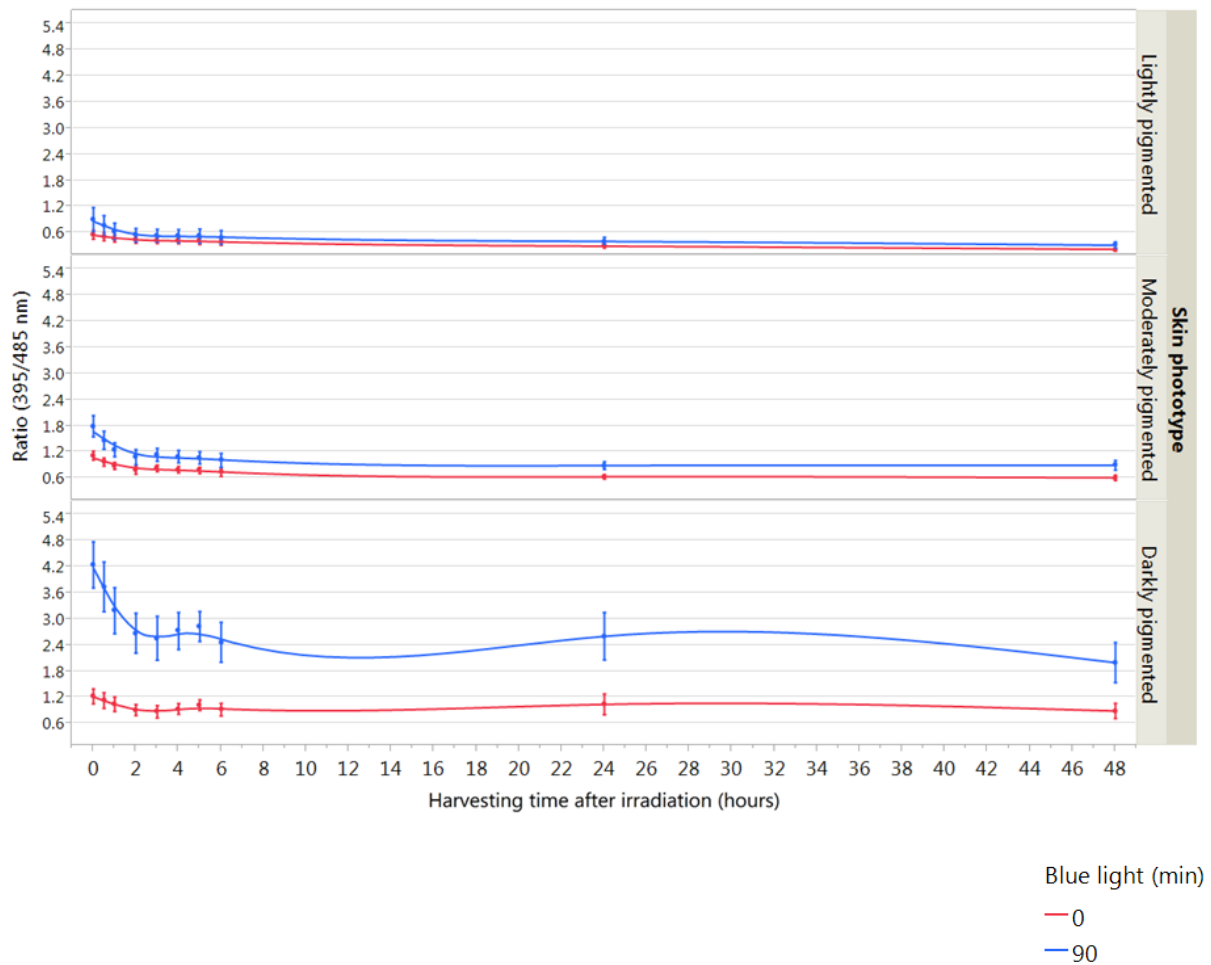


Figure 21. Intracellular redox status in NHEM in response to blue light. NHEM expressing Grx1-roGFP3 showed changes in ROS after an irradiation with 90 min of blue light for different harvesting time. Data are presented as mean \pm standard deviation. (N=3 repetitions, 3 replicates). Corresponding statistics summarized in Appendix 3.

For all the three skin phototypes the level of ROS decreased with time, after 6h ($p < 0.0001$) until 48h remained constant ($p < 0.0001$), and approached almost the same level as respective control values.

4.6 Gene expression analysis

The raw data obtained from RNA sequencing was subjected to distribution analysis and batch normalization. Followed by deep analysis of differential gene expression after the irradiation time 90 min with corresponding dose 64.8 J/cm^2 of blue treatment and cell harvesting of 48 hours.

4.6.1 Cluster analysis correlation

Hierarchical clustering using coloured heat maps showed the treated and non-treated samples in distinct clusters. Figure 22 illustrates the heat map with a strong matrix correlation between treated samples, which can be very well differentiated from the untreated samples from the three skin phototypes NHEM.

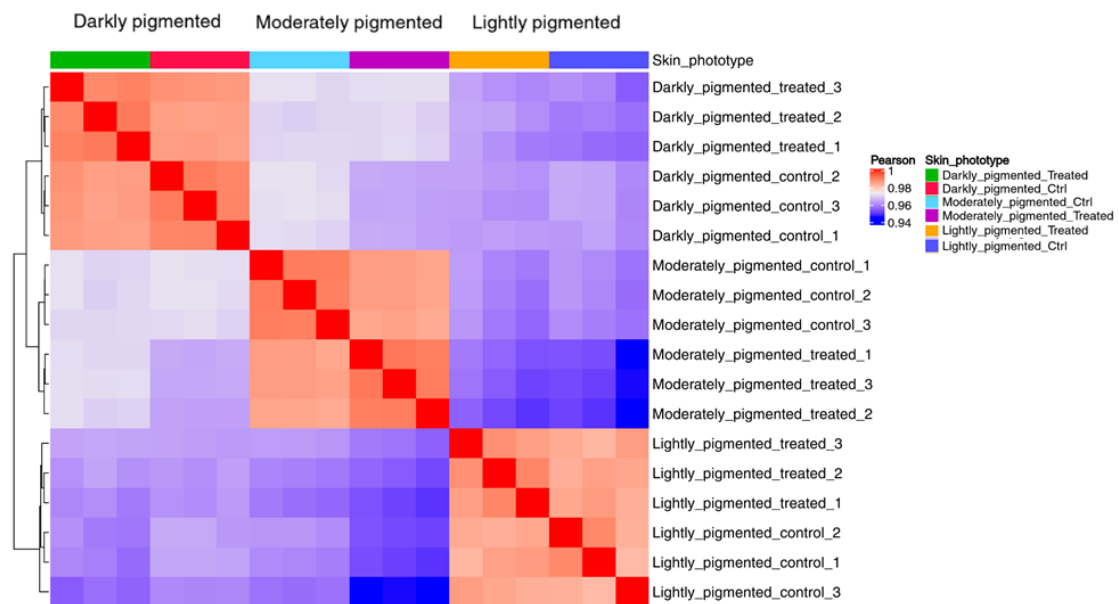


Figure 22. Cluster analysis. Pearson correlation heat map illustrating the cluster analysis of treated samples and non-treated samples of NHEM cells from three skin phototypes after treatment with blue light 90 min with cell harvesting after 48 hours. (N=1, 3 replicates).

4.6.2 Altered genes post blue light treatment

Out of the complete data set, 17221 genes were found to be differentially expressed for each respective three skin phototype NHEM after irradiation with blue light (90 min, 64.8 J/cm²). Amongst these genes, 3263 were significant for lightly pigmented, 4740 for moderately pigmented and 2409 for darkly pigmented.

Amongst the complete differentially expressed genes, a total of 7326 were significantly differentially or commonly expressed genes for among all three skin types. Out of this, moderately pigmented NHEM showed the highest number (2442) of significant genes differentially expressed from the two other skin type NHEM. Whereas darkly pigmented showed the least number of differentially expressed significant genes as compared to the two other skin type NHEM. Amongst the total number of significant genes, 605

genes were noticed to be commonly shared between the three skin type NHEM. Also, the highest amount (792) of commonly shared significant genes was observed between moderately and darkly pigmented NHEM. On the other hand, the lowest amount (183) of commonly shared significant genes was found between lightly and darkly pigmented NHEM (Figure 23).

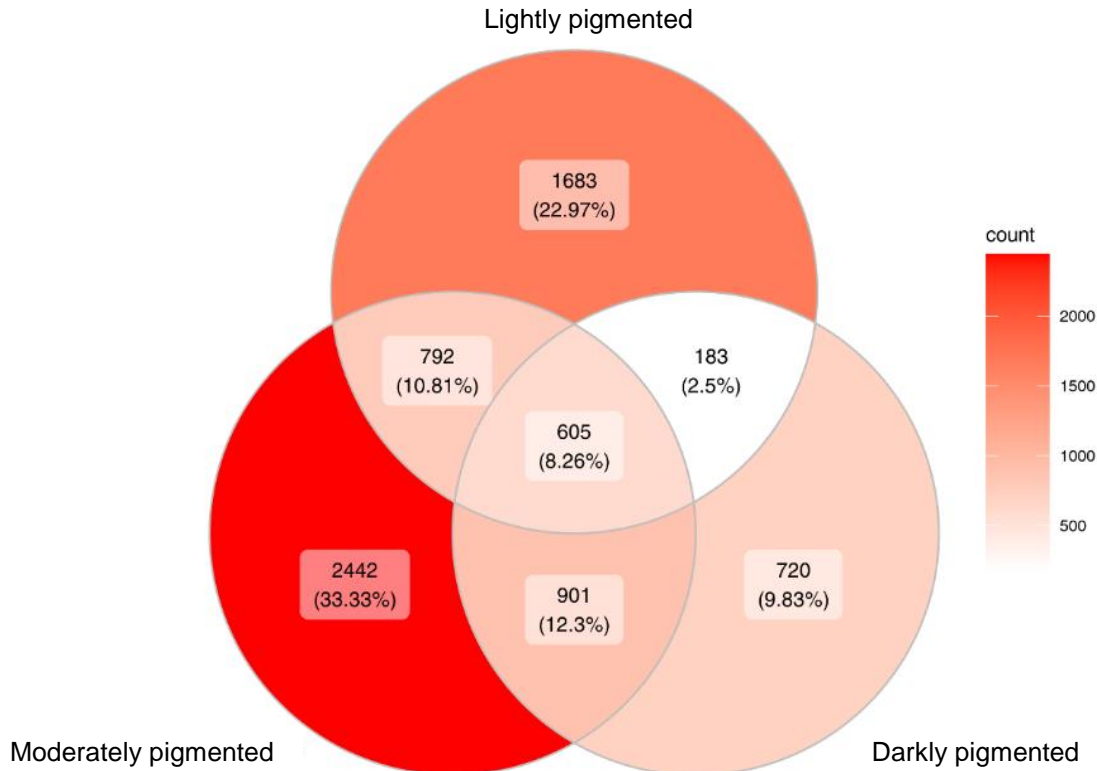


Figure 23. Significant count of genes. Venn diagram showing the number of genes significantly (adjusted p-value <0.05) commonly or differentially expressed in NHEM from the three skin phototypes after the blue light treatment 90 min and cell harvesting 48 hours.

Table 6 lists the number of significantly up- and down-regulated genes for each skin phototype NHEM. After the treatment with the respective dose of blue light, a maximum number of both up- and down-regulated genes were noted for moderately pigmented NHEM. Whereas among the two other skin phototypes, lightly pigmented had a little bit higher number of up-regulated genes as compared to darkly pigmented. Also, the down-regulated genes for the lightly pigmented were higher by 658 genes in comparison to darkly pigmented.

Table 6. Summary of differentially expressed genes. Number of significantly (adjusted p-value <0.05) up- and down-regulated genes.

Skin phototype	Lightly pigmented	Moderately pigmented	Darkly pigmented
Total number of up-regulated genes	1457	2324	1261
Total number of down-regulated genes	1806	2416	1148

Further, the common genes differentially expressed for NHEM were sorted by listing the top ten up- and down-regulated genes (Table 7).

Table 7. List of top ten up- and down- regulated differentially expressed genes. Top ten significantly (adjusted p-value <0.05) up- and down-regulated genes (gene symbol).

Up-regulated genes	Down-regulated genes
UTP14C	SPP1
SMIM38	CLDN1
LINC00304	PMP2
FBXW10	TMEM26
RNF112	ENPP1
ALDH8A1	SH2D4A
LOC100996583	ABCA1
TCTE1	FAXDC2
AOC3	MME
GAL3ST1	ADAM12

These genes encode proteins implicated in protein synthesis, membrane integrity, cell-cell interactions, transport, metabolism, cell differentiation and proliferation.

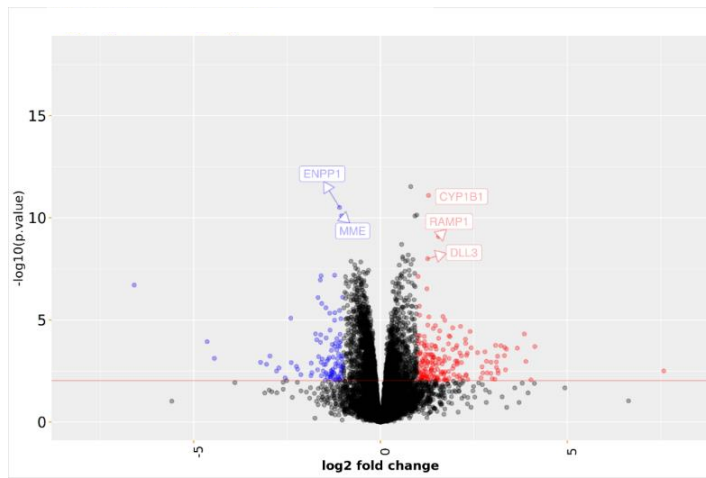
Next, the top most common up- and down-regulated genes for each of the three skin phototype NHEM were sorted from the differentially expressed genes (Table 8)

Table 8. List of top ten up- and down- regulated differentially expressed genes. Top most up- and down-regulated genes (gene symbol) for the three skin phototype NHEM.

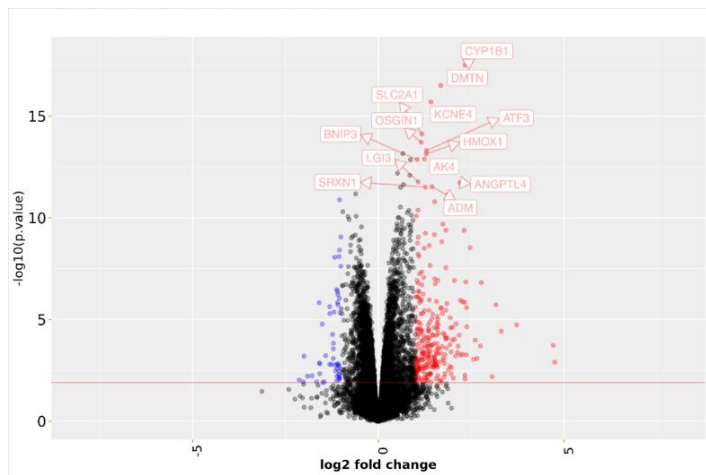
Regulation	Lightly pigmented	Moderately pigmented	Darkly pigmented
Up-regulated	UTP14C	UTP14C	LINC00304
	SMIM38	LOC100996583	UTP14C
	FBXW10	SECTM1	RNF112
	ALDH8A1	CYP1B1	LOC100996583
	LOC100996583	SMIM38	GAL3ST1
	TCTE1	SERPINF2	TRIM73
	RNF112	RNF112	CYP1B1
	AOC3	GAL3ST1	HLA-DRA
	GAL3ST1	TCTE1	SMIM38
	SSPO	MIR210HG	TCTE1
Down-regulated	SPP1	TMEM26	SPP1
	CLDN1	SH2D4A	FAXDC2
	PMP2	FAXDC2	SAPCD2
	ENPP1	ENPP1	PYHIN1
	ABCA1	ADAM12	THBS2
	MME	TM4SF18	PPARGC1A
	PYHIN1	PYHIN1	KU-MEL-3
	SH2D4A	DCAF12L1	LRRC1
	FAM83D	ANXA3	TM4SF18
	KIF14	ITFG2	ABCA1

Further, with the help of volcano plots (Figure 24), the regulation of top most significant genes was observed. The genes with large fold change are depicted that are also statistically significant. The red line serves as the threshold of significance and the most statistically significant genes are towards the top of the volcano plot. Statistically significant genes towards the right are the up-regulated genes whereas towards the left are the down-regulated genes (Figure 24).

(A)



(B)



(C)

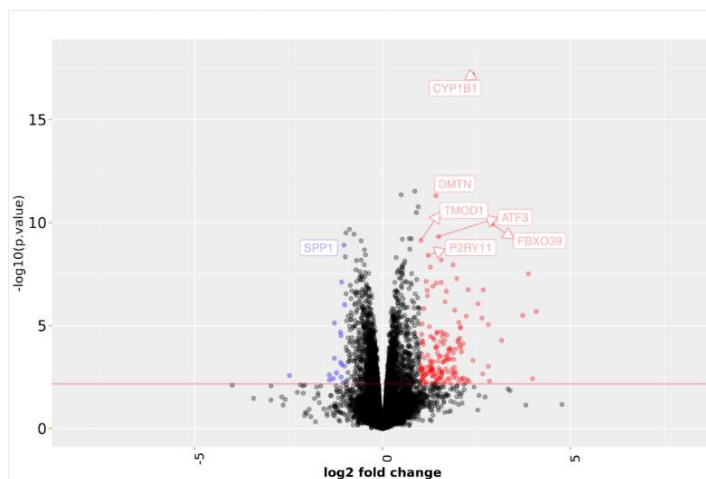


Figure 24. Volcano plots labelling top significant genes. Significantly up- and down-regulated genes for all the three skin phototype NHEM (A) Lightly pigmented, (B) Moderately pigmented and (C) Darkly pigmented.

4.6.3 De-regulated pathways after blue light treatment

GSEA (Gene Set Enrichment Analysis) was performed to ascertain whether the defined sets of genes exhibit statistical significant in their distribution within the ranked lists of differentially expressed genes. Also KEGG (Kyoto Encyclopedia of Genes and Genomes), a public database was used to obtain the detailed information of pathways involved in diverse cellular networks. Normalized enrichment score (NES) was used to classify the pathways into up-regulated and down-regulated categories.

Total 302 pathways were screened for each skin phototype NHEM (Table 9). Lightly pigmented had a total of 128 and 174 up- and down-regulated pathways, respectively. Whereas darkly pigmented had contrary trends with the counts of up- and down-regulated pathways to lightly pigmented NHEM. Moreover, moderately pigmented NHEM had the highest count of up-regulated pathways (220) and the lowest count of down-regulated pathways (82).

Table 9. Summary of differentially expressed KEGG pathways. Significantly up-regulated and down-regulated pathways for all the three skin phototype NHEM have been tabulated below with different significance level based on nominal p-value <0.05 and adjusted p-value <0.05.

Skin phototypes	Lightly pigmented	Moderately pigmented	Darkly pigmented
Total number of de-regulated pathways	302	302	302
Total number of up-regulated pathways	128	220	182
Significantly up-regulated pathways (nominal p-value)	15	89	38
Significantly up-regulated pathways (adjusted p-value)	4	56	6
Total number of down-regulated pathways	174	82	120
Significantly down-regulated pathways (nominal p-value)	41	17	9
Significantly down-regulated pathways (adjusted p-value)	14	13	0

Based on the adjusted p-value <0.05, the trend for the count of the up-regulated pathway was highest for the moderately pigmented NHEM (56) and almost similar for lightly (4) and darkly pigmented (6) NHEM. On the contrary, the number of down-regulated pathways with adjusted p-value <0.05 was approximately similar for

moderately (13) and lightly pigmented (14) NHEM and no down-regulated pathways were found for the darkly pigmented NHEM. There were no commonly shared significantly regulated pathways between the three skin phototypes. Although moderately pigmented NHEM shared commonly significant pathways with lightly pigmented (12) and darkly pigmented (4) NHEM. Moreover, moderately pigmented had the highest amount of differentially significant de-regulated pathways as compared to the other skin phototype NHEM, which had a very low count of differentially significantly de-regulated pathways, 6 for lightly pigmented and 2 for darkly pigmented (Figure 25).

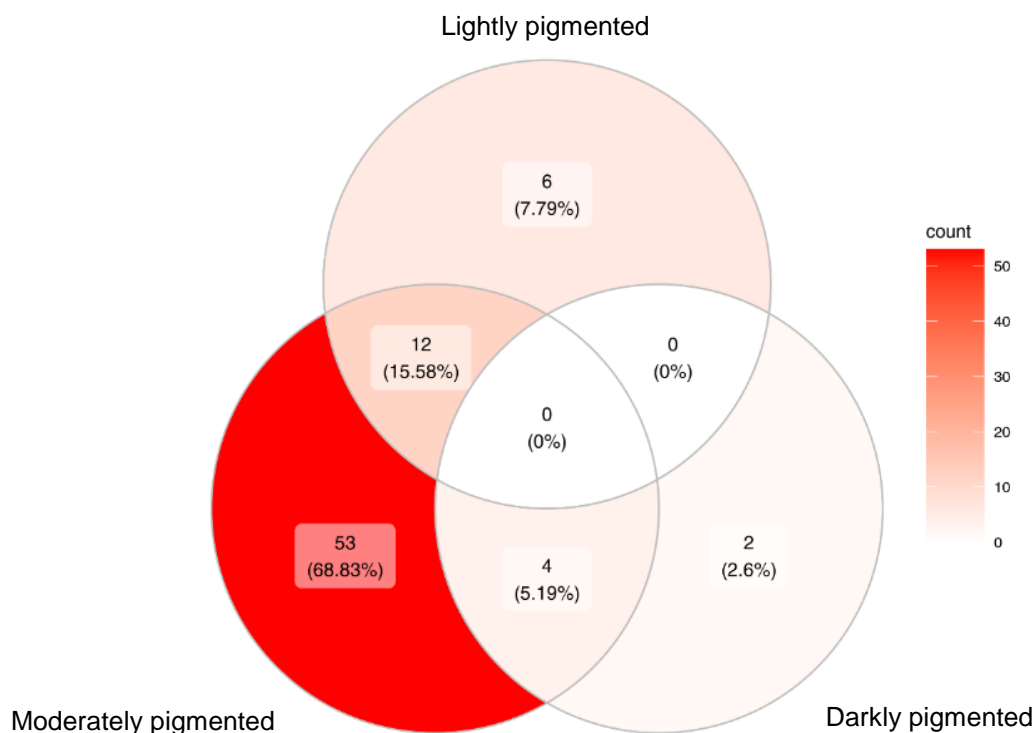


Figure 25. Number of significantly regulated pathways. Venn diagram depicting the count of significantly (adjusted p-value <0.05) commonly or differentially expressed pathways in the three skin phototype categories of NHEM after 90 min of blue light irradiation and cell harvesting 48 hours.

KEGG database sorts the complete gene sets into six main categories, namely:-

1. Metabolism
2. Genetic Information Processing
3. Environmental Information Processing
4. Cellular Processes
5. Organismal Systems
6. Human Diseases

Based on the above information provided by KEGG, the complete data set was studied for the networks and reactions affected due to our respective dose of blue light. The distribution is summarized in Figure 26.

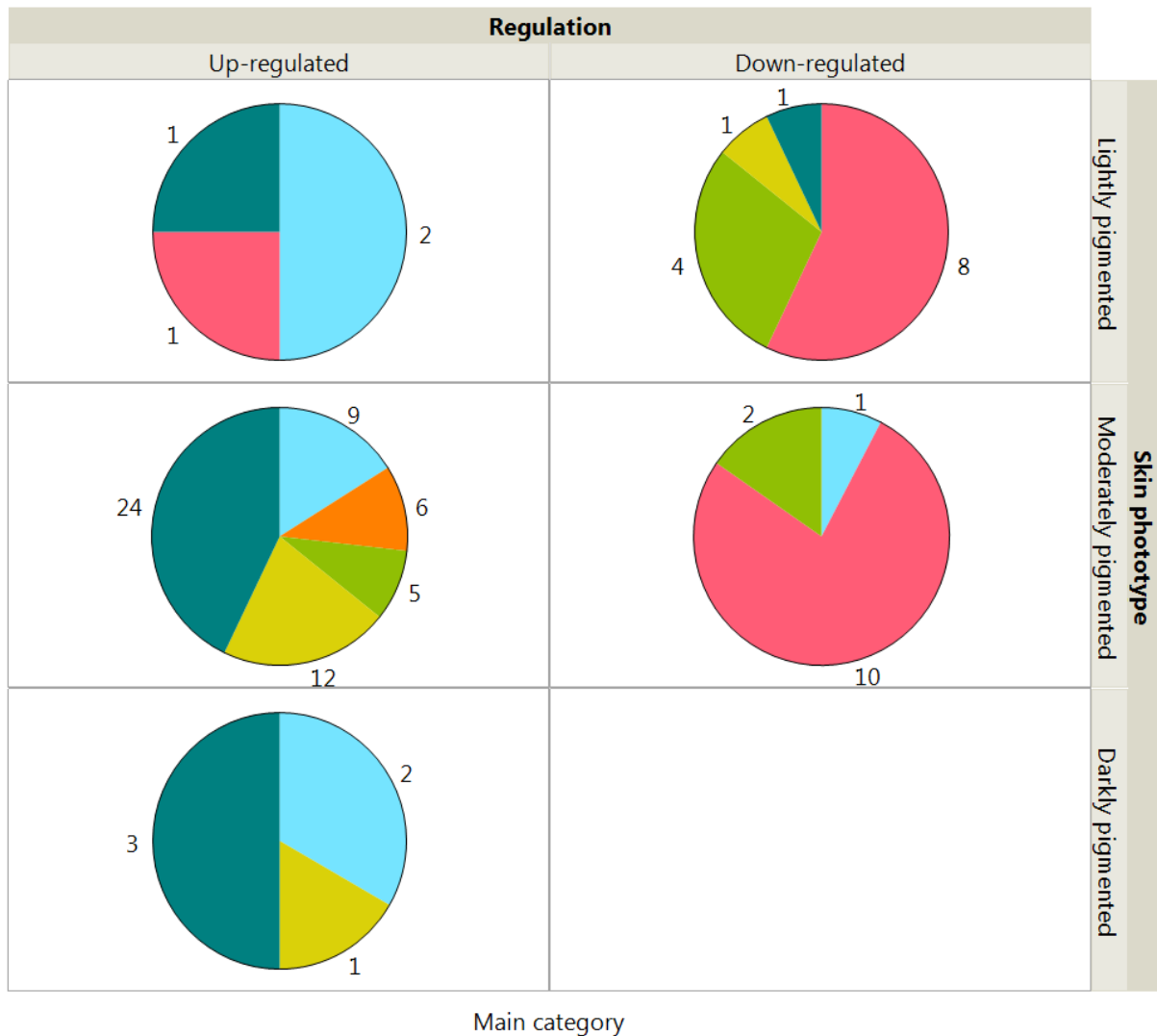


Figure 26. Significantly regulated pathways from KEGG. Significantly (adjusted p-value <0.05) up-regulated (NES >0) and down-regulated (NES <0) pathways from the six main category obtained from KEGG for all the three skin phototype NHEM. The numbers around the pie charts are the total number of up- and down-regulated pathways of the respective category.

The distribution obtained from sorting according to the KEGG 'Main Category', a significant up-regulation was observed in pathways belonging to category 'metabolism' for all the three skin phototype NHEM, except one pathway was significantly down-regulated for moderately pigmented NHEM. The number of up-regulated pathways belonging to this category were more in number for moderately pigmented NHEM as compared to the two other skin phototype NHEM.

The second category 'genetic information processing' had highly down-regulated pathways for moderately pigmented NHEM followed by lightly pigmented. Also, for the lightly pigmented NHEM only one pathway for this category was found to be up-regulated.

On the other hand, the significant pathways belonging to the third category 'environmental information processing' were found to be up-regulated for moderately pigmented only and no significant pathways were observed for other skin phototype NHEM.

Whereas pathways related to 'cellular process' were more up-regulated for moderately pigmented and in contrast it was more down-regulated for lightly pigmented NHEM.

Further, the fifth main category, 'organismal systems' pathways were more up-regulated for moderately pigmented NHEM and only one pathway for the darkly pigmented NHEM. Moreover, only one pathway was down-regulated for the lightly pigmented NHEM.

Lastly, the pathways related to the sixth category was found to be significantly up-regulated for all the three skin phototype NHEM, wherein higher in number for the moderately pigmented followed slightly for darkly pigmented and least for lightly pigmented NHEM.

Since the number of pathways in the main categories had a small sample size, we performed Fisher's Exact Test, as this test is suitable when the sample size is small.

Fisher's Exact Test was a further confirmation of the significance level of the KEGG pathways from the main category with significant adjusted p-value <0.05 for the three skin phototype NHEM. This test is applied when there are two variables and to find out whether the proportions of one variable is different depending on the value of the other variable. The result procured from this test is summarized in Table 10. The main category pathways belonging to lightly pigmented NHEM were strongly significant,

followed by moderately pigmented and no significance was observed for the darkly pigmented NHEM.

Table 10. Fisher's Exact Test. The result of the P value obtained from the Fisher's Exact Test for the main category with the significant KEGG pathways for the three skin phototype NHEM.

Skin phototype	Lightly pigmented	Moderately pigmented	Darkly pigmented
Fisher's Exact Test (P)	<0.0001	0.0114	0.8635

Furthermore, several individual pathways, which were significantly enriched after blue light irradiation with our dose, were sorted based on the six main categories to understand the sub-category type of these pathways (Table 11-16).

Amongst the metabolic pathways, after blue light treatment, sub-category xenobiotics biodegradation and metabolism were found to be up-regulated for all the three skin phototype NHEM (Table 11). This category comprises pathways like metabolism of xenobiotics by cytochrome P450, AHR pathway. Other related pathways to these pathways include steroid biosynthesis and terpenoid backbone biosynthesis. Besides, for moderately pigmented the sub-category carbohydrate metabolism was found to be significantly up-regulated, which constitutes of pathways like glycolysis/gluconeogenesis, pentose phosphate metabolism. Wherein the former is known to produce small amounts of ATP and NADH, and the latter produces NADPH and pentoses. Another interesting sub-category found to be up-regulated by blue light treatment includes metabolism of cofactors and vitamins comprising of the pathway porphyrin and chlorophyll metabolism (Table 11).

Table 11. List of significantly enriched KEGG pathways sorted for main category ‘Metabolism’. Significantly (adjusted p-value <0.05) up- and down-regulated pathways for all three skin phototype NHEM have been shown below. (A) Lightly pigmented, (B) Moderately pigmented and (C) Darkly pigmented.

(A)

Sub-category	Pathway name	NES	Adj. p-val.
1.3. Lipid metabolism	Steroid biosynthesis	1.96	0.0295
1.11. Xenobiotics biodegradation and metabolism	Metabolism of xenobiotics by cytochrome P450	1.89	0.0393

(B)

Sub-category	Pathway name	NES	Adj. p-val.
1.0 Global and overview maps	Carbon metabolism	1.78	0.0033
1.0 Global and overview maps	Biosynthesis of amino acids	1.93	0.0033
1.1. Carbohydrate metabolism	Glycolysis Gluconeogenesis	2.21	0.0033
1.1. Carbohydrate metabolism	Fructose and mannose metabolism	1.75	0.0323
1.1. Carbohydrate metabolism	Pentose phosphate pathway	1.72	0.0461
1.5. Amino acid metabolism	Lysine degradation	-1.81	0.0112
1.6. Metabolism of other amino acids	Glutathione metabolism	1.9	0.0072
1.8. Metabolism of cofactors and vitamins	Porphyry and chlorophyll metabolism	1.69	0.0482
1.11. Xenobiotics biodegradation and metabolism	AHR-Pathway	2.16	0.0033
1.11. Xenobiotics biodegradation and metabolism	Metabolism of xenobiotics by cytochrome P450	1.93	0.0072

(C)

Sub-category	Pathway name	NES	Adj. p-val.
1.9. Metabolism of terpenoids and polyketides	Terpenoid backbone biosynthesis	1.98	0.0288
1.11. Xenobiotics biodegradation and metabolism	AHR-Pathway	2.14	0.0192

Transcription, translation, replication and repair were the sub-categories found significant in the main-category ‘Genetic Information Processing’ for lightly and moderately pigmented NHEM (Table 12). All the pathways belonging to these sub-categories were down-regulated except for the ribosome pathway for the lightly pigmented was found to be significantly up-regulated.

Table 12. List of significantly enriched KEGG pathways sorted for main category ‘Genetic Information Processing’. Significantly (adjusted p-value <0.05) up- and down-regulated pathways for all three skin phototype NHEM have been shown below. (A) Lightly pigmented and (B) Moderately pigmented.

(A)

Sub-category	Pathway name	NES	Adj. p-val.
2.1. Transcription	Spliceosome	-1.8	0.0135
2.2. Translation	RNA transport	-1.94	0.0135
2.2. Translation	Ribosome biogenesis in eukaryotes	-1.77	0.0274
2.2. Translation	Ribosome	-1.66	0.0306
2.4. Replication and repair	DNA replication	-2.29	0.0135
2.4. Replication and repair	Mismatch repair	-2.01	0.0274
2.4. Replication and repair	Homologous recombination	-1.84	0.0274
2.4. Replication and repair	Nucleotide excision repair	-1.8	0.0393
2.4. Replication and repair	Base excision repair	-1.78	0.044

(B)

Sub-category	Pathway name	NES	Adj. p-val.
2.1. Transcription	Spliceosome	-1.97	0.0033
2.1. Transcription	Basal transcription factors	-1.94	0.0066
2.2. Translation	Ribosome biogenesis in eukaryotes	-2.29	0.0033
2.2. Translation	RNA transport	-1.93	0.0033
2.4. Replication and repair	DNA replication	-2.25	0.0033
2.4. Replication and repair	Base excision repair	-2.06	0.0033
2.4. Replication and repair	Mismatch repair	-2.07	0.0033
2.4. Replication and repair	Homologous recombination	-2.02	0.0033
2.4. Replication and repair	Fanconi anemia pathway	-2.21	0.0033
2.4. Replication and repair	Nucleotide excision repair	-1.68	0.0347

Besides, the pathways as part of the sub-category (main category ‘cellular processes’) cell growth and death are also down-regulated for the two NHEM, i.e., lightly pigmented and moderately pigmented (Table 13). Which included cell cycle, oocyte meiosis, p53 signalling. Although, the ferroptosis pathway was up-regulated for moderately pigmented NHEM. Apart from this the sub-category, transport and catabolism comprise pathways like autophagy, phagosome, mitophagy and lysosome were significantly up-regulated for moderately-pigmented NHEM.

Table 13. List of significantly enriched KEGG pathways sorted for main category ‘Cellular Processes’. Significantly (adjusted p-value <0.05) up- and down-regulated pathways for all three skin phototype NHEM have been shown below. (A) Lightly pigmented and (B) Moderately pigmented.

(A)

Sub-category	Pathway name	NES	Adj. p-val.
4.2. Cell growth and death	Cell cycle	-2.38	0.0135
4.2. Cell growth and death	Oocyte meiosis	-1.71	0.0274
4.2. Cell growth and death	p53 signaling pathway	-1.69	0.0393
4.2. Cell growth and death	Cellular senescence	-1.58	0.0393

(B)

Sub-category	Pathway name	NES	Adj. p-val.
4.1. Transport and catabolism	Autophagy	1.46	0.0497
4.1. Transport and catabolism	Phagosome	1.62	0.0175
4.1. Transport and catabolism	Mitophagy	1.9	0.0058
4.1. Transport and catabolism	Lysosome	1.75	0.0033
4.2. Cell growth and death	Cell cycle	-1.85	0.0033
4.2. Cell growth and death	Ferroptosis	2.05	0.0033
4.2. Cell growth and death	Oocyte meiosis	-1.51	0.0416

Further, the sub-categories part of ‘environmental information processing’ that were significantly up-regulated contained signal transduction and signalling molecules and interaction for the moderately pigmented NHEM (Table 14). Amongst this, TNF signalling which is known to play a role in inducing a wide range of pathways, for example, apoptosis and cell survival, as well as inflammation and immunity, were compared for the three NHEM to assess the effects of blue light treatment.

Table 14. List of significantly enriched KEGG pathways sorted for main category ‘Environmental Information Processing’. Significantly (adjusted p-value <0.05) up- and down-regulated pathways for all three skin phototype NHEM have been shown below for moderately pigmented.

Sub-category	Pathway name	NES	Adj. p-val.
3.2. Signal transduction	TNF signaling pathway	1.54	0.0416
3.2. Signal transduction	HIF-1 signaling pathway	2.35	0.0033
3.3. Signaling molecules and interaction	Cytokine-cytokine receptor interaction	1.83	0.0033
3.3. Signaling molecules and interaction	Cell adhesion molecules (CAMs)	1.65	0.0176
3.3. Signaling molecules and interaction	Viral protein interaction with cytokine and cytokine receptor	1.89	0.0087
3.3. Signaling molecules and interaction	Neuroactive ligand-receptor interaction	1.59	0.0283

Some of the pathways belonging to the sub-category of the endocrine system, the immune system, the digestive system, the excretory and the nervous system were also found to be significantly regulated in the main category ‘organismal system’ (Table 15). The above sub-categories were significantly up-regulated for moderately and darkly pigmented NHEM, respectively. Whereas, one of the pathway progesterone-mediate

oocyte maturation belonging to the endocrine system sub-category was found significantly down-regulated for the lightly pigmented NHEM.

Table 15. List of significantly enriched KEGG pathways sorted for main category 'Organismal Systems'. Significantly (adjusted p-value <0.05) up- and down-regulated pathways for all three skin phototype NHEM have been shown below. (A) Lightly pigmented, (B) Moderately pigmented and (C) Darkly pigmented.

(A)

Sub-category	Pathway name	NES	Adj. p-val.
5.2. Endocrine system	Progesterone-mediated oocyte maturation	-1.64	0.0464

(B)

Sub-category	Pathway name	NES	Adj. p-val.
5.1. Immune system	Th1 and Th2 cell differentiation	1.58	0.0349
5.1. Immune system	Intestinal immune network for IgA production	2.24	0.0033
5.1. Immune system	Hematopoietic cell lineage	1.87	0.0102
5.1. Immune system	Antigen processing and presentation	1.76	0.0171
5.2. Endocrine system	Ovarian steroidogenesis	1.85	0.0102
5.2. Endocrine system	Relaxin signaling pathway	1.82	0.0033
5.2. Endocrine system	Adipocytokine signaling pathway	1.71	0.0175
5.4. Digestive system	Cholesterol metabolism	1.78	0.0181
5.4. Digestive system	Bile secretion	1.69	0.032
5.5. Excretory system	Collecting duct acid secretion	1.82	0.0246
5.6. Nervous system	Synaptic vesicle cycle	1.6	0.0441
5.8. Development	Osteoclast differentiation	1.55	0.0349

(C)

Sub-category	Pathway name	NES	Adj. p-val.
5.1. Immune system	Intestinal immune network for IgA production	1.9	0.0483

The sub-category cancer, immune diseases, cardiovascular diseases, endocrine and metabolic disease and also infectious disease in the category: bacterial, viral and parasitic as part of the main category 'human diseases' were found to be significantly regulated (Table 16). Amongst this list, the few commonly shared pathways like chemical carcinogenesis were selected for further comparison for the evaluation of the blue light irradiation. As chemical carcinogenesis, found to be up-regulated for lightly and moderately pigmented NHEM, this pathway is involved when there is environmental exposure to chemical carcinogens. Moreover, rheumatoid arthritis was found to be remarkably up-regulated for moderately and darkly pigmented NHEM, which is part of the immune disease sub-category. In this disease, it is known to have abnormal activation of the immune system resulting in elevation of pro-inflammatory cytokines and chemokines levels. Moreover, rheumatoid arthritis was found to be remarkably up-regulated for moderately and darkly pigmented NHEM, which is part of

the immune disease sub-category. In this disease, it is known to have abnormal activation of the immune system resulting in elevation of pro-inflammatory cytokines and chemokines levels. And, previously we noted, some pathways of the sub-category signalling molecules and interaction from the main-category 'environmental information processing' were found to be up-regulated as well (Table 14)

Table 16. List of significantly enriched KEGG pathways sorted for main category 'Human Diseases'. Significantly (adjusted p-value <0.05) up- and down-regulated pathways for all three skin phototype NHEM have been shown below. (A) Lightly pigmented, (B) Moderately pigmented and (C) Darkly pigmented.

(A)

Sub-category	Pathway name	NES	Adj. p-val.
6.1. Cancers: Overview	Chemical carcinogenesis	1.76	0.0464
6.9. Infectious diseases: Viral	Human immunodeficiency virus 1 infection	-1.52	0.0393

(B)

Sub-category	Pathway name	NES	Adj. p-val.
6.1. Cancers: Overview	Chemical carcinogenesis	1.93	0.0072
6.1. Cancers: Overview	Central carbon metabolism in cancer	1.92	0.0087
6.1. Cancers: Overview	Pathways in cancer	1.42	0.0146
6.2. Cancers: Specific types	Basal cell carcinoma	1.77	0.0163
6.2. Cancers: Specific types	Thyroid cancer	1.75	0.0226
6.2. Cancers: Specific types	Breast cancer	1.54	0.0292
6.3. Immune diseases	Rheumatoid arthritis	2.34	0.0033
6.3. Immune diseases	Graft-versus-host disease	1.94	0.0087
6.3. Immune diseases	Autoimmune thyroid disease	1.93	0.0146
6.3. Immune diseases	Allograft rejection	1.89	0.0171
6.3. Immune diseases	Inflammatory bowel disease (IBD)	1.73	0.0255
6.6. Cardiovascular diseases	Fluid shear stress and atherosclerosis	1.76	0.0058
6.7. Endocrine and metabolic diseases	Type I diabetes mellitus	1.85	0.0189
6.7. Endocrine and metabolic diseases	Non-alcoholic fatty liver disease (NAFLD)	1.45	0.0461
6.8. Infectious diseases: Bacterial	Vibrio cholerae infection	1.7	0.0255
6.8. Infectious diseases: Bacterial	Tuberculosis	1.71	0.0058
6.8. Infectious diseases: Bacterial	Staphylococcus aureus infection	2.04	0.0033
6.9. Infectious diseases: Viral	Human T-cell leukemia virus 1 infection	1.5	0.0175
6.9. Infectious diseases: Viral	Kaposi sarcoma-associated herpesvirus infection	1.56	0.02
6.9. Infectious diseases: Viral	Influenza A	1.57	0.0292
6.9. Infectious diseases: Viral	Human cytomegalovirus infection	1.44	0.0372
6.9. Infectious diseases: Viral	Hepatitis C	1.5	0.0413
6.9. Infectious diseases: Viral	Epstein-Barr virus infection	1.41	0.0461
6.10. Infectious diseases: Parasitic	Leishmaniasis	1.65	0.0323

(C)

Sub-category	Pathway name	NES	Adj. p-val.
6.3. Immune diseases	Rheumatoid arthritis	1.8	0.0483
6.8. Infectious diseases: Bacterial	Staphylococcus aureus infection	2.23	0.0192
6.9. Infectious diseases: Viral	Herpes simplex virus 1 infection	1.8	0.0192

Moreover, based on our observation from the different experiments conducted using blue light (90 min, 64.8 J/cm²) and from the literature search, some important pathways affected by light treatment were selected and evaluated from this data set.

Amongst the selected pathways (illustrated in Figure 27) were oxidative phosphorylation and glycolysis/gluconeogenesis which are part of the metabolic pathways and are involved in the ATP production. Both these pathways were found to be up-regulated after the treatment with blue light for all the skin phototype NHEM cells. On the other hand, the apoptosis pathway had an up-regulated trend for moderately and darkly pigmented, but it was not significant for any of the skin phototypes. The p53 signalling pathway was also assessed as p53 activation is induced by stress signals, and we observed that this pathway was down-regulated for both lightly and moderately pigmented NHEM cells, but it was up-regulated for darkly pigmented NHEM, although not reaching a relevant level of significance.

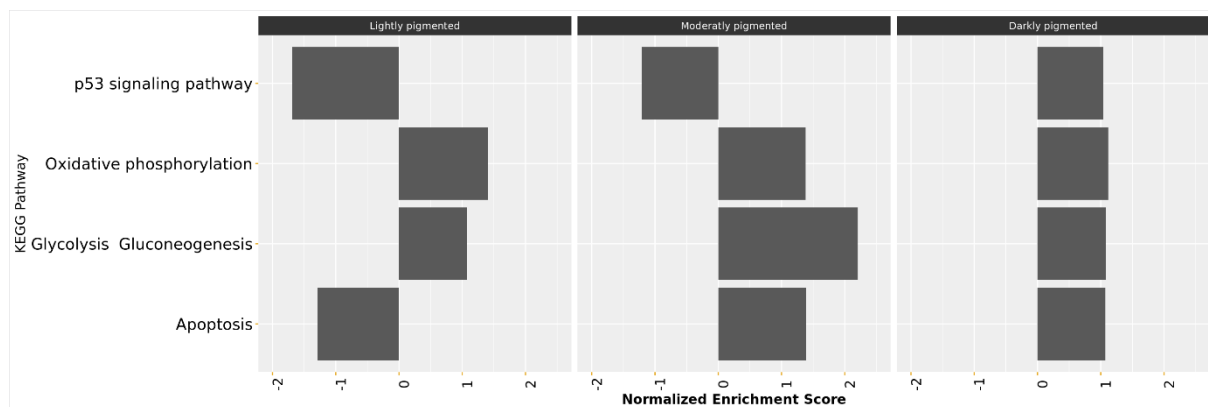


Figure 27. Selected pathways for further analysis of gene expression data. Pathways related to metabolism, apoptosis and stress signaling with NES for all the three skin phototype NHEM cells. Bars represent mean.

Further, some other important players in regulating a wide range of cellular functions including immunity, inflammation, and cell signalling to cell death are the signalling pathways like TNF, TGF-beta, NF-Kappa B, MAPK, AMPK and FoxO signalling pathway. In our data set, we observed a down-regulation of TGF-beta signalling pathway for all the three skin phototypes and the AMPK signalling pathway had the opposite trend. On the other hand, the two other pathways i.e. NF-Kappa B signalling and MAPK signalling pathway were found to be down-regulated for lightly and darkly pigmented NHEM, whereas up-regulated for moderately pigmented NHEM. Moreover,

TNF and FoxO signalling pathway had the same trend with up-regulation for moderately and darkly pigmented and down-regulation for lightly pigmented (Figure 28).

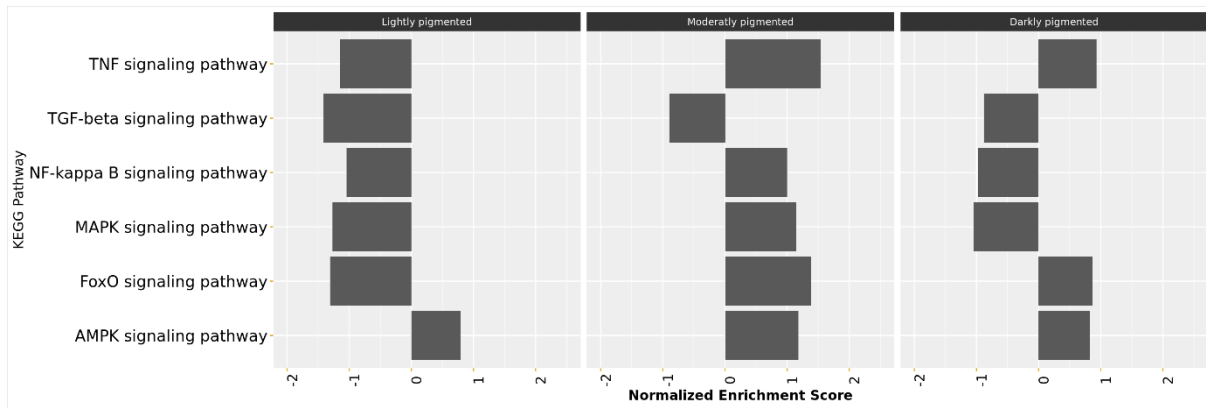


Figure 28. Important signalling pathways selected for further analysis. Signalling pathway with NES for all the three skin phototype. Bars represent mean.

4.6.4 Significant MicroRNAs (miRNAs) after blue light treatment

Two miRNAs, MIR4664 and MIR3189 were found to be significantly regulated in our RNA sequencing data (Table 17). MIR4664 was significant for both lightly and moderately pigmented NHEM cells, whereas MIR3189 was found to be significantly regulated for darkly pigmented NHEM cells.

Table 17. List of significantly regulated miRNAs. Significant (adjusted p-value <0.05) miRNAs for all three skin phototype NHEM have been shown below. (A) Lightly pigmented, (B) Moderately pigmented and (C) Darkly pigmented.

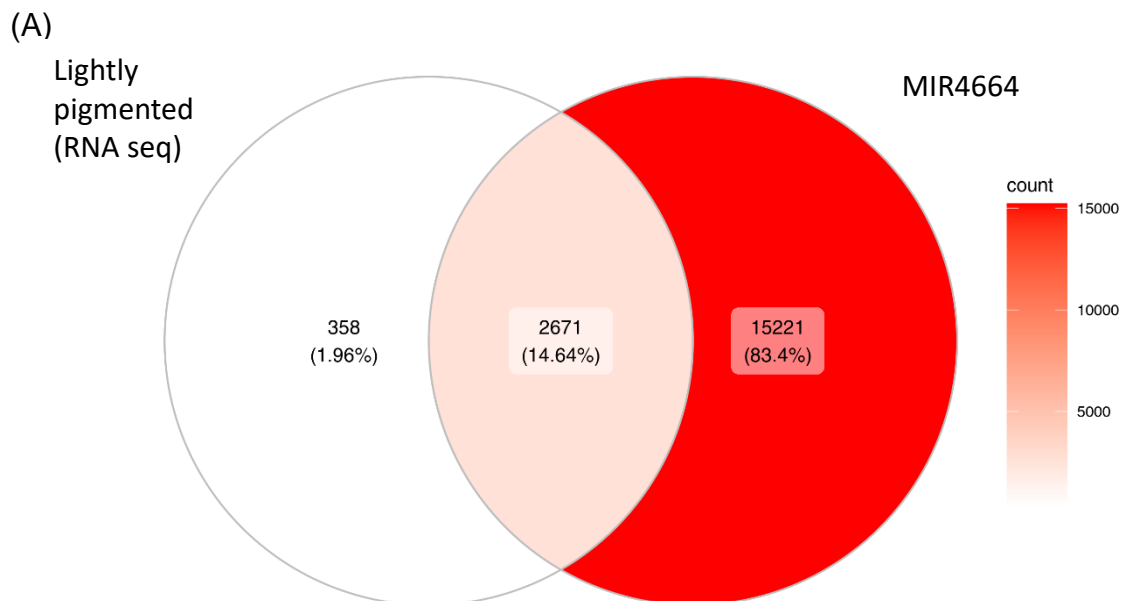
Skin phototype	Lightly pigmented	Moderately pigmented	Darkly pigmented
miRNAs	MIR4664	MIR4664	MIR3189
log Fold change	0.888714	0.909552	2.250505
Adjusted p-value	0.020844	0.008566	0.035314

Then possible target genes were searched using the miRWalk database (Table 18).

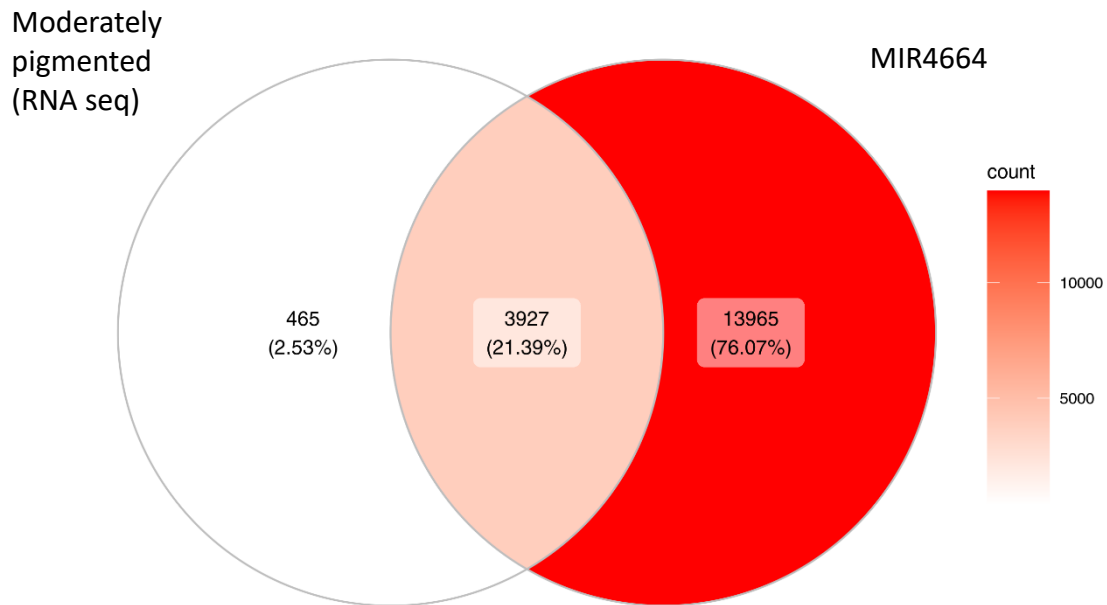
Table 18. Total number of possible target genes. The total number of possible target genes found in the miRWalk database search.

miRNA	Number of possible target genes
hsa-miR-4664-3p	52243
hsa-miR-4664-5p	45970
hsa-miR-3189-3p	62937
hsa-miR-3189-5p	46633

Next, the common target genes amongst the significant gene in our data and possible targets obtained from the miRWalk database were identified (Figure 29). The common genes between RNA seq dataset and MIR4664 dataset for lightly pigmented skin phototype were 2671 and 3927 for moderately pigmented skin phototype NHEM. 1953 genes were found to be common between RNA seq dataset and MIR3189 dataset for darkly pigmented skin phototype NHEM. Further, a total of 481 genes were obtained as the common genes amongst all the three skin phototypes NHEM (Figure 29).



(B)



(C)

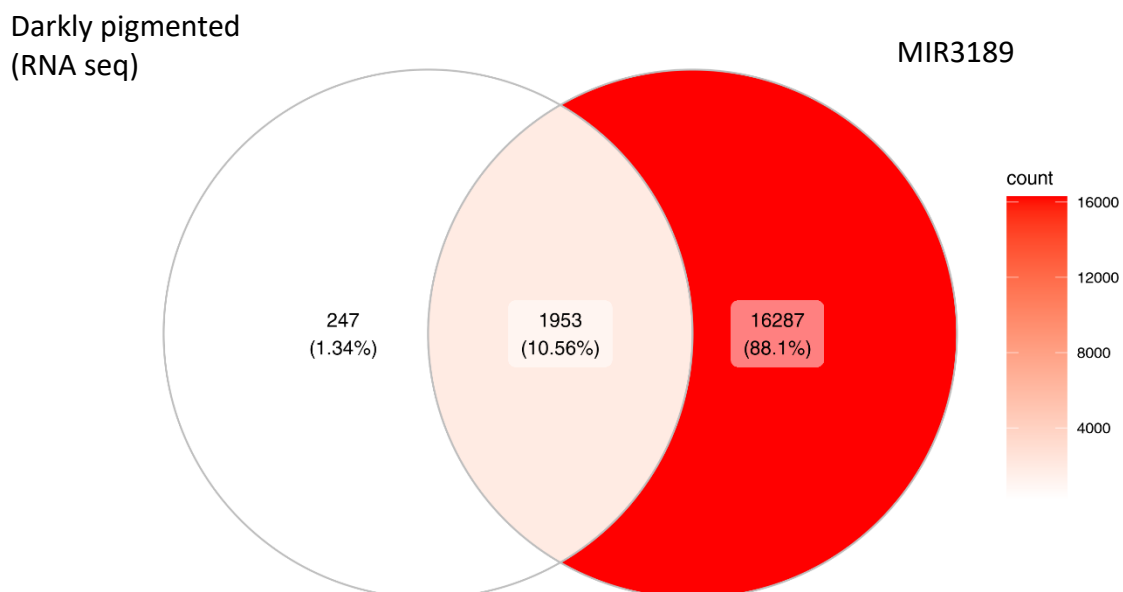
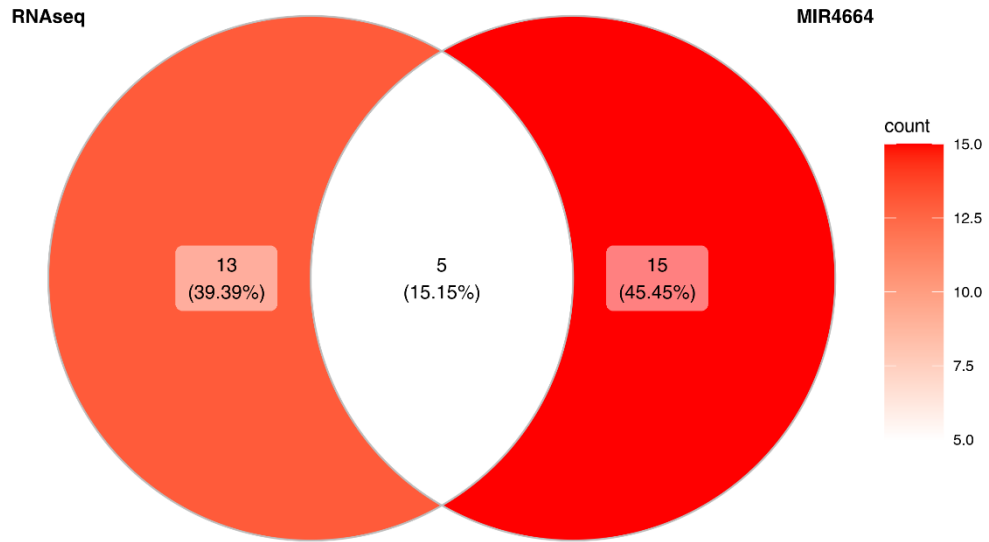


Figure 29. Number of common target genes. Venn diagram depicting the common target genes between the significant gene list obtained from RNA seq and list of possible target genes obtained from miRWalk search for all three skin phototypes (A) Lightly pigmented, (B) Moderately pigmented, and (C) Darkly pigmented.

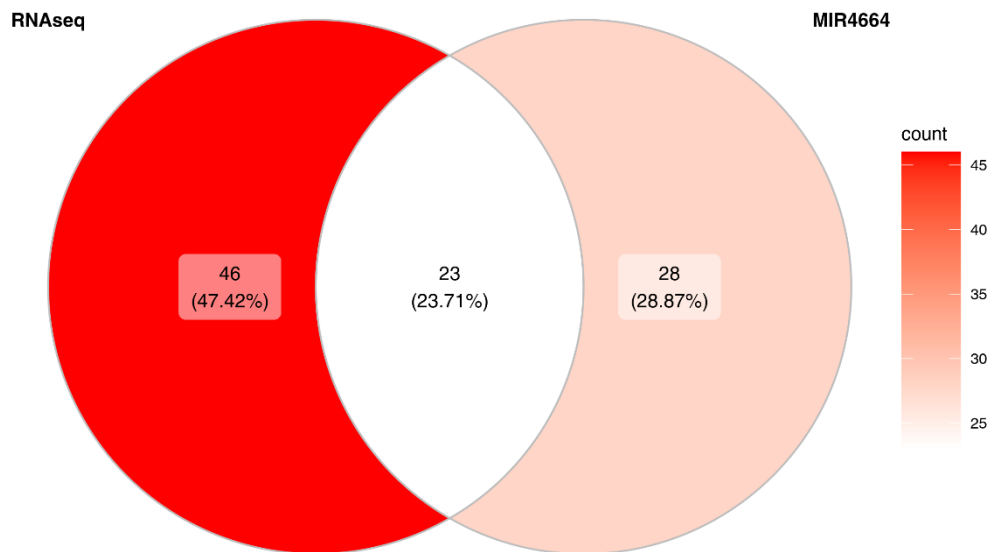
Afterwards, the pathway analysis was performed for these common genes using the KEGG database and parallel-analysis with the significant pathways obtained in the

initial gene expression analysis were analysed to understand common regulated pathways (Figure 30).

(A)



(B)



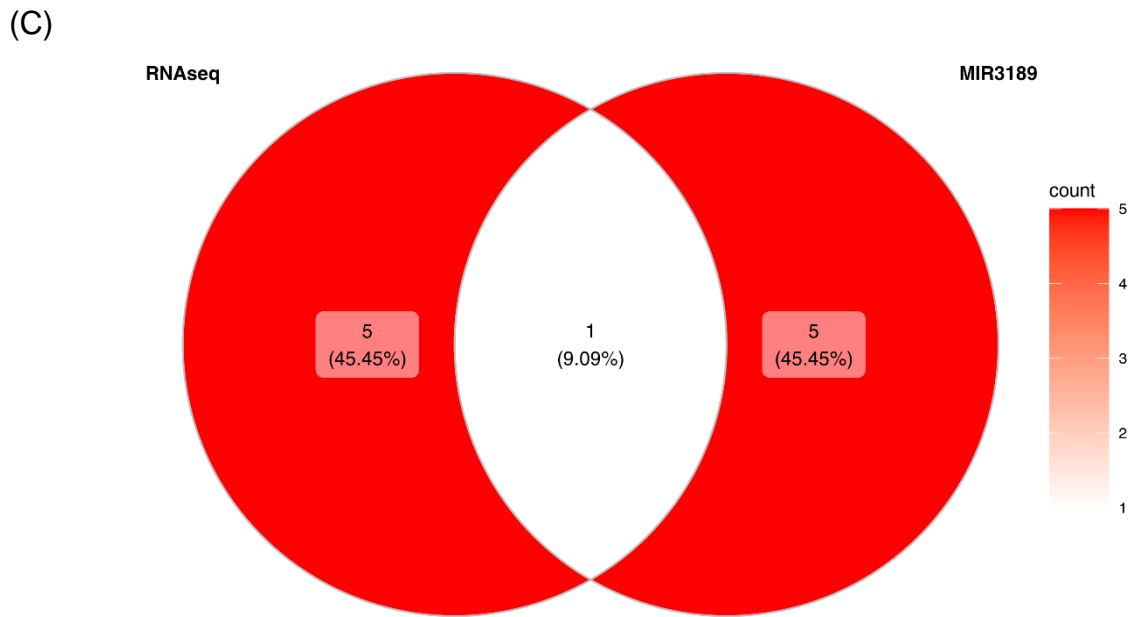


Figure 30. Number of common pathways. Venn diagram depicting the common KEGG pathways between the significant pathway list obtained from RNA seq and list of pathways belonging to possible binding sites obtained from miRWalk search for all three skin phototypes (A) Lightly pigmented, (B) Moderately pigmented and (C) Darkly pigmented.

In total 5 pathways were found to be common for lightly pigmented, 23 for moderately pigmented and 1 for darkly pigmented between the RNA seq dataset and miRWalk dataset. The common pathways with the main and sub-category as listed in Table 19 were obtained from a KEGG database analysis.

Table 19. Common pathways. The total number of common pathways found between the RNA seq data and pathways for miRNA for all three skin phototypes (A) lightly pigmented, (B) moderately pigmented and (C) darkly pigmented.

(A)

Pathway name	Main Category	Sub-category
Steroid biosynthesis	1. Metabolism	1.3. Lipid metabolism
DNA replication	2. Genetic Information Processing	2.4. Replication and repair
Cell cycle	4. Cellular Processes	4.2. Cell growth and death
Oocyte meiosis	4. Cellular Processes	4.2. Cell growth and death
p53 signaling pathway	4. Cellular Processes	4.2. Cell growth and death

(B)

Pathway name	Main Category	Sub-category
Carbon metabolism	1. Metabolism	1.0 Global and overview maps
Biosynthesis of amino acids	1. Metabolism	1.0 Global and overview maps
Glycolysis/Gluconeogenesis	1. Metabolism	1.1. Carbohydrate metabolism
Fructose and mannose metabolism	1. Metabolism	1.1. Carbohydrate metabolism
Pentose phosphate pathway	1. Metabolism	1.1. Carbohydrate metabolism
Lysine degradation	1. Metabolism	1.5. Amino acid metabolism
Mismatch repair	2. Genetic Information Processing	2.4. Replication and repair
Homologous recombination	2. Genetic Information Processing	2.4. Replication and repair
Fanconi anemia pathway	2. Genetic Information Processing	2.4. Replication and repair
Nucleotide excision repair	2. Genetic Information Processing	2.4. Replication and repair
HIF-1 signaling pathway	3. Environmental Information Processing	3.2. Signalling trasnduction
Cell adhesion molecules	3. Environmental Information Processing	3.2. Signalling molecules and interaction
TNF signaling pathway	3. Environmental Information Processing	3.2. Signalling trasnduction
Cell cycle	4. Cellular Processes	4.2. Cell growth and death
Oocyte meiosis	4. Cellular Processes	4.2. Cell growth and death
Autophagy	4. Cellular Processes	4.2. Cell growth and death
Fluid shear stress and atherosclerosis	6. Human Diseases	6.6. Cardiovascular diseases
Human T-cell leukemia virus 1 infection	6. Human Diseases	6.8. Infectious diseases: Viral
Kaposi sarcoma-associated herpesvirus infection	6. Human Diseases	6.8. Infectious diseases: Viral
Vibrio cholerae infection	6. Human Diseases	6.8. Infectious diseases: Bacterial
Influenza A	6. Human Diseases	6.8. Infectious diseases: Viral
Human cytomegalovirus infection	6. Human Diseases	6.8. Infectious diseases: Viral
Epstein-Barr virus infection	6. Human Diseases	6.8. Infectious diseases: Viral

(C)

Pathway name	Main Category	Sub-category
Terpenoid backbone biosynthesis	1. Metabolism	1.9 Metabolism of terpenoids and polyketides

4.6.5 Alteration in aryl-hydrocarbon receptor (AHR) pathway and related genes

The analysis of gene expression data suggests that among the complete gene set that was altered, CYP1B1 was observed to be highly up-regulated after 48 hours of blue light irradiation (90 min, 64.8 J/cm²) (Figure 13). This in turn, points toward a possible role of the transcription factor, aryl hydrocarbon receptor after blue light treatment. Moreover, pathway analysis also showed an up-regulated trend for AHR pathway and other pathways related to it, like metabolism of xenobiotics by cytochrome P450,

chemical carcinogenesis, tryptophan metabolism and steroid hormone biosynthesis based on the normalized enrichment score (Figure 31).

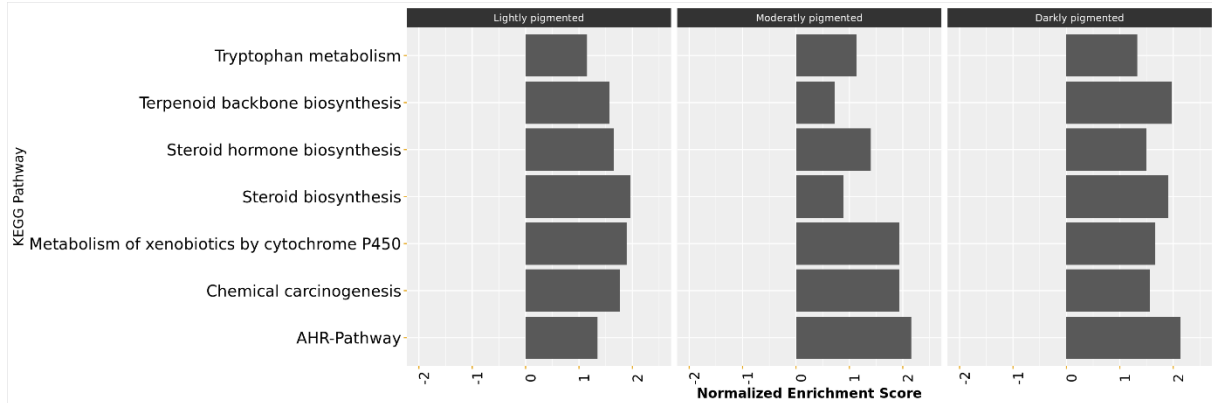


Figure 31. AHR pathway and other related pathways. AHR pathway and other related pathways with NES for all the three skin phototype NHEM. Bars represent mean.

In Figure 32, the coloured heat map reveals the expression pattern of the different genes involved in the AHR pathway.

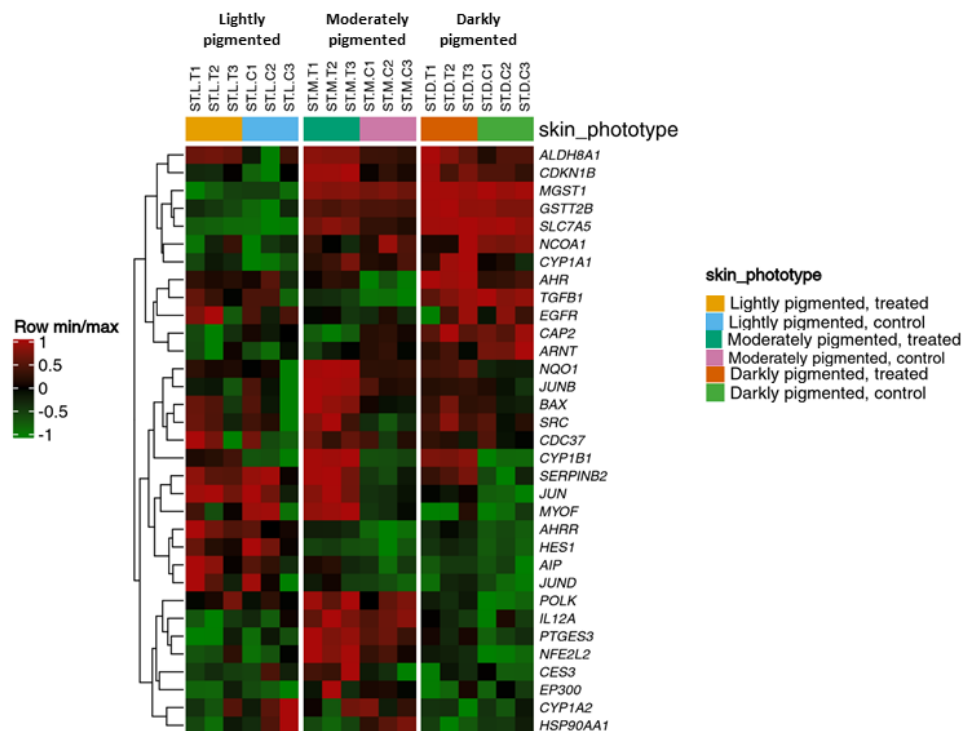


Figure 32. AHR pathway heat map. Pearson correlation heat map illustrating up- and down-regulation of the AHR pathway related genes from three skin phototypes after treatment with blue light for 90 min and cell harvesting after 48 hours. (T: light treated, C: non-treated control). Red: up-regulated expression of the genes, green: down-regulated expression of the genes.

The entire list of genes involved in the AHR pathway is known as 'AHR gene battery' as shown in Figure 33. The trend for these genes has been summarized after blue light irradiation (90 min, 64.8 J/cm²) and harvesting time 48 hours thereafter.

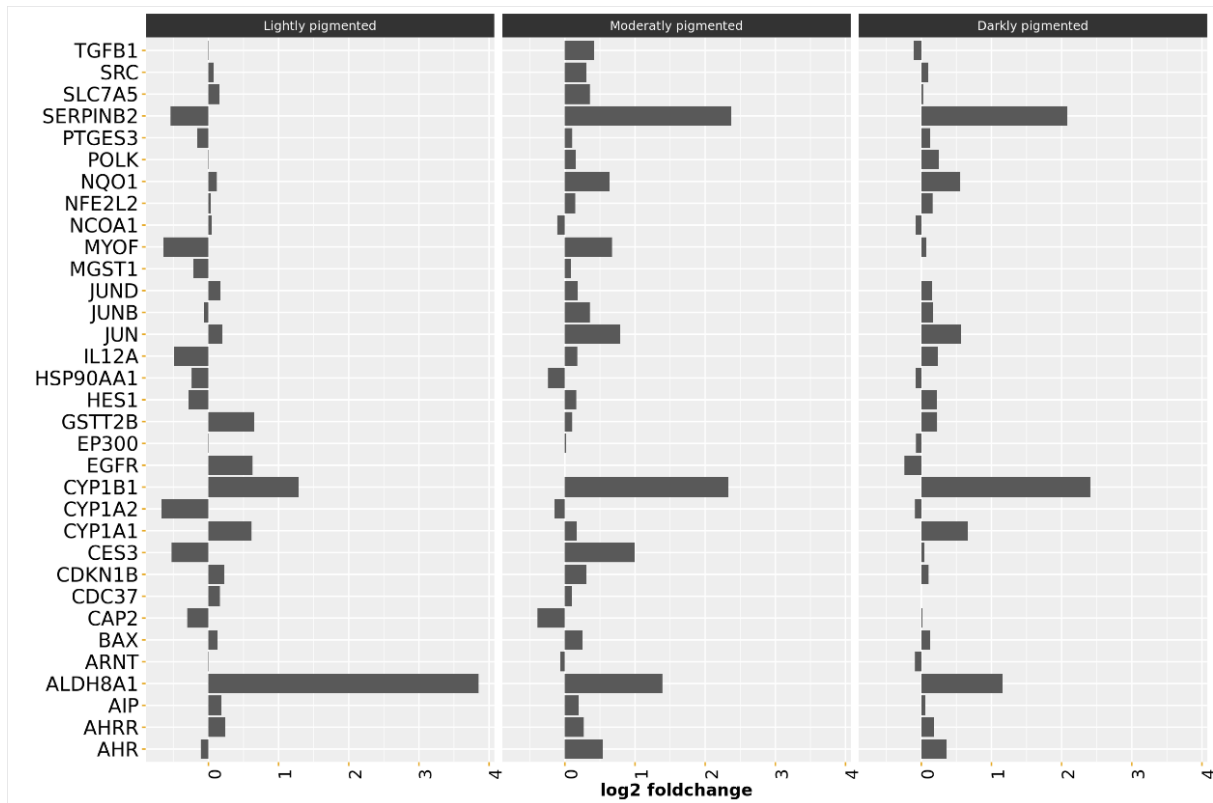


Figure 33. AHR gene battery. Genes involved in AHR pathway summarized for all the three skin phototype NHEM. Bars represent mean.

Genes like CYP1A1, aryl hydrocarbon receptor (AHR), cyclin-dependent kinase 1 B (CDKN1B), nuclear factor erythroid 2 like 2 (NFE2L2, also known as Nrf 2), NAD(P)H quinone oxidoreductase 1 (NQO1), aldehyde dehydrogenase 8 family member A1 (ALDH8A1), aryl hydrocarbon receptor repressor (AHRR) were also found to be up-regulated amongst the genes related to AHR pathway. Others like aryl hydrocarbon receptor nuclear translocator (ARNT), CYP1A2, heat shock protein 90 alpha family class A member 1 (HSP90AA1) were found to be down-regulated.

Using STRING database, the proteins encoded by above genes were obtained (AHR, CYP1B1 and CYP1A1 were used as an input for the search).and, an overview of the protein-protein interaction is illustrated in Figure 34.

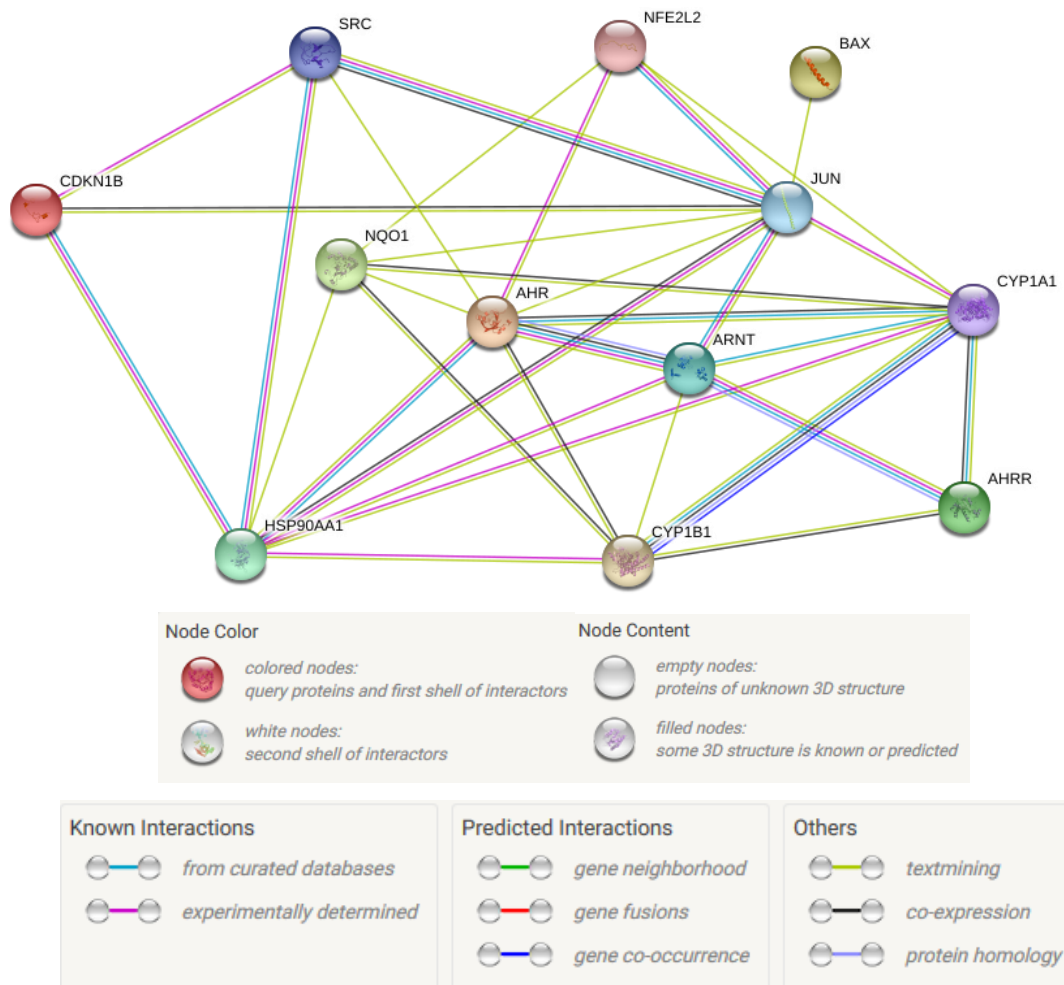


Figure 34. Overview of protein-protein interaction. Protein-protein interaction of the genes involved in AHR pathway as obtained from STRING database. AHR, CYP1B1 and CYP1A1 were used as an input for the search.

4.6.6 Effects of blue light on melanogenesis

The process of production of the pigment melanin is known as melanogenesis. This process is regulated by a varied amount of internal as well as external factors. After blue light treatment, the melanogenesis pathway was found to be up-regulated for all skin phototypes (Figure 35). As, tyrosine serves as the precursor for the melanin synthesis, the regulation of this pathway was assessed following blue light irradiation. We observed an up-regulation of the tyrosine metabolism pathway. Amongst the core molecular pathways influencing the melanin production, c-AMP signaling pathway also plays an important role, as it is known to activate several melanogenic genes. This pathway was also found to be up-regulated in our data set.

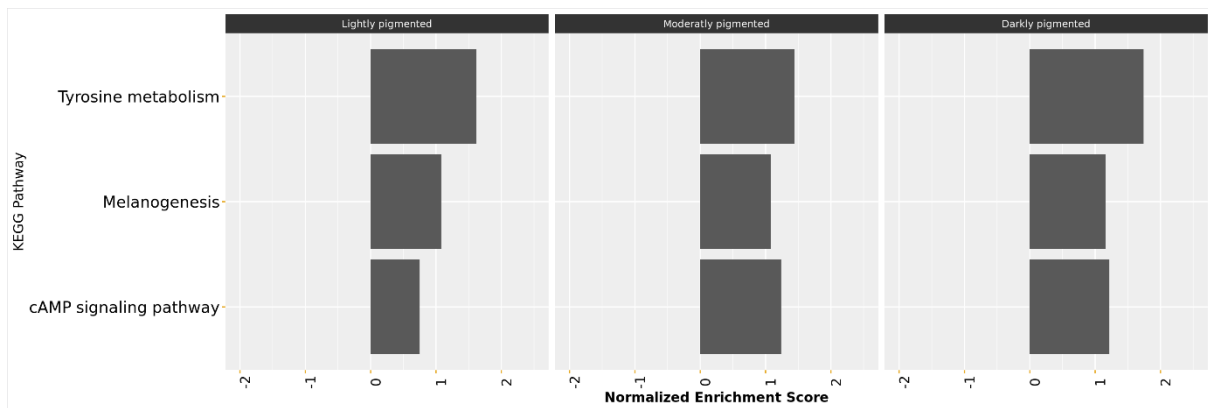


Figure 35. Melanogenesis and related pathways. Pathways involved in the melanin synthesis with NES and adjusted p-value for all the three skin phototype NHEM. Bars represent mean.

Many genes involved in melanogenesis, were found to be significantly regulated after blue light irradiation. Tyrosinase (TYR) is an important enzyme in the melanin synthesis pathway and is involved in the conversion of tyrosine to L-DOPA, which is the rate-limiting step of this process. This enzyme is encoded by the TYR gene, which was found to be significantly up-regulated in our gene set (Figure 36).



Figure 36. Genes involved in melanin synthesis. Genes involved directly or indirectly in melanin synthesis for all the three skin phototype NHEM. Bars represent mean.

The STRING database was used to search for TYR. The database provided the information about protein encoded by TYR and interaction with other proteins like transient receptor potential cation channel subfamily C member 1 (TRPC1), OCA2 melanosomal transmembrane protein (OCA2), premelanosome protein (PMEL), Dopachrome tautomerase (DCT), Microphthalmia-associated transcription factor (MITF) and MLANA (Melan-A) (Figure 37). The genes encoded by these proteins (obtained from STRING) and other important genes involved in the melanogenesis

pathway (from literature search) were selected for further analysis (Figure 36). Amongst these, OCA2, opsin 3 (OPN 3) and TRPC1 were found to be up-regulated. Whereas MITF, c-AMP response element (CREB) were found to be down-regulated.

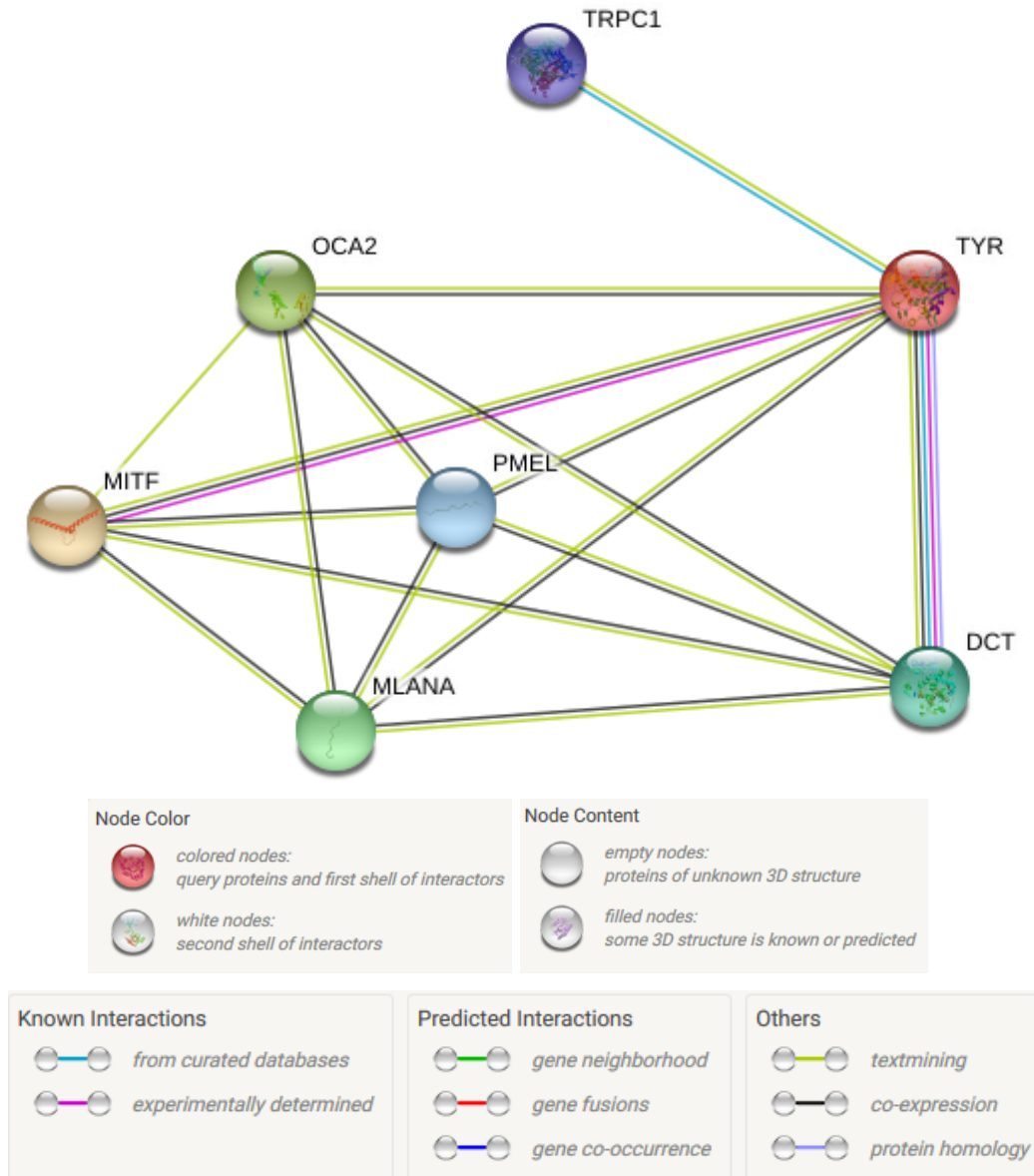


Figure 37. Overview of protein-protein interaction. Protein-protein interaction of the genes involved in melanogenesis pathway as obtained from STRING database. TYR was used as an input for the search.

The melanogenesis pathway was obtained from the KEGG database and a multi-plot was built combining the data for all the three skin phototype NHEM (Figure 38).

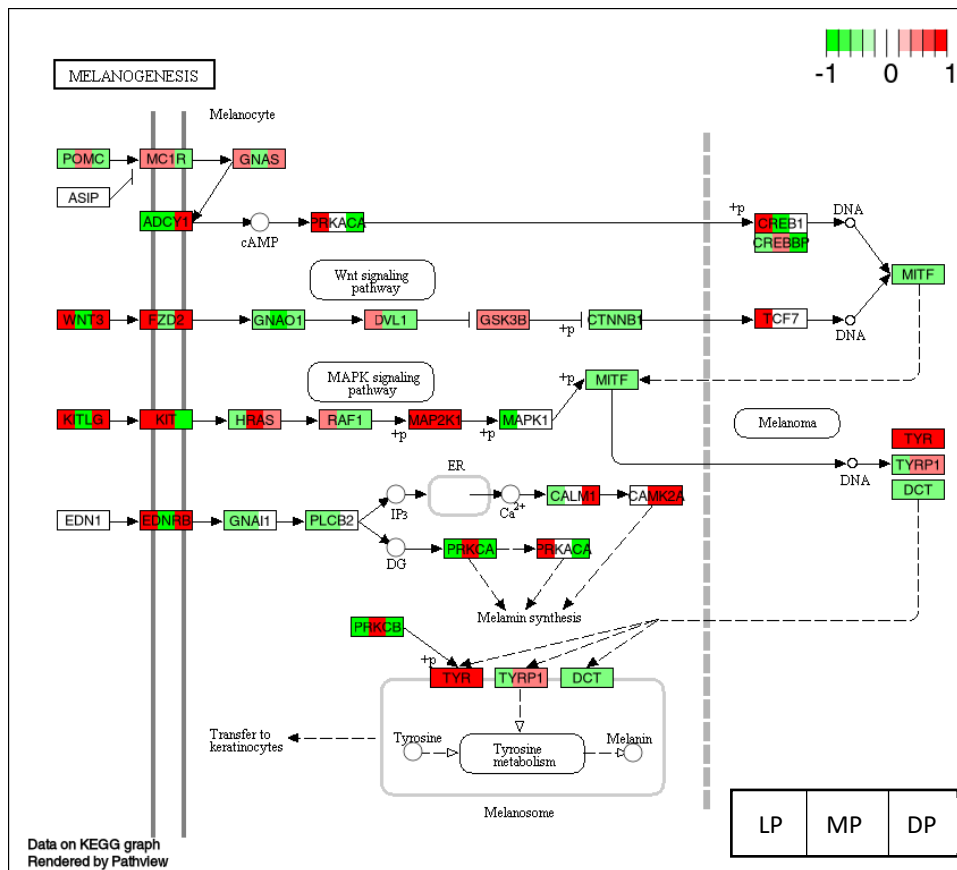


Figure 38. Overview of melanogenesis pathway. Multiplot of melanogenesis pathway as obtained from KEGG database based on the NES. Each box allotted for a gene has been divided into three skin phototypes (from left to right), lightly pigmented, moderately pigmented and darkly pigmented.

5. Discussion

Currently, different effects of PBM have been reported in the literature on cell metabolism, viability, proliferation, apoptosis and redox status. These outcomes vary depending on the cell type and different irradiation parameters. The influence of PBM on melanocytes has been shown mainly to affect the pigmentation. Moreover, the role of PBM on melanocytes has received far less attention than its neighbouring skin cells, keratinocytes and fibroblasts. Therefore, the present study aimed at understanding the impact of PBM using blue light (453 nm) on human melanocytes.

Briefly, the effects of different doses of blue light on NHEM cells were assessed using a cell viability XTT assay followed by an investigation of the role of blue light (both stimulatory and inhibitory doses obtained from viability assay) in modulating the amount of melanin production. An irradiation time of 90 min with a corresponding dose of 64.8 J/cm² was chosen to analyse known effects of light as this dose showed the highest increase in melanin content for all three skin phototype NHEM cells. Further functional assays were carried out using the selected dose to investigate the photobiomodulatory effects reported in the literature. Thus, ATP measurement, redox status analysis and cell apoptosis examined for safety concerns of the selected dose. Subsequently, a comprehensive evaluation of gene expression profiles of all three skin phototypes was performed. This analysis found multiple genes and pathways deregulated, and also two significant miRNAs. Amongst these, the key findings have been discussed.

5.1 Blue light doses resulted in a biphasic dose response

To evaluate the role of blue light on melanocytes, different doses (listed in Table 1) were applied on NHEM cells and using viability assay, the change in metabolic activity was assessed. Mitochondrial enzymes of metabolically active cells are known to reduce the tetrazolium salt (XTT) and the coloured end product is measured directly by absorbance reading⁶⁷. It resulted in a biphasic dose-response curve wherein lower doses or the short-term irradiation affected the cell metabolism positively and led to an increase in the activity. On the other hand, higher doses or long-term irradiation led to a decrease in cell metabolism. Maximum acceleration of approximately 23% in the activity was achieved for the dose 5.4 J/cm². Whereas amongst all doses evaluated

for the study, the maximum decrease of 31% was obtained for the highest dose after 24 hours of light treatment.

Many authors have found the same results^{68, 15}, that has been based on 'Arndt-Schulz law' dose-dependent model^{69, 70}. Similar findings have been also been reported by Castellano-Pellicena, I. et al., 2019⁷¹, blue light led to an induction in metabolic activity of cultured keratinocytes using 453 nm of blue light. Further, in our study, 48 hours harvesting after irradiation for doses of 5.4, 21.6, and 64.8 J/cm² lead to a suppression in the activity of NHEM cells. The opposite trend has been shown by AlGhamdi, K.M., et al, 2015⁵³ using short-term irradiation, using blue (457 nm) and red laser (635 nm) after 72 hours of harvesting time.

Since we saw an inhibition in the metabolic activity with different doses after 48 hours, we did not proceed for 72 hours of harvesting after irradiation. Also for the cells to survive in the 96-well plate for three days after irradiation, the initial number for the seeding of cells would have been lower, and that could have been another factor affecting the cell response to blue light in a different manner.

5.2 Blue light induces hyperpigmentation

Melanocytes have the main function of producing the pigment melanin, and blue light has been reported to induce pigmentation^{47, 52}. Hence, to elucidate whether blue light (453 nm) can modulate the amount of melanin production in these cells selected doses were applied on NHEM cells followed by an estimation of the melanin content. Selected doses included 5.4, 21.6, and 64.8 J/cm² based on the outcome of the viability assay for their stimulatory and inhibitory effects. The blue light doses 5.4 and 21.6 J/cm² did not show a significant change in the melanin amount. On the other hand, the melanin assay revealed an increase in melanin amount after application of dose 64.8 J/cm² post 48 hours of irradiation for all the three skin phototype NHEM cells. The same observations were reflected in gene expression analysis as well with an increase in the melanogenesis pathway. Additionally, a significant up-regulation of the gene TYR, encoding for tyrosinase enzyme was observed, which is located in melanocytes and is responsible for catalysing the first rate-limiting step in the conversion of tyrosine to L-DOPA in the melanin synthesis pathway^{72, 73}. Moreover, a significant up-regulation was observed for tyrosine metabolism, as this amino acid is the natural principle substrate for melanin⁷⁴.

In addition, significant up-regulation was observed in OCA2 melanosomal transmembrane protein (OCA2, formerly known as P gene). It is located in melanocytes and predicted to be involved in the transport of tyrosine within the melanocytes⁷⁵ and as well it is known to regulate the pH of the melanosome and the melanosome maturation^{76, 77}. AlGhamdi, K.M et al.⁵⁴ have shown that the stage I melanosomes were significantly higher in the treated group as compared to the non-treated group, which points towards an induction of melanogenesis. Furthermore, OPN3 was observed to be up-regulated. It belongs to the family of light-sensitive G-protein coupled receptors. Opsins have recently been identified for their role in phototherapy^{78, 79}. Regazzetti, C., et al., 2018⁵⁸ have demonstrated the role of Opsin 3 (OPN 3) as a sensor for blue light in melanocytes and demonstrated an increase in pigmentation. Another proposed downstream target of opsins is transient receptor potential (TRP) channels, which are known to be activated by light⁸⁰. Gene expression analysis also revealed a significant up-regulation of TRPC1 in NHEM cells after blue light treatment. Moreover, it is known that OPN 3 and other opsins signal via a pathway involving cyclic nucleotides (c-AMP and c-GMP)⁷⁸. This would match with our KEGG pathway analysis depicting an up-regulation in the cAMP pathway.

Although c-GMP pathway was only up-regulated for moderately and darkly pigmented NHEM after blue light irradiation. In addition, several melanogenic genes can be indirectly be activated by c-AMP synthesis.

Besides this MITF, the master regulator of melanocyte development and melanogenic genes was observed to be down-regulated. This could be because this gene has been reported to be up-regulated immediately after light exposure and later returns to its basal level⁵⁸.

5.3 No induction of cell death via apoptosis by blue light

Cellular apoptosis is a downstream response seen after light treatment. PBM is known to have an effect on the cell apoptosis level depending on the dose and other irradiation parameters. We also evaluated the possibility of whether our dose could have a stimulatory or inhibitory effect on cell apoptosis due to long-term irradiation, using flow cytometry analysis.

Although to our surprise, the dose used in our study did not result in a significant apoptosis between the untreated control and treated samples for two of the harvesting time points (24 and 48 hours) for all the three skin phototypes NHEM.

From the gene expression profiles, it was noted that the majority of cell growth and death pathways were found to be significantly down-regulated. Single gene expression depicts a slightly up-regulation of TP53, which codes for p53, which might be due to a light-induced stress. On the other hand, there is also a slight up-regulation of MDM2, which is an antagonist of TP53. The former encodes a nuclear-localized E3 ubiquitin ligase. As a result, this leads to reduced cellular stress and a subsequent down-regulation of genes involved in caspase cascade like CASP9, CASP3. This finding is reflected in FACS analysis, where no significant apoptosis was observed for all NHEM after blue light treatment. In addition, the apoptotic pathways were also not significantly regulated and the caspase cascade responsible for the execution of this programmed cell death was slightly down-regulated due to a non-significant expression of the respective adaptors. Similar findings have been reported by Becker, A., et al., 2016⁸¹, the group observed no occurrence of apoptosis after 30 min of blue light treatment with 23 mW/cm² after 24 hours of harvesting time. In contrast to this, Oh, P.S., et al., 2014⁸² obtained opposing trends in their investigation while assessing the effects of blue light on melanoma cells. They found the induction of apoptotic cell death by a mitochondrial-mediated pathway. The authors also observed an increase in phosphorylation of p53 in the early phase of irradiation, which decreased after long exposure times.

Although an overall, up-regulation was observed in the apoptosis pathway for moderately and darkly pigmented NHEM. As well as, p53 signalling pathway showed a slight up-regulation for darkly pigmented NHEM but it was not significant. All these observations might be the reason for more cell death for darkly pigmented NHEM cells noticed in flow cytometry results, followed by moderately pigmented NHEM cells.

Moreover, the TNF signalling pathway is up-regulated for both the NHEM cells, suggesting a possible increase in inflammation. Also the NF- κ B pathway is up-regulated in moderately pigmented, which is involved in inflammation and induced responses. Hence, there is a stimulation of regulated mechanisms to remove unwanted and damaged components. Pathways like autophagy, phagosome, mitophagy, lysosome and ferroptosis were up-regulated in moderately pigmented cells.

An acceleration in these pathways occurs for the removal of cell debris and further cleansing. Cytokine-cytokine receptor interaction is up-regulated as well, which enhances the restoration of homeostasis. Likewise, up-regulation of cell adhesion molecules (CAMs) add to that and are up-regulated. They are known to play an important role in homeostasis, immune response and inflammation⁸³. This could also further add to the reason for more pathways related to cancer, immune disease and infectious disease being significantly up-regulated in moderately pigmented NHEM.

5.4 Blue lights increases ATP amount

So far, with the available knowledge from the current research reported on PBM mechanisms, it is clear that mitochondria are inevitably affected by it. Mitochondria are known as the “powerhouse of the cell” as they are involved in energy generation in the form of ATP, which is obtained via the process of oxidative phosphorylation. PBM has been attributed to act directly on the complex IV (also known as cytochrome c oxidase) of the cellular respiratory chain that is located in the mitochondrial membrane⁸⁴. To assess the PBM effects on NHEM using the selected dose for this study, we performed an ATP assay based on luminescence. Our findings suggested a significant increase in ATP levels 24 and 48 hours of harvesting after irradiation for all skin phototype NHEM. In accordance with Liebmann, J., et al., 2010⁸⁵, who have provided evidence that the cellular ATP was elevated after blue light (453 nm) irradiation.

In the gene expression analysis, an up-regulation was observed in oxidative phosphorylation and glycolysis or gluconeogenesis pathways, which is in accordance with the results obtained from ATP measurements.

5.5 Blue light increases ROS level

Reactive oxygen species (ROS) are considered as an important secondary messenger for downstream signalling. PBM has been reported to alter the cell redox potential, which accounts for the primary changes induced by light¹³. Flavins and Flavin-containing cytochrome⁸⁶ found within the mitochondrial respiratory chain are known to be excited by blue light and produce ROS^{87, 88}. Further, to investigate the role of blue light treatment on the mitochondrial function, the redox status analysis of the cell is an important step. Hence, to estimate the changes in the redox level in NHEM using

the selected dose for this study, we utilized live redox sensor Grx1-roGFP3. Different dyes and chemicals used to assess the level of ROS changes in the system have many disadvantages and, therefore this sensor was transduced into our cells to measure real-time changes inside the cell after irradiation with our respective dose 64.8 J/cm². For all the skin phototype NHEM, maximum acceleration in ROS levels were seen immediately after the irradiation, and from 30 min to 2 hours, there is an exponential decrease. Whereas after two hours of the light treatment, the levels start shifting towards the basal level and finally, after six hours after irradiation, the curve flattens completely. Rohringer, S. et al.⁸⁹ showed that only blue (475 nm) LED light induced a significant increase in ROS production, whereas the red (635 nm) and green (516 nm) LED light did not result in a significant increase in ROS formation in the endothelial cells. Similar results were also communicated by Liebel, F. et L:⁹⁰ about the significant increase in ROS production following exposure to visible light (400-700 nm).

Conspicuously, the replication and repair pathways are significantly down-regulated, indicating the possibility of the stress level being well maintained by the cellular system. This is also reflected by the quick reduction in the rapid ROS increase observed shortly after irradiation, which might rely on the concept of 'mitohormesis' (mitochondrial hormesis). It is well known that the mitochondria are an important source of ROS within the mammalian cells⁹¹. Besides, the mitochondrial respiratory chain has the photoacceptors or chromophores for blue light absorption^{92, 86, 93}. ROS are the signalling molecules, produced in mitochondria due to stress, and this triggers the retrograde response. This process results in transcriptional changes in the nucleus, which in turn activates the cellular defense mechanism, serving as the protective shield and prevent further damage to the cell.

Besides, this process also activates detoxification routes that finally result in alleviation of the initial signalling molecules, and this might explain the fast recovery of the sudden burst in ROS in NHEM. In more detail, expression of genes like SDHA, COX4I1, COX5A, COX5B, ATP5F1A, ATP6V1A that encodes for the mitochondrial respiratory chain complexes I-V were found to be up-regulated after blue light treatment. That led to an increase in energy metabolism and as a result, an up-regulation in oxidative phosphorylation was observed. This was confirmed in the ATP measurements with an increase in the ATP amount for NHEM. This might also trigger the AMPK system, which acts as a sensor of the cellular energy status and is activated by oxidative stress as

well. Which further results in an activation of FOXOs via phosphorylation. This is reflected in an overall up-regulation in AMPK and FOXO signalling pathways of NHEM. Additionally, to assert the assumption of counteracting the oxidative stress, the metabolism of xenobiotics by cytochrome P450 was observed to be significantly up-regulated in NHEM 48 hours after irradiation with blue light. Nrf2, a critical transcription factor known to activate a group of stress-dependent genes and a key enhancer of cytoprotective genes to oxidative stress as well as a potential target of AMPK. In the inactive state, Nrf2 is bound to Kelch-like ECH-associated protein 1 (Keap1). Upon inactivation of the latter, Nrf2 translocates to the nucleus and binds to the antioxidant response element (ARE). Finally, this triggers the activation of transcription of genes involved in xenobiotic metabolism and disposition, anti-oxidant defense and redox signalling.

Moreover, the enzyme tyrosinase is known to use superoxide radical as a substrate for melanogenesis and this might have a role in protecting melanocytes from the harmful effects of ROS^{94, 95}. Hence, showing that melanin can act as photosensitizer^{96, 97}. Melanin has been reported to be an important regulator to balance ROS in melanocytes that could alter the response of melanocytes to arsenic and UV radiation when compared to keratinocytes^{98, 99}. Thus, melanocytes have the mechanism to manage ROS to prevent DNA damage.

The results obtained from redox changes showed a higher increase in the amount of ROS formation in the darkly pigmented NHEM as compared to the other two skin phototype NHEM, which could possibly explain the higher number of dead cells following blue light treatment as measured by flow cytometry.

5.6 AHR as a possible target for oxidative stress management from blue light

Moreover, after 48 hours of blue light treatment, gene expression revealed a strong and significant up-regulation of CYP1B1, as well as an up-regulation of the CYP1A1 gene. They are crucial in the detoxification of polycyclic aromatic compounds like polycyclic aromatic hydrocarbons (PAHs) and halogenated aromatic hydrocarbons (HAHs), for example, 2,3,7,8-tetrachlorodibenzo-para-dioxin (TCDD)^{100, 101}, whose activation can be extensively toxic due to production of highly reactive electrophiles, termed as reactive oxygen metabolites (ROMs)¹⁰². Both CYP1B1 and CYP1A1 are

regulated by AHR, which is a basic-helix/loop/helix per-Arnt-sim (bHLH/PAS) superfamily member and a ligand-activated transcription factor. Significant up-regulation of the AHR pathway in NHEM after blue light treatment was noted from KEGG pathways.

AHR senses numerous intracellular and extracellular signals including endogenous compounds, foreign chemicals, gas molecules, gravity, heat, osmotic pressure, photons (light) ¹⁰³, oxygen level, redox potential and changes to circadian rhythm, control adaptation to the cellular environment ¹⁰⁴. Its role in the cellular response to light has been reported ^{105, 106}. Tyrosine and tryptophan are known to absorb UV radiation or visible light and even a stronger absorption observed for tryptophan, making it more susceptible to photolytic destruction ¹⁰⁷. The photoproducts formed as a result include 6-formylindolo[3,2-*b*]carbazole (FICZ) and 6, 12-diformylindolo[3, 2-*B*]carbazole (dFICZ) ^{108, 109}. Amongst these two photoproducts, FICZ has a stronger affinity for AHR.

The skin epidermis has an abundant source of amino acid-like tryptophan (Trp) and upon irradiation (90 min, 64.8 J/cm²) of human melanocytes with blue light (453 nm), Trp might be photo-oxidized to produce photo products like TCDD; FICZ or dFICZ that act as major AHR ligands and CYP1 substrates ^{110, 111, 78}. AHR in its non-activated state is located in the cytoplasm and upon activation by a ligand, it translocates into the nucleus. In the nucleus, it binds with ARNT to form the active heterodimer. This heterodimer is known to bind further to xenobiotics response elements (XRE) to modulate the expression of targets ¹¹². This, in turn, up-regulates the transcription of a battery of xenobiotic-metabolizing enzymes (XMEs) ¹¹³, which are termed as 'AHR gene battery'.

Amongst these, CYP1A1, CYP1A2, CYP1B1, NQO1 and ALDH3A1 are involved in phase I and UGT1A, GSTA1 in phase II of xenobiotic metabolism ^{102, 114}.

Apart from CYP1B1 and CYP1A1, in our data set, gene expression analysis also revealed the up-regulation of other genes, NQO1, ALDH8A1, GSTT2B in NHEM after blue light treatment. NQO1 has been extensively studied for its role in chemoprotection ^{102, 103} and ALDH8A1 is involved in tryptophan catabolism ¹¹⁵. Whereas, GSTT2B is part of the phase II XMEs known for cellular detoxification. Also pathways like chemical carcinogenesis, metabolism of cytochrome P450, steroid hormone biosynthesis and tryptophan metabolism were found to be up-regulated in NHEM following blue light

treatment. These observations further affirm the role of AHR being involved as a sensor of blue light. Similar findings have been reported by Becker, A., et al., 2016⁸¹, showing that blue light (453 nm) exposed keratinocytes had a significant increase in the transcription of genes related to the electron transport chain, cytochrome P450-related genes as well as steroid hormone synthesis related genes.

Besides AHR, AHRR was also observed to be slightly up-regulated. The latter differs from AHR as it has a trans-repressor domain at C-terminal domain whereas AHR and ARNT have a transactivation domain at the same terminal. As a result, it can suppress AHR activity by binding to ARNT and XRE¹¹⁶. Hence, this serves as a negative regulatory loop to maintain homeostasis¹¹².

Correspondingly, AHR-activated CYP1 enzymes might play an interesting role in regulating pigmentation in melanocytes. It has been reported that AHR regulates the process of melanogenesis by coordinating the expression of melanogenic enzymes^{117, 118, 119}, as well as it might be also be involved in protecting melanocytes from oxidative damage by promoting mitochondrial biogenesis¹²⁰. This is in line with our gene expression results wherein an up-regulation of the AHR pathway as well as related genes like CYP1B1 was observed and hence underlining the role of AHR in modulating the melanin content.

5.7 Conclusion and outlook

We have provided an overview of the effects of PBM using blue light (453 nm) dose 64.8 J/cm² on human melanocytes, which revealed major cellular changes including induction of melanogenesis with no significant cell death via apoptosis as well as an increase in ATP and ROS level, the most persistent and significant findings reported after light treatment. Furthermore, gene expression analysis highlighted the role of AHR and its gene battery in response to oxidative stress for detoxification process post blue light treatment, besides the possibility of its role in the regulation of the melanogenic enzymes as well.

Additionally, all the three skin phototype NHEM cells illustrated almost the same overall outcome for different assays conducted *in vitro* as well as gene expression results showed the same regulation for different significant genes and pathways. Although still some variations were noticed in a few results. These variations could be attributed to the fact that these cells were obtained from different donors.

Nevertheless, this study supports some initial interesting findings as an effect of PBM using blue light on melanocytes, which could have a potential implication for hypopigmentary disorders like vitiligo, depigmented lesions or scars. However, further experiments with more cell lines and donors are necessary to validate these outcomes.

6. Summary

In this study, we assessed the impact of PBM using blue light on melanocytes. Blue light wavelength belongs to the shorter wavelength range in the electromagnetic spectrum and is the nearest one to UV radiation. The effects of UV radiation on the skin has been studied in great depth, but in the last decade, the focus has started to shift towards understanding the role of the shorter wavelength range on the human body and even other wavelengths belonging to VIS light spectrum. VIS light represents almost half of the solar light coming on the earth. It has been shown that low levels of VIS and NIR light can have beneficial effects, and therefore, it is being used to treat various conditions and diseases in the medical field. In the past, the use of this therapy has progressed but still, there is a lot that needs to be studied to unravel the cellular and molecular mechanisms involved to assess the effects as a whole. From the literature search, it was noted that in the skin, the consequences of blue light on keratinocytes and fibroblasts have been explored more as compared to melanocytes. Wide ranges of inhibitory and stimulatory effects on biological processes have been reported. At the same time, these outcomes might not be the same for every cell type as different irradiation parameters can bring out different impact and every cell has own mechanisms to deal with varied type and amount of stimuli. Hence, this study aimed to evaluate the effects of blue light wavelength (453 nm) on melanocytes.

In vitro experiments were carried out using NHEM cells with the application of different doses of blue light to assess the dose-effect, which resulted in a biphasic dose-response curve. Next, blue light was tested in NHEM cells for its response on melanin production following 90 min of irradiation with a dose of 64.8 J/cm², the cells were harvested 48 hours after irradiation and an increased melanin concentration was noted. The same results occurred in all the three pigmented skin phototype of NHEM cells. Further, this dose was selected, and other parameters were evaluated, for example, possible induction of apoptosis, influence on ATP level and consequences on the redox status of the cells. No significant apoptosis was induced, and an increase in the ATP level was identified as well as the ROS production increased with a sudden burst immediately after irradiation and later with time, it shifted to basal levels.

Finally, gene expression analysis was performed, which revealed an array of genes and pathways explaining the other *in vitro* data. Pathways like glycolysis and oxidative phosphorylation were up-regulated, reflecting the results of ATP measurements.

Moreover, the overall pattern for the pathways related to cell growth and death was down-regulated, and apoptosis pathway itself was not significantly regulated, which is reflected by the FACS analysis where no significant apoptosis was observed. Additionally the caspase cascade was slightly down-regulated. The utmost important gene CYP1B1 was strongly significantly up-regulated. This gene belongs to 'AHR gene battery', involved in the production of phase I and phase II enzymes of xenobiotic metabolism. They are well known for their role in preventing damage due to oxidative stress. This outcome is in line with the observation obtained from ROS measurements. Thus, an increase in ROS levels activates the 'AHR gene battery' triggering the anti-inflammatory response as also downstream pathways like the steroid hormone synthesis. Furthermore, an increase in the melanogenesis pathway and tyrosine metabolism was noted, which is in agreement with the increase in melanin content assay. Moreover, gene expression profiles revealed an up-regulation of tyrosinase enzyme, AHR pathway as well as tryptophan metabolism. All these findings suggest the possible role of AHR as a potential regulator of xenobiotic effects in human melanocytes on exposure to blue light dose (64.8 J/cm^2) via photo-oxidation of tryptophan and possibly mediating pigmentation by modulating the melanogenic enzymes.

7. References

1. U.S. National Library of Medicine: Fact Sheet Medical Subject Headings (MeSH®). 2015. Online: <http://wayback.archive-it.org/org-350/20180312141553/https://www.nlm.nih.gov/pubs/factsheets/mesh.html>, Stand: 29.06.2020.
2. Arany, PR: Photobiomodulation: poised from the fringes. *Photomed Laser Surg*, 30: 507-509, 2012.
3. Anders, JJ, Lanzafame, RJ, Arany, PR: Low-level light/laser therapy versus photobiomodulation therapy. *Photomed Laser Surg*, 33: 183-184, 2015.
4. Nobel Media: Niels Ryberg Finson - Biographical. 2020. Online: <https://www.nobelprize.org/prizes/medicine/1903/finsen/biographical/>, Stand: 23.06.2020.
5. Mester, E, Szende, B, Tota, JG: Effect of laser on hair growth of mice. *Kiserl Orvostud*, 19: 628-631, 1967.
6. Mester, E, Szende, B, Gärtner, P: [The effect of laser beams on the growth of hair in mice]. *Radiobiol Radiother (Berl)*, 9: 621-626, 1968.
7. Mester, E, Nagylucskay, S, Döklen, A, Tisza, S: Laser stimulation of wound healing. *Acta Chir Acad Sci Hung*, 17: 49-55, 1976.
8. Hadis, MA, Zainal, SA, Holder, MJ, Carroll, JD, Cooper, PR, Milward, MR, Palin, WM: The dark art of light measurement: accurate radiometry for low-level light therapy. *Lasers Med Sci*, 31: 789-809, 2016.
9. Chung, H, Dai, T, Sharma, SK, Huang, YY, Carroll, JD, Hamblin, MR: The nuts and bolts of low-level laser (light) therapy. *Ann Biomed Eng*, 40: 516-533, 2012.
10. Verhoeven, G: The reflection of two fields – electromagnetic radiation and its role in (aerial) imaging. *AARGnews*, 55: 13-18, 2017.
11. Diffey, B, Kochevar, I: Basic principles of photobiology. In: *Photodermatology*. edited by HENRY, W. L., New York [u.a.], Informa healthcare, 2007, pp 15-27.
12. Sutherland, J: Biological effects of polychromatic light. *Photochem Photobiol*, 76: 164-170, 2002.
13. Karu, TI: Primary and secondary mechanisms of action of visible to near-IR radiation on cells. *J Photochem Photobiol B*, 49: 1-17, 1999.
14. Sowa, P, Rutkowska-Talipska, J, Rutkowski, K, Kosztyla-Hojna, B, Rutkowski, R.: Optical radiation in modern medicine. *Postepy Dermatol Alergol*, 30: 246-251, 2013.

15. Huang, YY, Chen, AC, Carroll, JD, Hamblin, MR: Biphasic dose response in low level light therapy. *Dose Response*, 7: 358-383, 2009.
16. Karu, TI: Cellular and molecular mechanisms of photobiomodulation (Low-Power Laser Therapy). *IEEE J Sel Top Quantum Electron*, 20: 143-148, 2014.
17. Giese, AC: Photosensitization of organisms with special reference to natural photosensitizers. In: *Lasers in Biology and Medicine*. edited by HILLENKAMPF F, P. R., SACCHI C, New York: Plenum press, 1980, pp 299-314.
18. Spikes, JD: Photosensitization. In: *The Science of Photobiology, 2nd edition*. edited by SMITH, K. C., New York: Plenum Press, 1989, pp 79-111.
19. Karu, TI, Pyatibrat, LV, Kolyakov, SF, Afanasyeva, NI: Absorption measurements of cell monolayers relevant to mechanisms of laser phototherapy: reduction or oxidation of cytochrome c oxidase under laser radiation at 632.8 nm. *Photomed Laser Surg*, 26: 593-599, 2008.
20. Karu, TI: Multiple roles of cytochrome c oxidase in mammalian cells under action of red and IR-A radiation. *IUBMB Life*, 62: 607-610, 2010.
21. Hamblin, MR: Mechanisms and applications of the anti-inflammatory effects of photobiomodulation. *AIMS Biophys*, 4: 337-361, 2017.
22. Avci, P, Gupta, A, Sadasivam, M, Vecchio, D, Pam, Z, Pam, N, Hamblin, MR: Low-level laser (light) therapy (LLLT) in skin: stimulating, healing, restoring. *Semin Cutan Med Surg*, 32: 41-52, 2013.
23. Haake, A, Holbrook, K: The structure and development of skin. In: *Fitzpatrick's dermatology in general medicine*. edited by FREEDBERG, I. M., FITZPATRICK, T. B., New York, McGraw-Hill, Health Professions Division, 1999, pp 70-114.
24. Kolarsick, PAJ, Kolarsick, MA, Goodwin, C: Anatomy and physiology of the skin. *J Dermatol Nurses Assoc*, 3: 203-213, 2011.
25. Lucas, JB: The physiology and biomechanics of skin flaps. *Facial Plast Surg Clin North Am*, 25: 303-311, 2017.
26. Kanitakis, J: Anatomy, histology and immunohistochemistry of normal human skin. *Eur J Dermatol*, 12: 390-399, 2002.
27. Seifert, AW, Maden, M: New insights into vertebrate skin regeneration. *Int Rev Cell Mol Biol*, 310: 129-169, 2014.

-
28. Freinkel, RK, Woodley, DT: *The biology of the skin*, New York, NY, Parthenon, 2001.
 29. Wong, R, Geyer, S, Weninger, W, Guimberteau, JC, Wong, JK: The dynamic anatomy and patterning of skin. *Exp Dermatol*, 25: 92-98, 2016.
 30. Menon, GK: New insights into skin structure: scratching the surface. *Adv Drug Deliv Rev*, 54: S3-S17, 2002.
 31. Cichorek, M, Wachulska, M, Stasiewicz, A, Tyminska, A: Skin melanocytes: biology and development. *Postepy Dermatol Alergol*, 30: 30-41, 2013.
 32. Plonka, PM, Passeron, T, Brenner, M, Tobin, DJ, Shibahara, S, Thomas, A, Slominski, A, Kadekaro, AL, Hershkovitz, D, Peters, E, Nordlund, JJ, Abdel-Malek, Z, Takeda, K, Paus, R, Ortonne, JP, Hearing, VJ, Schallreuter, KU: What are melanocytes really doing all day long...? *Exp Dermatol*, 18: 799-819, 2009.
 33. Goding, CR: Melanocytes: The new Black. *Int J Biochem Cell Biol*, 39: 275-279, 2007.
 34. Seiji, M, Fitzpatrick, TB: The reciprocal relationship between melanization and tyrosinase activity in melanosomes (melanin granules). *J Biochem*, 49: 700-706, 1961.
 35. Kobayashi, N, Nakagawa, A, Muramatsu, T, Yamashina, Y, Shirai, T, Hashimoto, MW, Ishigaki, Y, Ohnishi, T, Mori, T: Supranuclear melanin caps reduce ultraviolet induced DNA photoproducts in human epidermis. *J Invest Dermatol*, 110: 806-810, 1998.
 36. Yamaguchi, Y, Brenner, M, Hearing, VJ: The regulation of skin pigmentation. *J Biol Chem*, 282: 27557-27561, 2007.
 37. Haass, NK, Herlyn, M: Normal human melanocyte homeostasis as a paradigm for understanding melanoma. *J Invest Dermatol Symp Proc*, 10: 153-163, 2005.
 38. Miot, LD, Miot, HA, Silva, MG, Marques, ME: Fisiopatologia do melasma [Physiopathology of melasma]. *An Bras Dermatol*, 84: 623-635, 2009.
 39. Simon, JD, Peles, D, Wakamatsu, K, Ito, S: Current challenges in understanding melanogenesis: bridging chemistry, biological control, morphology, and function. *Pigment Cell Melanoma Res*, 22: 563-579, 2009.
 40. Kauser, S, Schallreuter, KU, Thody, AJ, Gummer, C, Tobin, DJ: Regulation of human epidermal melanocyte biology by beta-endorphin. *J Invest Dermatol*, 120: 1073-1080, 2003.

41. Pfeifer, GP, Besaratinia, A: UV wavelength-dependent DNA damage and human non-melanoma and melanoma skin cancer. *Photochem Photobiol Sci*, 11: 90-97, 2012.
42. Sage, E, Girard, P-M, Francesconi, S: Unravelling UVA-induced mutagenesis. *Photochem Photobiol Sci*, 11: 74-80, 2012.
43. Ash, C, Dubec, M, Donne, K, Bashford, T: Effect of wavelength and beam width on penetration in light-tissue interaction using computational methods. *Lasers Med Sci*, 32: 1909-1918, 2017.
44. Baron, ED, Suggs, AK: Introduction to photobiology. *Dermatol Clin*, 32: 255-266, vii, 2014.
45. Garza, ZCF, Born, M, Hilbers, PAJ, van Riel, NAW, Liebmann, J: Visible blue light therapy: Molecular Mechanisms and Therapeutic Opportunities. *Curr Med Chem*, 25: 5564-5577, 2018.
46. Zhao, ZC, Zhou, Y, Tan, G, Li, J: Research progress about the effect and prevention of blue light on eyes. *Int J Ophthalmol*, 11: 1999-2003, 2018.
47. Kleinpenning, MM, Smits, T, Frunt, MHA, van Erp, PEJ, van de Kerkhof, PCM, Gerritsen, RMJP: Clinical and histological effects of blue light on normal skin. *Photodermatol Photoimmunol Photomed*, 26: 16-21, 2010.
48. Kushibiki, T, Tajiri, T, Ninomiya, Y, Awazu, K: Chondrogenic mRNA expression in prechondrogenic cells after blue laser irradiation. *J Photochem Photobiol B*, 98: 211-215, 2010.
49. Lavi, R, Ankri, R, Sinyakov, M, Eichler, M, Friedmann, H, Shainberg, A, Breitbart, H, Lubart, R: The plasma membrane is involved in the visible light-tissue interaction. *Photomed Laser Surg*, 30: 14-19, 2012.
50. Kushibiki, T, Hirasawa, T, Okawa, S, Ishihara, M: Blue laser irradiation generates intracellular reactive oxygen species in various types of cells. *Photomed Laser Surg*, 31: 95-104, 2013.
51. Buravlev, EA, Zhidkova, TV, Vladimirov, YA, Osipov, AN: Effects of laser and LED radiation on mitochondrial respiration in experimental endotoxic shock. *Lasers Med Sci*, 28: 785-790, 2013.
52. Duteil, L, Cardot-Leccia, N, Queille-Roussel, C, Maubert, Y, Harmelin, Y, Boukari, F, Ambrosetti, D, Lacour, JP, Passeron, T: Differences in visible light-induced pigmentation according to wavelengths: a clinical and histological study in

-
- comparison with UVB exposure. *Pigment Cell Melanoma Res*, 27: 822-826, 2014.
53. AlGhamdi, KM, Kumar, A, Ashour, AE, AlGhamdi, AA: A comparative study of the effects of different low-level lasers on the proliferation, viability, and migration of human melanocytes in vitro. *Lasers Med Sci*, 30: 1541-1551, 2015.
54. AlGhamdi, KM, Kumar, A, Al-Ghamdi, AA, Al-Rikabi, AC, Mubarek, M, Ashour, AE: Ultra-structural effects of different low-level lasers on normal cultured human melanocytes: an in vitro comparative study. *Lasers Med Sci*, 31: 1819-1825, 2016.
55. Bennet, D, Viswanath, B, Kim, S, An, JH: An ultra-sensitive biophysical risk assessment of light effect on skin cells. *Oncotarget*, 8: 47861-47875, 2017.
56. Yuan, Y, Yan, G, Gong, R, Zhang, L, Liu, T, Feng, C, Du, W, Wang, Y, Yang, F, Li, Y, Guo, S, Ding, F, Ma, W, Idiatullina, E, Pavlov, V, Han, Z, Cai, B, Yang, L: Effects of blue light emitting diode irradiation on the proliferation, apoptosis and differentiation of bone marrow-derived mesenchymal stem cells. *Cell Physiol Biochem*, 43: 237-246, 2017.
57. Nakashima, Y, Ohta, S, Wolf, AM: Blue light-induced oxidative stress in live skin. *Free Radic Biol Med*, 108: 300-310, 2017.
58. Regazzetti, C, Sormani, L, Debayle, D, Bernerd, F, Tulic, MK, De Donatis, GM, Chignon-Sicard, B, Rocchi, S, Passeron, T: Melanocytes sense blue light and regulate pigmentation through Opsin-3. *J Invest Dermatol*, 138: 171-178, 2018.
59. Mignon, C, Uzunbajakava, NE, Castellano-Pellicena, I, Botchkareva, NV, Tobin, DJ: Differential response of human dermal fibroblast subpopulations to visible and near-infrared light: Potential of photobiomodulation for addressing cutaneous conditions. *Lasers Surg Med*, 50: 859-882, 2018.
60. Kuch, N: Co-cultures of fibroblasts and keratinocytes under the influence of blue light. *Medical Research Center*. Hochschule Mannheim, University of Applied Sciences, 2016.
61. Backman, TWH, Girke, T: systemPipeR: NGS workflow and report generation environment. *BMC Bioinformatics*, 17: 388, 2016.
62. Bray, NL: Fast RNA-seq quantification. *Nat Biotechnol*, 34: 525-527, 2016.
63. Gu, Z, Eils, R, Schlesner, M: Complex heatmaps reveal patterns and correlations in multidimensional genomic data. *Bioinformatics* 32: 2847-2849, 2016.

-
64. Sergushichev, AA: An algorithm for fast preranked gene set enrichment analysis using cumulative statistic calculation. *bioRxiv*: 060012, 2016.
 65. Geistlinger, L, Csaba, G, Zimmer, R: Bioconductor's enrichment browser: seamless navigation through combined results of set- & network-based enrichment analysis. *BMC Bioinformatics*, 17: 45, 2016.
 66. Dweep, H, Sticht, C, Kharkar, A, Pandey, P, Gretz, N: Parallel analysis of mRNA and microRNA microarray profiles to explore functional regulatory patterns in polycystic kidney disease: Using PKD/Mhm Rat Model. *PLoS One*, 8: e53780, 2013.
 67. Scudiero, DA, Shoemaker, RH, Paull, KD, Monks, A, Tierney, S, Nofziger, TH, Currens, MJ, Seniff, D, Boyd, MR: Evaluation of a soluble tetrazolium/formazan assay for cell growth and drug sensitivity in culture using human and other tumor cell lines. *Cancer Res Treat*, 48: 4827-4833, 1988.
 68. Lanzafame, RJ, Stadler, I, Andrew, F, Connelly, R, Peter, STA, Brondon, P, Olson, D: Reciprocity of exposure time and irradiance on energy density during photoradiation on wound healing in a murine pressure ulcer model. *Lasers Surg Med*, 39: 534-542, 2007.
 69. Schulz, H: Über die Theorie der Arzneimittelwirkung. In, *Virchows Archiv*, 1877, pp 423-434.
 70. Schulz, H: Über Hefegifte. In, *Pflügers Archiv Gesamte Physiologie*, 1888, pp 517-541.
 71. Castellano-Pellicena, I, Uzunbajakava, NE, Mignon, C, Raafs, B, Botchkarev, VA, Thornton, MJ: Does blue light restore human epidermal barrier function via activation of Opsin during cutaneous wound healing? *Lasers Surg Med*, 51: 370-382, 2019.
 72. Lai, X, Wichers, HJ, Soler-Lopez, M, Dijkstra, BW: Structure and function of human tyrosinase and tyrosinase-related proteins. *Chemistry (Easton)*, 24: 47-55, 2018.
 73. D'Mello, SA, Finlay, GJ, Baguley, BC, Askarian-Amiri, ME: Signaling pathways in melanogenesis. *Int J Mol Sci*, 17, 2016.
 74. Kitano, Y, Hu, F: Melanin versus protein synthesis in melanocytes in vitro. *Exp Cell Res*, 64: 83-88, 1971.

-
75. Rinchik, EM, Bultman, SJ, Horsthemke, B, Lee, S-T, Strunk, KM, Spritz, RA, Avidano, KM, Jong, MTC, Nicholls, RD: A gene for the mouse pink-eyed dilution locus and for human type II oculocutaneous albinism. *Nature*, 361: 72-76, 1993.
 76. Puri, N, Brillant, M: The function of the pink-eyed dilution protein. *Pigment Cell Res*, 11: 174, 1998.
 77. Yang, Q, Yi, S, Li, M, Xie, B, Luo, J, Wang, J, Rong, X, Zhang, Q, Qin, Z, Hang, L, Feng, S, Fan, X: Genetic analyses of oculocutaneous albinism types 1 and 2 with four novel mutations. *BMC Med Genet*, 20: 106, 2019.
 78. Hamblin, MR: Mechanisms and Mitochondrial redox signaling in photobiomodulation. *Photochem Photobiol*, 94: 199-212, 2018.
 79. Serrage, H, Heiskanen, V, Palin, WM, Cooper, PR, Milward, MR, Hadis, M, Hamblin, MR: Under the spotlight: mechanisms of photobiomodulation concentrating on blue and green light. *Photochem Photobiol Sci*, 18: 1877-1909, 2019.
 80. Gu, Q, Wang, L, Huang, F, Schwarz, W: Stimulation of TRPV1 by Green laser light. *Evid Based Complement Alternat Med*, 2012: 857123, 2012.
 81. Becker, A, Klapczynski, A, Kuch, N, Arpino, F, Simon-Keller, K, De La Torre, C, Sticht, C, van Abeelen, FA, Oversluizen, G, Gretz, N: Gene expression profiling reveals aryl hydrocarbon receptor as a possible target for photobiomodulation when using blue light. *Sci Rep*, 6: 33847, 2016.
 82. Oh, PS, Na, KS, Hwang, H, Jeong, HS, Lim, S, Sohn, MH, Jeong, HJ: Effect of blue light emitting diodes on melanoma cells: involvement of apoptotic signaling. *J Photochem Photobiol B*, 142: 197-203, 2015.
 83. Harjunpaa, H, Lloret Asens, M, Guenther, C, Fagerholm, SC: Cell adhesion molecules and their roles and regulation in the immune and tumor microenvironment. *Front Immunol*, 10: 1078, 2019.
 84. Karu, TI: Laser biostimulation: a photobiological phenomenon. *J Photochem Photobiol B*, 3: 638-640, 1989.
 85. Liebmann, J, Born, M, Kolb-Bachofen, V: Blue-light irradiation regulates proliferation and differentiation in human skin cells. *J Invest Dermatol*, 130: 259-269, 2010.
 86. Cooper, GM, Hausman, RE: *The cell: a molecular approach*, Washington, DC, ASM Press, 2007.

-
87. Swartz, TE, Corchnoy, SB, Christie, JM, Lewis, JW, Szundi, I, Briggs, WR, Bogomolni, RA: The photocycle of a flavin-binding domain of the blue light photoreceptor phototropin. *J Biol Chem*, 276: 36493-36500, 2001.
 88. Cheon, MW, Kim, TG, Lee, YS, Kim, SH: Low level light therapy by Red–Green–Blue LEDs improves healing in an excision model of Sprague–Dawley rats. *Pers Ubiquit Comput*, 17: 1421-1428, 2012.
 89. Rohringer, S, Holnthoner, W, Chaudary, S, Slezak, P, Priglinger, E, Strassl, M, Pill, K, Muhleder, S, Redl, H, Dungel, P: The impact of wavelengths of LED light-therapy on endothelial cells. *Sci Rep*, 7: 10700, 2017.
 90. Liebel, F, Kaur, S, Ruvolo, E, Kollias, N, Southall, MD: Irradiation of skin with visible light induces reactive oxygen species and matrix-degrading enzymes. *J Invest Dermatol*, 132: 1901-1907, 2012.
 91. Murphy, MP: How mitochondria produce reactive oxygen species. *Biochem J*, 417: 1-13, 2009.
 92. Bouly, JP, Schleicher, E, Dionisio-Sese, M, Vandenbussche, F, Van der Straeten, D, Bakrim, N, Meier, S, Batschauer, A, Galland, P, Bittl, R, Ahmad, M: Cryptochrome blue light photoreceptors are activated through interconversion of flavin redox states. *J Biol Chem*, 282: 9383-9391, 2007.
 93. Osborne, NN, Núñez-Álvarez, C, Del Olmo-Aguado, S: The effect of visual blue light on mitochondrial function associated with retinal ganglions cells. *Exp Eye Res*, 128: 8-14, 2014.
 94. Videira IF, MD, Magina S: Mechanisms regulating melanogenesis. *An Bras Dermatol*, 88: 76-83, 2013.
 95. Tsatmali, M, Ancans, J, Thody, AJ: Melanocyte function and its control by melanocortin peptides. *J Histochem Cytochem*, 50: 125-133, 2002.
 96. Slominski A, TD, Shibahara S, Wortsman J: Melanin pigmentation in mammalian skin and its hormonal regulation. *Physiol Rev*, 84: 1155-1228, 2004.
 97. Chiarelli-Neto, O, Ferreira, AS, Martins, WK, Pavani, C, Severino, D, Faião-Flores, F, Maria-Engler, SS, Aliprandini, E, Martinez, GR, Di Mascio, P, Medeiros, MHG, Baptista, MS: Melanin photosensitization and the effect of visible light on epithelial cells. *PLoS One*, 9: e113266-e113266, 2014.
 98. Suzukawa, AA, Vieira, A, Winnischofer, SM, Scalfio, AC, Mascio, PD, da Costa Ferreira, AM, Ravanat, J-C, de Luna Martins, D, Rocha, MEM, Martinez, GR:

- Novel properties of melanins include promotion of DNA strand breaks, impairment of repair, and reduced ability to damage DNA after quenching of singlet oxygen. *Free Radic Biol Med*, 52: 1945-1953, 2012.
99. Jenkins, NC, Grossman, D: Role of melanin in melanocyte dysregulation of reactive oxygen species. *Biomed Res Int*, 2013: 908797-908797, 2013.
100. Mimura, J, Fujii-Kuriyama, Y: Functional role of AhR in the expression of toxic effects by TCDD. *Biochim Biophys Acta*, 1619: 263-268, 2003.
101. Nebert, DW, Dalton, TP, Okey, AB, Gonzalez, FJ: Role of aryl hydrocarbon receptor-mediated induction of the CYP1 enzymes in environmental toxicity and cancer. *J Biol Chem*, 279: 23847-23850, 2004.
102. Nebert, DW, Roe, AL, Dieter, MZ, Solis, WA, Yang, Y, Dalton, TP: Role of the aromatic hydrocarbon receptor and [Ah] gene battery in the oxidative stress response, cell cycle control, and apoptosis. *Biochem Pharmacol*, 59: 65-85, 2000.
103. Nebert, DW: Aryl hydrocarbon receptor (AHR): "pioneer member" of the basic-helix/loop/helix per-Arnt-sim (bHLH/PAS) family of "sensors" of foreign and endogenous signals. *Prog Lipid Res*, 67: 38-57, 2017.
104. Rothhammer, V, Quintana, FJ: The aryl hydrocarbon receptor: an environmental sensor integrating immune responses in health and disease. *Nat Rev Immunol*, 19: 184-197, 2019.
105. Gu, Y-Z, Hogenesch, JB, Bradfield, CA: The PAS Superfamily: Sensors of environmental and developmental signals. *Annu Rev Pharmacol Toxicol*, 40: 519-561, 2000.
106. Foley, JF: The arylhydrocarbon receptor sees the light. *Sci STKE*, 2007: tw182, 2007.
107. Rannug, A, Fritsche, E: The aryl hydrocarbon receptor and light. *Biol Chem*, 387: 1149-1157, 2006.
108. Rannug, A, Rannug, U, Rosenkranz, HS, Winqvist, L, Westerholm, R, Agurell, E, Grafström, AK: Certain photooxidized derivatives of tryptophan bind with very high affinity to the Ah receptor and are likely to be endogenous signal substances. *J Biol Chem*, 262: 15422-15427, 1987.

-
109. Rannug, U, Rannug, A, Sjöberg, U, Li, H, Westerholm, R, Bergman, J: Structure elucidation of two tryptophan-derived, high affinity Ah receptor ligands. *Chem Biol*, 2: 841-845, 1995.
 110. Wincent, E, Amini, N, Luecke, S, Glatt, H, Bergman, J, Crescenzi, C, Rannug, A, Rannug, U: The suggested physiologic aryl hydrocarbon receptor activator and cytochrome P4501 substrate 6-formylindolo[3,2-b]carbazole is present in humans. *J Biol Chem*, 284: 2690-2696, 2009.
 111. Smirnova, A, Wincent, E, Vikström Bergander, L, Alsberg, T, Bergman, J, Rannug, A, Rannug, U: Evidence for new light-independent pathways for generation of the endogenous aryl hydrocarbon receptor agonist FICZ. *Chem Res Toxicol*, 29: 75-86, 2016.
 112. Larigot, L, Juricek, L, Dairou, J, Coumoul, X: AhR signaling pathways and regulatory functions. *Biochim Open*, 7: 1-9, 2018.
 113. Shimada, T: Xenobiotic-Metabolizing Enzymes Involved in activation and detoxification of carcinogenic polycyclic aromatic hydrocarbons. *Drug Metab Pharmacokinet*, 21: 257-276, 2006.
 114. Schrenk, D: Impact of dioxin-type induction of drug-metabolizing enzymes on the metabolism of endo- and xenobiotics. *Biochem Pharmacol*, 55: 1155-1162, 1998.
 115. Davis, I, Yang, Y, Wherritt, D, Liu, A: Reassignment of the human aldehyde dehydrogenase ALDH8A1 (ALDH12) to the kynurenine pathway in tryptophan catabolism. *J Biol Chem*, 293: 9594-9603, 2018.
 116. Hahn, ME, Allan, LL, Sherr, DH: Regulation of constitutive and inducible AHR signaling: complex interactions involving the AHR repressor. *Biochem Pharmacol*, 77: 485-497, 2009.
 117. Luecke, S, Backlund, M, Jux, B, Esser, C, Krutmann, J, Rannug, A: The aryl hydrocarbon receptor (AHR), a novel regulator of human melanogenesis. *Pigment Cell Melanoma Res*, 23: 828-833, 2010.
 118. Jux, B, Kadow, S, Luecke, S, Rannug, A, Krutmann, J, Esser, C: The aryl hydrocarbon receptor mediates UVB radiation-induced skin tanning. *J Invest Dermatol*, 131: 203-210, 2011.

119. Furue, M, Tsuji, G: Chloracne and hyperpigmentation caused by exposure to hazardous aryl hydrocarbon receptor ligands. *Int J Environ Res Public Health*, 16: 4864, 2019.
120. Wang, X, Li, S, Liu, L, Jian, Z, Cui, T, Yang, Y, Guo, S, Yi, X, Wang, G, Li, C, Gao, T, Li, K: Role of the aryl hydrocarbon receptor signaling pathway in promoting mitochondrial biogenesis against oxidative damage in human melanocytes. *J Dermatol Sci*, 96: 33-41, 2019.

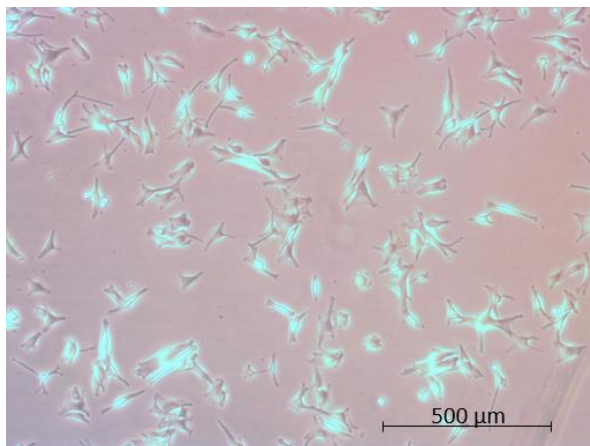
8. Appendix

Appendix 1. Statistics for Figure 13. Value significantly different for the untreated control vs treated (90 min) are indicated by nominal p-value <0.05.

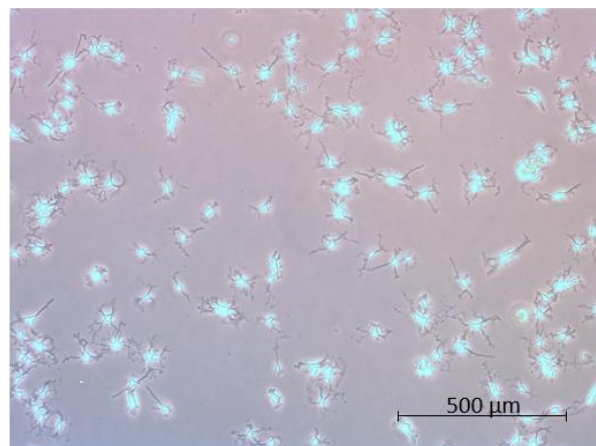
Treatment	p-value
Untreated control vs 2.5 min	<0.0001
Untreated control vs 5 min	<0.0001
Untreated control vs 7.5 min	<0.0001
Untreated control vs 10 min	<0.0001
Untreated control vs 15 min	<0.0001
Untreated control vs 20 min	<0.0001
Untreated control vs 30 min	<0.0001
Untreated control vs 60 min	<0.0001
Untreated control vs 90 min	<0.0001

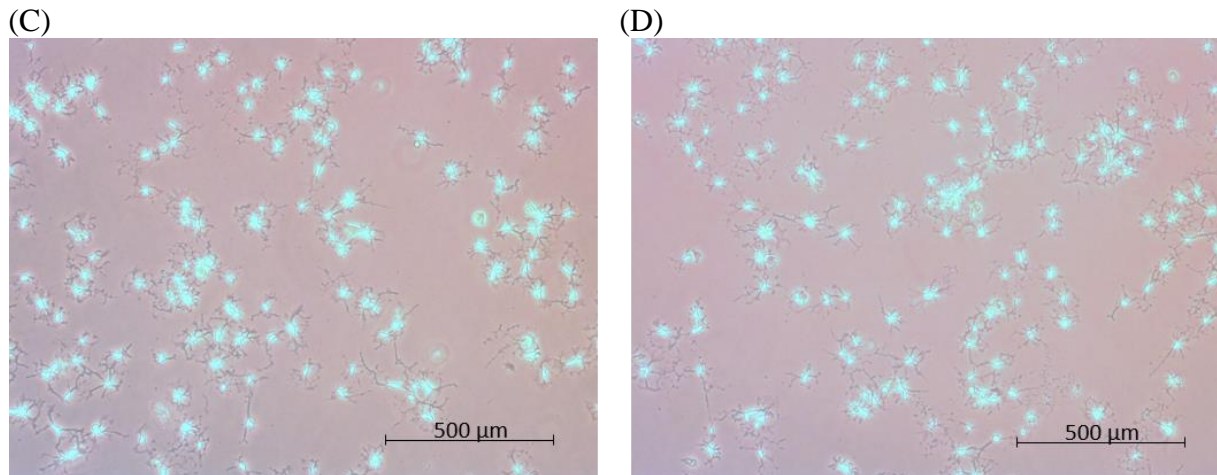
Appendix 2. NHEM cell morphology. (A) before staurosporine treatment and (B) after 1 hour (C) after 2 hours, (D) after 4 hours of treatment with staurosporine (1 μ m). Phase contrast images acquired using inverted light microscope with 5x magnification

(A)



(B)





Appendix 3. Statistics for Figure 21. Value significantly different for the untreated control vs treated (90 min) are indicated by nominal p-value <0.05.

Harvesting time post irradiation (hours)	Skin phototype	p-value
0	Lightly pigmented	<0.0001
	Moderately pigmented	<0.0001
	Darkly pigmented	<0.0001
0.5	Lightly pigmented	<0.0001
	Moderately pigmented	<0.0001
	Darkly pigmented	<0.0001
1	Lightly pigmented	<0.0001
	Moderately pigmented	<0.0001
	Darkly pigmented	<0.0001
2	Lightly pigmented	<0.0001
	Moderately pigmented	<0.0001
	Darkly pigmented	<0.0001
3	Lightly pigmented	<0.0001
	Moderately pigmented	<0.0001
	Darkly pigmented	<0.0001
4	Lightly pigmented	<0.0001
	Moderately pigmented	<0.0001
	Darkly pigmented	<0.0001
5	Lightly pigmented	<0.0001
	Moderately pigmented	<0.0001
	Darkly pigmented	<0.0001
9	Lightly pigmented	<0.0001
	Moderately pigmented	<0.0001
	Darkly pigmented	<0.0001
24	Lightly pigmented	<0.0001
	Moderately pigmented	<0.0001
	Darkly pigmented	<0.0001
48	Lightly pigmented	<0.0001
	Moderately pigmented	<0.0001
	Darkly pigmented	<0.0001

9. Curriculum vitae and Publications

Personal information

Name	Aparna Chauhan
Date of birth	14.04.1992
Place of birth	Ghaziabad, India
Nationality	Indian
Marital status	Unmarried
Father's name	Ravindra Pal Singh Chauhan
Mother's name	Saraswati Chauhan

Education

November 2017-Present	Promotion, Dr. sc. hum. (scientiarum humanarum) , Medical Research Center, Medical Faculty of Mannheim of the Heidelberg University, Germany Thesis title: Impact of photobiomodulation on human skin melanocytes.
August 2013-June 2015	Master of Science in Applied Microbiology Banaras Hindu University, Varanasi, India Master's dissertation title: Study of <i>BHMTG742A</i> and <i>PEMTG744C</i> polymorphisms and maternal risk for Down syndrome.
July 2010-May 2013	Bachelor of Science , Microbiology honours University of Delhi, Gargi College, Delhi India

Work experience

April 2016-October 2017	Junior Research Fellow, CSIR-Institute of Genomics and Integrative Biology, New Delhi, India Project title: Ultrastructural characterization, functional and inflammatory regulators of type 2 diabetes induced impaired skin health.
-------------------------	---

Publications

- Jaiswal, SK, Sukla, KK, **Chauhan, A**, Lakhotia, AR, Kumar, A, Rai, AK: Choline metabolic pathway gene polymorphisms and risk for Down syndrome: An association study in a population with folate-homocysteine metabolic impairment. *Eur J Clin Nutr*, 71: 45-50, 2017.

- Gupta, A, **Chauhan, A**, Priya, A, Mantri, B, Wadhokar, M, Dalave, K, Shah, B, Gokhale, RS, Batra, VV, Singh, A: Lesional skin in vitiligo exhibits delayed in vivo reepithelialization compared to the nonlesional skin. *Wound Rep Reg*, 28: 307-314, 2020.

Abbreviations

ABCA1	ATP binding cassette subfamily A member 1
ADAM12	Disintegrin and metalloproteinase domain-containing protein 12
AMPK	AMP-activated protein kinase
AHR	Aryl hydrocarbon receptor
AHRH	Aryl hydrocarbon receptor repressor
AIP	Aryl hydrocarbon receptor interacting protein
ALDH8A1	Aldehyde dehydrogenase 8 family member A1
ANOVA	Analysis of variance
ANXA3	Annexin A3
AOC3	Membrane primary amine oxidase
ARE	Antioxidant response element
ARNT	Aryl hydrocarbon receptor nuclear translocator
ATP	Adenosine triphosphate
ATP5F1A	ATP synthase subunit alpha
ATP6V1A	V-type protein ATPase catalytic subunit A
BAX	BCL2 associated X, apoptosis regulator
bHLH/PAS	basic-helix/loop/helix per-Arnt-sim
cAMP	Cyclic adenosine monophosphate
CAMs	Cell adhesion molecules
CAP2	Cyclase associated actin cytoskeleton regulatory protein 2
CASP3	Caspase 3
CASP9	Caspase 9
CDC37	Cell division cycle 37, HSP90 cochaperone
CDKN1B	Cyclin-dependent kinase 1B
cGMP	Cyclic guanosine monophosphate
COX	Cytochrome c oxidase
COX4I1	Cytochrome c oxidase subunit 4 isoform 1
COX5A	Cytochrome c oxidase subunit 5A
COX5B	Cytochrome c oxidase subunit 5B
CLDN1	Claudin-1
CREB	c-AMP response element

CYP1A2	Cytochrome P450 family 1 subfamily A member 2
CYP1B1	Cytochrome P450 family 1 subfamily B member 1
DCAF12L1	DDB1-and CUL4-associated factor 12-like protein 1
DCT	Dopachrome tautomerase
dFICZ	6, 12-diformylindolo[3, 2- <i>B</i>]carbazole
ECM	Extracellular-matrix
EGFR	Epidermal growth factor receptor
ENPP1	Ectonucleotide pyrophosphate/phosphodiesterase 1
EP300	E1A binding protein p300
FACS	Fluorescence-activated cell sorting
FAM83D	Family with sequence similarity 83 member D
FAXDC2	Fatty acid hydroxylase domain containing 2
FBXW10	F-box and WD repeat domain containing 10
FBS	Fetal bovine serum
FDR	False discovery rate (also called adjusted p-value)
FICZ	6-formylindolo[3,2- <i>b</i>]carbazole
FITC	Fluorescein isothiocyanate
FOXOs	Forkhead box protein O
GAL3ST1	Galactose-3-O-sulfotransferase 1
GSEA	Gene Set Enrichment Analysis
GSTA1	Glutathione S-transferase alpha 1
GSTT2B	Glutathione S-transferase theta 2B
HAHs	Halogenated aromatic hydrocarbons
HeNe	Helium-Neon
HES1	Hes family bHLH transcription factor 1
HLA-DRA	Major histocompatibility complex, class II, DR alpha
HSP90AA1	Heat shock protein 90 alpha family class A member 1
IL12A	Interleukin 12A
IQR	Interquartile range
IR	Infrared
ITFG2	Integrin alpha FG-GAP repeat containing 2
JUN	Jun proto-oncogene, AP-1 transcription factor subunit
JUNB	JunB proto-oncogene, AP-1 transcription factor subunit

JUND	JunD proto-oncogene, AP-1 transcription factor subunit
Keap1	Kelch-like ECH-associated protein 1
KEGG	Kyoto Encyclopedia of Genes and Genomes
KIF14	Kinase family member 14
L-DOPA	Dihydroxyphenylalanine
LEDs	Light-emitting diodes
LINC00304	Long intergenic non-protein coding RNA 304
LLLT	Low-level laser (or light) therapy
LRRC1	Leucine rich repeat containing 1
MDM2	E3 ubiquitin-protein ligase Mdm2
MGST1	Microsomal glutathione S-transferase 1
Min	Minutes
MIR210HG	MIR210 host gene (a long noncoding RNA)
MITF	Microphthalmia-associated transcription factor
MLANA	Melan-A
MME	Membrane metalloendopeptidase
MYOF	Myoferlin
NAALT	North American Association for Light Therapy
NADH	Nicotinamide adenine dinucleotide
NCOA1	Nuclear receptor coactivator 1
NES	Normalised enrichment score
NFE2L2	Nuclear factor erythroid 2 like 2, also known as Nrf2
NF- κ B	Nuclear factor kappa B
NGS	Next generation sequencing
NHEM	Normal Human Epidermal Melanocytes
NIR	Near infrared
NQO1	NAD(P)H quinone oxidoreductase 1
OCA2	OCA2 melanosomal transmembrane protein
OPN3	Opsin 3
PAHs	Polycyclic aromatic hydrocarbons
PBM	Photobiomodulation
PBS	Phosphate buffer saline
PI	Propidium iodide

PMEL	Premelanosome protein
PMP2	Peripheral myelin protein 2
PMS	N-methyl dibenzopyrazine methyl sulfate
POLK	DNA polymerase kappa
PPARGC1A	PPARG coactivator 1 alpha
PS	Phosphatidylserine
PTGES3	Prostaglandin E synthase 3
PYHIN1	Pyrin and HIN domain family member 1
RIN	RNA integrity number
RNA	Ribonucleic acid
RNF112	Ring finger protein 112
ROMs	Reactive oxygen metabolites
ROS	Reactive oxygen species
RT	Room temperature
SAPCD2	Suppressor APC domain containing 2
SD	Standard deviation
SDHA	Succinate dehydrogenase complex flavoprotein subunit A
SECTM1	Secreted and transmembrane 1
SERPINB2	Serpin family B member 2
SH2D4A	SH2 domain containing 4A
SLC7A5	Solute carrier family 7 member 5
SMIM38	Small integral membrane protein 38
SPP1	Secreted phosphoprotein 1
SRC	SRC proto-oncogene, non-receptor tyrosine kinase
SSPO	SCO-Spondin
TCDD	2,3,7,8-tetrachlorodibenzo-para-dioxin
TCTE1	T-complex-associated-testis-expressed 1
TGF- β	Transforming growth factor beta
THBS2	Thrombospondin 2
TMEM26	Transmembrane protein 26
TM4SF18	Transmembrane 4 L six family member 18
TNF	Tumor necrosis factor
TP53	Tumor protein 53

TRIM73	Tripartite motif containing 73
Trp	Tryptophan
TRPC1	Transient potential cation subfamily C member 1
TYR	Tyrosinase
UGT1A	UDP glucuronosyltransferase family 1 member 4 complex locus
UTP14C	UTP14C small subunit processome component
UV	Ultraviolet
VIS	Visible
WALT	World Association for Laser Therapy
XMEs	Xenobiotics-metabolizing enzymes
XRE	Xenobiotics response elements
XTT	Sodium 3'-[1-(phenylaminocarbonyl)-3, 4-tetrazolium] bis (4methoxy-6-nitro) benzene sulfonic acid hydrate

Acknowledgements

First of all, I would like to express my deepest gratitude to Prof. Norbert Gretz for providing me the opportunity to work in his group. I am thankful for his supervision, support, patience and invaluable advice all throughout this period.

I am very grateful to Prof. Yvonne Samstag (Spokesperson), Research Training Group 'Elucidation of molecular mechanisms as foundation for an evidence-based complementary and integrative medicine' (Train4CIM) for having me as one of the fellows of this group. In addition, a big thanks to the whole team for their help and valuable feedbacks during our meetings, seminars and courses, especially Minguem Jeong, Divya Lairikyengbam and Karina for the friendship, love and our fun get-togethers. As well as, the Ministry of Science, Research and the Arts, Baden-Württemberg and graduate academy, Heidelberg University for financing the fellowship for a period of 3 years.

I would like to dedicate a special thanks to Sina Schwalm and Edda Eustachi for their assistance in all the administrative work as well as the nice conversations during this period.

I would like to express my deepest appreciation for Dr. Carsten Sticht, who not only helped in gene expression analysis but also provided with his generous guidance through the thesis writing process. I would also extend my thanks to Dr. Carolina De La Torre for her work and support. I would thank Camela Jost, Maria Muciek and Elisabeth Wuehl for their help and technical support. Additionally, I would like to thank Stefanie Uhlig, Institute of Transfusion Medicine Immunology, for her support in the flow cytometry experiments. My greatest thanks to Dr. Prama Pallavi for her collaboration in new experimental set-up and her insightful suggestions and immense positive conversations. My biggest thanks to all my colleagues at ZMF for their enormous help, support and motivation. In particular, special thanks to my former colleague Stefania Palumbo for her brainstorming and help during several experiments, as well as Daniela Nardozi for her help in all upcoming questions and problems.

Moreover, I am extremely thankful to my very good friend Wiktoria Banczyk and her family for their generosity, advice and valuable time spent together filled with fun and laughter. In addition, a special mention and thanks to Tiziana Picascia, Erika, Elenora Scaccia for several exciting activities and trips we did together.

My PhD would not have been completed without the unconditional love and moral support of my family and friends in India. Especially my parents, my sister and brother and my best friend Anup, to whom I express my gratitude for believing in me all the time and being with me through thick and thin.

Finally, I am infinitely grateful to everyone for his or her deep trust in me, which encouraged me to grow and reach this goal.